NASA TECHNICAL MEMORANDUM

NASA TM X-1198

NASA TM X-1198

AERODYNAMIC CHARACTERISTICS OF A 0.0667-SCALE MODEL OF THE X-15A-2 RESEARCH AIRPLANE AT TRANSONIC SPEEDS

by James C. Patterson, Jr.

Langley Research Center

Langley Station, Hampton, Va.

NATIONAL AERONAUTICS AND SPACE ADMINISTRATION • WASHINGTON, D. C. • MARCH 1966

NASA TM X-1198

AERODYNAMIC CHARACTERISTICS OF A 0.0667-SCALE MODEL OF THE X-15A-2 RESEARCH AIRPLANE AT TRANSONIC SPEEDS

By James C. Patterson, Jr.

Langley Research Center
Langley Station, Hampton, Va.

NATIONAL AERONAUTICS AND SPACE ADMINISTRATION

For sale by the Clearinghouse for Federal Scientific and Technical Information
Springfield, Virginia 22151 – Price $3.00

AERODYNAMIC CHARACTERISTICS OF A 0.0667-SCALE MODEL OF THE X-15A-2 RESEARCH AIRPLANE AT TRANSONIC SPEEDS

By James C. Patterson, Jr.
Langley Research Center

SUMMARY

An experimental investigation has been conducted in the Langley 8-foot transonic pressure tunnel of a 0.0667-scale model of a modified version of the X-15 research airplane at Mach numbers from 0.60 to 1.20, over an angle-of-attack range from approximately -4° to 20°, and at Reynolds numbers based on the mean geometric chord from 2.074×10^6 to 2.172×10^6.

The results indicate that the static longitudinal, directional, and lateral stability of the configuration, less the externally mounted fuel tanks, has been reduced at lifting conditions compared with that of the X-15 research airplane.

The addition of the externally mounted fuel tanks resulted in a reduction in the longitudinal and directional stability such that the configuration was longitudinally unstable at zero lift below a Mach number of 1.10 and directionally unstable or neutrally stable at a higher angle of attack of 16°. The effective dihedral was increased by the addition of the tanks except for an angle of attack of 16° at Mach numbers ranging from 0.60 to 0.90.

INTRODUCTION

The X-15, a rocket-powered research airplane designed for hypersonic speeds at very high altitudes (see ref. 1), has been modified to extend the Mach number capabilities of this aircraft from 6.0 to 8.0 and is designated as the X-15A-2. This increase in Mach number has been made possible through an increase in fuel capacity by the addition of two externally mounted, jettisonable, propellant tanks 3.12 feet (0.951 m) in diameter and 23.54 feet (7.17 m) long, full scale. The fuselage has also been lengthened 2.42 feet (0.738 m) to provide sufficient room for the installation of two 50-gallon (0.19-m^3) spherical liquid hydrogen tanks to provide fuel for ramjet engines to be tested in the future.

To determine the effects of these modifications on the static stability and control characteristics at transonic speeds, a 0.0667-scale model of the X-15A-2 has been tested

in the Langley 8-foot transonic pressure tunnel. The results of the present investigation were obtained for a Mach number range from 0.60 to 1.20, at angles of attack from approximately -4° to 20°, and at angles of sideslip of 0° and 4°.

To expedite the publication of the data obtained through this investigation, no attempt has been made to analyze completely the results shown. Only a brief discussion is given of a comparison of the results of the X-15 and X-15A-2 model investigations.

SYMBOLS

Longitudinal and lateral results are presented about the stability and body axes systems, respectively. All moments are referenced to a point located at the 20-percent-wing-mean-geometric-chord station which is 24.69 inches (62.71 cm) from the nose of the model (see fig. 1). The units used for the physical quantities defined in this paper are given both in the U.S. Customary Units and in the International System of Units (SI). (See ref. 2.)

b wing span

c chord

$\bar{c}$ wing mean geometric chord

C_D drag coefficient, $\frac{\text{Drag}}{qS}$

$C_{D,o}$ drag coefficient at $C_L = 0$

C_L lift coefficient, $\frac{\text{Lift}}{qS}$

C_{L_α} lift-curve slope, per deg

$C_{L,(L/D)_{max}}$ lift coefficient at maximum lift-drag ratio

C_l rolling-moment coefficient, $\frac{\text{Rolling moment}}{qSb}$

C_{l_β} effective-dihedral parameter, $\frac{\Delta C_l}{\Delta \beta}$, per deg

C_m pitching-moment coefficient, $\frac{\text{Pitching moment}}{qS\bar{c}}$

$C_{m_{C_L}}$ static longitudinal stability parameter, $\frac{\partial C_m}{\partial C_L}$

C_n yawing-moment coefficient, $\frac{\text{Yawing moment}}{qSb}$

C_{n_β} static directional stability parameter, $\frac{\Delta C_n}{\Delta \beta}$, per deg

C_Y side-force coefficient, $\frac{\text{Side force}}{qS}$

C_{Y_β} side-force parameter, $\frac{\Delta C_Y}{\Delta \beta}$, per deg

$(L/D)_{max}$ maximum lift-drag ratio

M Mach number

q free-stream dynamic pressure

S wing area

α angle of attack of fuselage center line, deg

β angle of sideslip of fuselage center line, deg

δ_h deflection of horizontal tail, positive when trailing edge is down, deg

δ_v deflection of vertical tail, positive when trailing edge is to left, deg

Subscripts:

L left horizontal tail

R right horizontal tail

Model components:

B_{11} modified fuselage

H_9 horizontal tail

T_{11} externally mounted fuel tanks

T_{12} helium tank located behind the upper vertical tail

V_L lower vertical tail

V_{L_7} lower vertical tail: 10° single-wedge airfoil, quarter-chord line swept back 23.41°, aspect ratio of 0.412, taper ratio of 0.784

V_{L_8} lower vertical tail: identical with V_{L_7} without jettisonable portion of tail, aspect ratio of 0.143, taper ratio of 0.917

V_{L_9} lower vertical tail: identical with V_{L_7} with span decreased by approximately one-third

V_U upper vertical tail

V_{U_5} upper vertical tail: 10° single-wedge airfoil, quarter-chord line swept back 23.41°, aspect ratio of 0.5158, taper ratio of 0.741

V_{U_6} upper vertical tail: identical with V_{U_5} with a span increase of 1.07 inches (2.718 cm)

W_2 wing

X_{16} modified side fairings

APPARATUS AND METHODS

Model

The 0.0667-scale model of the X-15 research airplane used during the investigation of reference 1 has been altered to simulate the proposed modified configuration used in the present investigation (see fig. 1). The modifications made to the airplane consist of an increase in fuselage length, the addition of two fuel tanks attached to either side of the fuselage just below the wing, and an extension of the fuselage side fairing to approximately the base of the fuselage to house hydrogen peroxide tanks used by the auxiliary power units. A spherical helium tank has also been added just behind the upper vertical tail to be used to maintain adequate fuel pressure with the increase in fuel supply. (See fig. 1(c).) A photograph of the model is presented as figure 2.

The basic vertical-tail configuration $V_{U_5}V_{L_7}$ used in this investigation is the same as that of reference 1. This component was altered during this investigation by varying the height of both the upper and lower vertical tail. Additional information is given in figure 1(b) and in table I. The speed brakes, deflected at 35°, are the same as those used in reference 1.

The code designation for the basic configuration is $B_{11}X_{16}W_2H_9T_{12}V_{U5}V_{L7}$ and with externally mounted fuel tanks installed is $B_{11}X_{16}W_2H_9T_{12}V_{U5}V_{L7}T_{11}$. All data presented were obtained for the basic configuration unless otherwise noted.

Test Facility

The results of the present investigation obtained at subsonic and transonic speeds, covering the Mach number range from 0.60 to 1.20 at stagnation pressures of 1.00 and 0.85 atmospheres $\left(1.01 \times 10^5 \text{ and } 0.86 \times 10^5 \text{ N/m}^2\right)$, respectively, were obtained in the Langley 8-foot transonic pressure tunnel which is capable of continuous operation throughout the transonic speed range.

Measurements and Corrections

Measurements of forces and moments were obtained from a six-component, electrical strain-gage balance internally mounted and sting supported. These measurements, considered free of any appreciable effects from wall shock reflections, are presented in coefficient form based on the total wing area, span, and mean geometric chord.

The static pressures at the base of the model and in the balance chamber were measured by pressure transducers. These measurements were used to adjust the force and moment results to the condition of free-stream static pressure at the base of the fuselage.

The measured angle of attack has been corrected for tunnel flow angularity and sting and balance deflections and is estimated to be accurate within $\pm 0.10^\circ$.

PRESENTATION OF RESULTS

The results of the present investigation are presented in the following order:

	Figure
Longitudinal aerodynamic characteristics:	
Effect of horizontal-tail deflection. $\beta = 0^\circ$	3
Effect of externally mounted fuel tanks. $\beta = 0^\circ$	4
Effect of speed brakes. Configuration $V_{U5}V_{L8}$; $\beta = 0^\circ$	5
Lateral aerodynamic characteristics:	
Effect of horizontal-tail differential deflection. $\beta = 0^\circ$	6
Effect of externally mounted fuel tanks. $\beta = 0^\circ$ and 4°	7
Effect of right externally mounted fuel tank. $\beta = 0^\circ$ and 4°	8
Variation with angle of attack of lateral stability derivatives for externally mounted fuel tanks	9

Figure

Effect of speed brakes. $\beta = 0^{\circ}$ 10
Effect of vertical-tail size. $\beta = 0^{\circ}$ and 4° 11
Variation with angle of attack of lateral stability derivatives for various vertical-tail configurations 12
Effect of vertical-tail deflection. $\beta = 0^{\circ}$; $\delta_h = 0^{\circ}$ 13

Analysis:
Variation with Mach number of longitudinal stability parameter for speed brakes and externally mounted fuel tanks. Control surfaces undeflected 14
Variation with Mach number of lift-curve slope for speed brakes and externally mounted fuel tanks. Control surfaces undeflected 15
Variation with Mach number of $C_{L,(L/D)_{max}}$, $(L/D)_{max}$, and $C_{D,o}$ for speed brakes and externally mounted fuel tanks. Control surfaces undeflected 16
Variation with Mach number of lateral stability derivatives for various vertical-tail configurations. $\delta_h = 0^{\circ}$ 17
Variation with Mach number of lateral stability derivatives for externally mounted fuel tanks 18

DISCUSSION

A brief discussion is given of the comparison of the results of this investigation with the results found in reference 1. The effect of externally mounted fuel tanks, the changes in vertical-tail size, and the effect of speed brakes are discussed. No data were obtained at a Mach number of 0.90 during this investigation; therefore, the trends found in reference 1 were used in fairing the data presented in the analysis figures at this Mach number.

Longitudinal Stability Characteristics

The static longitudinal stability parameter for both the basic configuration of the present investigation and for the basic configuration of reference 1 are shown in figure 14. A comparison of the results of the two basic configurations, without the externally mounted fuel tanks, indicates a reduction in the stability at the higher lift coefficients for the configuration of this investigation throughout the Mach number range. This loss in stability could possibly be attributed to a forward shift in center of lift as a result of the extended fuselage of the configuration. The stability level was further reduced by the speed brakes as it was in reference 1.

The addition of the externally mounted fuel tanks had a substantial destabilizing effect on the basic configuration of this investigation. At zero lift, the tanks-on configuration was longitudinally unstable up to a Mach number of approximately 1.10. At the higher lift coefficients, the configuration was stable although the static margin was reduced to approximately one-half that of the basic configuration throughout the Mach number range.

Maximum Lift-Drag Ratio

The maximum lift-drag ratio $(L/D)_{max}$, the lift coefficient at maximum lift-drag ratio $C_{L,(L/D)_{max}}$, and the drag coefficient at zero lift $C_{D,o}$ of the basic configuration, with and without speed brakes and externally mounted fuel tanks, are shown in figure 16 with some corresponding values from reference 1. There was a small increase in $(L/D)_{max}$ and $C_{L,(L/D)_{max}}$ of the basic configuration compared with the results of reference 1 up to a Mach number of 1.15. The results with the speed brakes were approximately the same for both of the basic configurations throughout the Mach number range.

The addition of the externally mounted fuel tanks resulted in a decrease in the maximum lift-drag ratio of approximately 1.0 throughout the Mach number range.

Lateral Stability Characteristics

Tests were conducted at sideslip angles of 0^o and 4^o with a horizontal-tail deflection of 0^o. The lateral stability derivatives obtained from these data for the basic model and for the basic model with the four alternate vertical-tail configurations are shown in figure 17.

The directional stability level of the basic configuration (vertical tail $V_{U5}V_{L7}$) was essentially the same as that of reference 1 at the lower angle of attack (0^o); however, there was a decided decrease in stability at the higher angle of attack (16^o) throughout the Mach number range (fig. 17(a)).

The various changes in vertical-tail size (fig. 17(a)) indicate the effect of aspect ratio on the directional stability. The loss in stability resulting from the change from $V_{U5}V_{L7}$, the basic vertical-tail configuration, to $V_{U5}V_{L8}$ is recovered by an extension to the upper vertical tail, $V_{U6}V_{L8}$, although the area added to the upper vertical tail is less than one-half that removed from the lower tail. (See fig. 1(b) and table I.)

The effective dihedral of the basic configuration (fig. 17(b)) was generally similar to that of reference 1 throughout the Mach number range at an angle of attack of 0^o. At the higher angle of attack, however, there was an increase in effective dihedral except for some decrease in effective dihedral between Mach numbers of 0.75 and 0.95. The results

obtained with the four additional vertical-tail configurations show that the upper-vertical-tail extension, $V_{U6}V_{L8}$, was very effective throughout the Mach number and angle-of-attack range as it was directionally.

The addition of the externally mounted fuel tanks resulted in a reduction in the longitudinal and directional stability such that the configuration was longitudinally unstable at zero lift below a Mach number of 1.10 and directionally unstable or neutrally stable at a higher angle of attack of 16°. The effective dihedral was increased by the addition of the tanks except for an angle of attack of 16° at Mach numbers ranging from 0.60 to 0.90.

CONCLUDING REMARKS

Results of an investigation to determine the effects of modifications made to the X-15 research airplane on the static stability and control characteristics throughout the transonic speed range indicate that the static longitudinal, directional, and lateral stability of the modified configuration, less the externally mounted fuel tanks, was reduced under lifting conditions throughout the Mach number range. There was, however, an increase in the effective dihedral at Mach numbers below 0.75 and above 0.95 compared with the X-15 model.

The addition of the externally mounted fuel tanks resulted in a reduction in the longitudinal and directional stability; thus the configuration was longitudinally unstable at zero lift below a Mach number of 1.10 and directionally unstable or neutrally stable at a higher angle of attack of 16°. The effective dihedral was increased by the addition of the tanks except for an angle of attack of 16° at Mach numbers ranging from 0.60 to 0.90.

Langley Research Center,
National Aeronautics and Space Administration,
Langley Station, Hampton, Va., October 11, 1965.

REFERENCES

1. Osborne, Robert S.: Stability and Control Characteristics of a 0.0667-Scale Model of the Final Version of the North American X-15 Research Airplane (Configuration 3) at Transonic Speeds. NASA TM X-758, 1963.

2. Mechtly, E. A.: The International System of Units – Physical Constants and Conversion Factors. NASA SP-7012, 1964.

TABLE I.- DIMENSIONS OF 0.0667-SCALE MODEL OF THE X-15A-2 RESEARCH AIRPLANE

Wing:				
Airfoil section	Modified NACA 66-005			
Total area	127.728 in^2	(824.050 cm^2)		
Exposed area	66.816 in^2	(431.070 cm^2)		
Total span	17.89 in.	(45.441 cm)		
Exposed span	12.02 in.	(30.531 cm)		
Total aspect ratio	2.50			
Exposed aspect ratio	2.15			
Leading-edge sweepback	36.75°			
Quarter-chord-line sweepback	25.64°			
Trailing-edge sweepforward	17.75°			
Root chord at center line	11.914 in.	(30.262 cm)		
Exposed root chord	8.8 in.	(22.352 cm)		
Tip chord	2.38 in.	(6.045 cm)		
Total taper ratio	0.20			
Exposed taper ratio	0.27			
Mean geometric chord based on total area	8.22 in.	(20.879 cm)		
Longitudinal distance from fuselage nose to 20-percent wing mean geometric chord	24.69 in.	(62.713 cm)		
Dihedral	0°			
Incidence	0°			
Horizontal tail (in plane of surface):				
Airfoil section	Modified NACA 66-005			
Total area	73.850 in^2	(476.451 cm^2)		
Exposed area	32.832 in^2	(211.819 cm^2)		
Total span	14.978 in.	(38.044 cm)		
Exposed span	9.008 in.	(22.880 cm)		
Exposed aspect ratio	2.48			
Leading-edge sweepback	50.58°			
Quarter-chord-line sweepback	45°			
Trailing-edge sweepback	19.28°			
Root chord at center line	8.175 in.	(20.765 cm)		
Exposed root chord	5.6 in.	(14.224 cm)		
Tip chord	1.686 in.	(4.282 cm)		
Mean geometric chord based on exposed area	3.986 in.	(10.124 cm)		
Dihedral	-15°			
		V_{U_5}		V_{U_6}
Upper vertical tail (exposed panel):				
Airfoil section (wedge)		10°		10°
Area		26.09 in^2 (168.322 cm^2)		32.252 in^2 (208.077 cm^2)
Span		3.67 in. (9.322 cm)		4.743 in. (12.047 cm)
Aspect ratio		0.52		0.70
Taper ratio		0.74		0.664
Leading-edge seeepback		30°		30°
Trailing-edge sweepback		0°		0°
Mean geometric chord		7.11 in. (18.059 cm)		6.80 in. (17.272 cm)
Movable portion –				
Area		16.79 in^2 (108.322 cm^2)		22.93 in^2 (147.935 cm^2)
Span		2.48 in. (6.299 cm)		3.55 in. (9.017 cm)
Root chord		7.49		7.49
Tip chord		6.05		5.43
	V_{L_7}		V_{L_8}	V_{L_9}
Lower vertical tail (exposed panel):				
Airfoil section (wedge)	10°		10°	10°
Area	21.93 in^2 (141.484 cm^2)		9.3 in^2 (60.000 cm^2)	15.90 in^2 (102.580 cm^2)
Mean span	3.01 in. (7.645 cm)		1.19 in. (3.023 cm)	2.10 in. (5.334 cm)
Aspect ratio	0.412		0.143	0.277
Taper ratio	0.784		0.917	0.85
Mean geometric chord	7.285		7.83	7.56
Leading-edge sweepback	30°		30°	30°
Trailing-edge sweepback	0°		0°	0°
Movable portion –				
Area	12.63 in^2 (81.484 cm^2)			6.57 in^2 (42.387 cm^2)
Mean span	1.82 in. (4.623 cm)			0.91 in. (2.311 cm)
Root chord	7.49 in. (19.025 cm)			7.49 in. (19.025 cm)
Tip chord	6.40 in. (16.256 cm)			6.95 in. (17.653 cm)
Fuselage:				
Length	41.29 in. (104.877 cm)			
Maximum depth	3.733 in. (9.482 cm)			
Maximum width with side fairings	5.868 in. (14.905 cm)			
Maximum width without side fairings	3.733 in. (9.482 cm)			
Fineness ratio without side fairings	11.06			
Base diameter	3.197 in. (8.120 cm)			
Speed brake (one side):				
Area	3.514 in^2 (22.671 cm^2)			
Chord	2.678 in. (6.802 cm)			
Average span	1.306 in. (3.322 cm)			

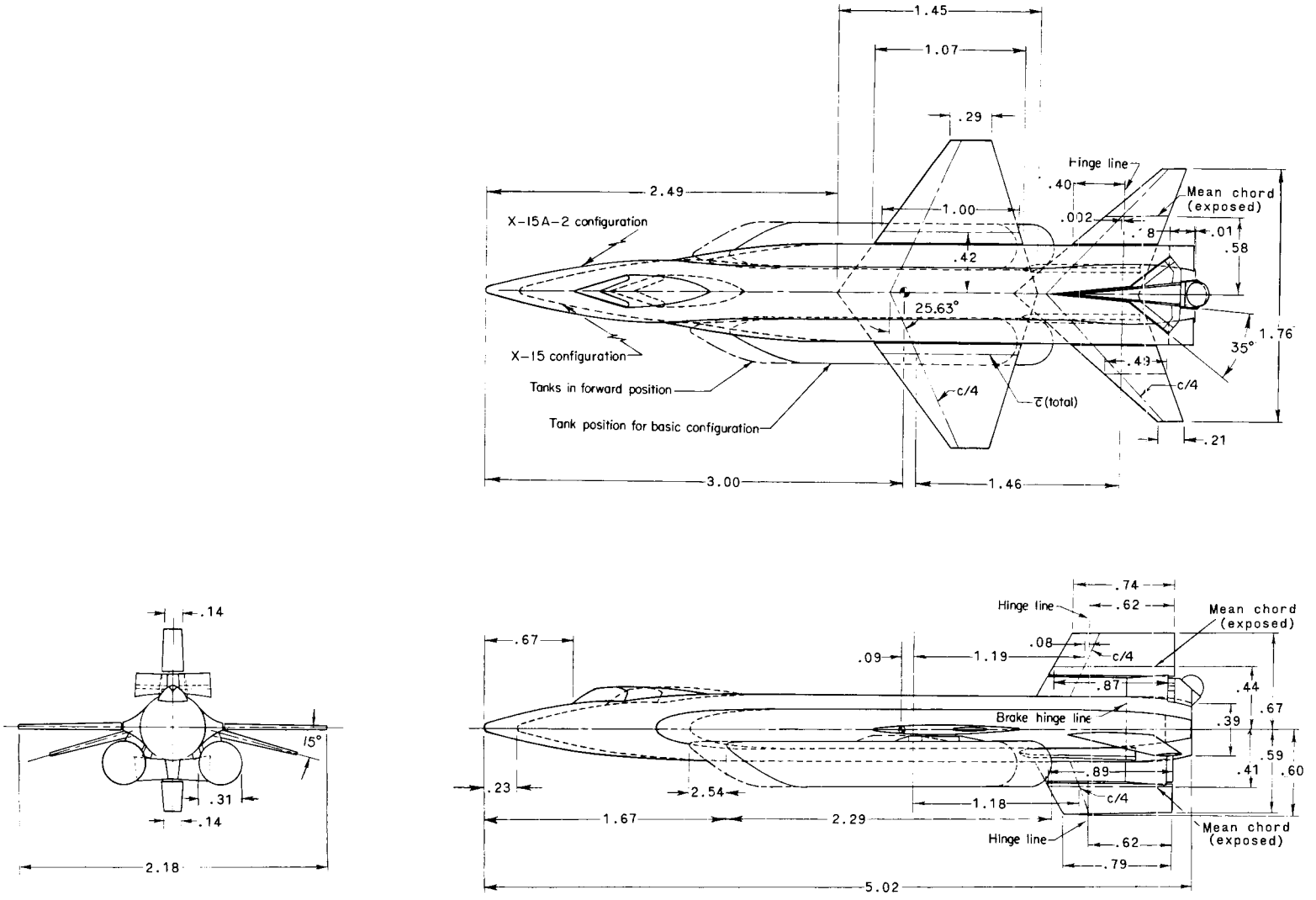

(a) Details of 0.0667-scale model of X-15A-2 and X-15 research airplanes.

Figure 1.- Drawing of modified and original X-15 research airplane. All dimensions have been nondimensionalized by using wing-mean-geometric-chord length of 8.22 inches (20.88 cm) as a reference.

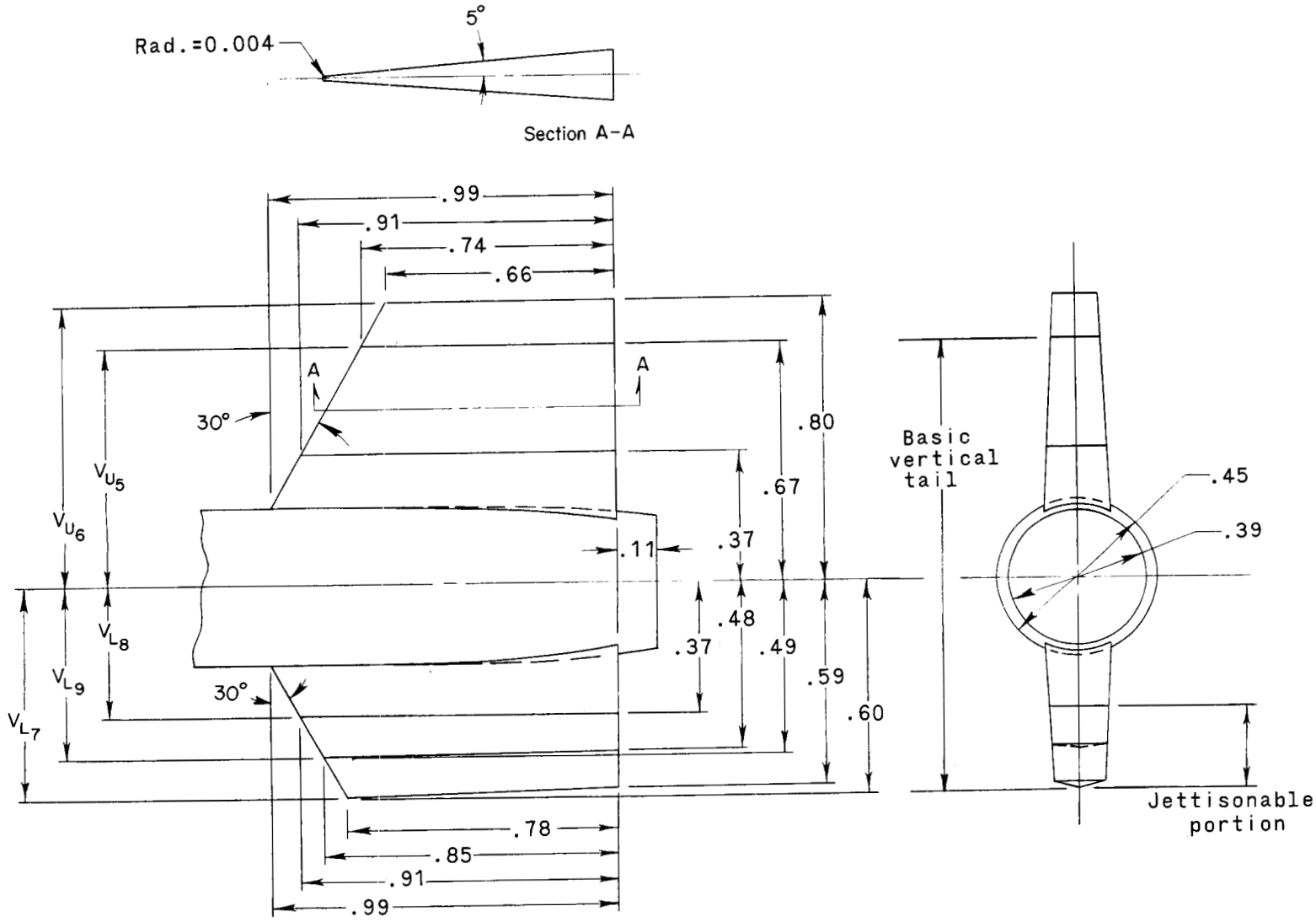

(b) Details of vertical tail.

Figure 1.- Continued.

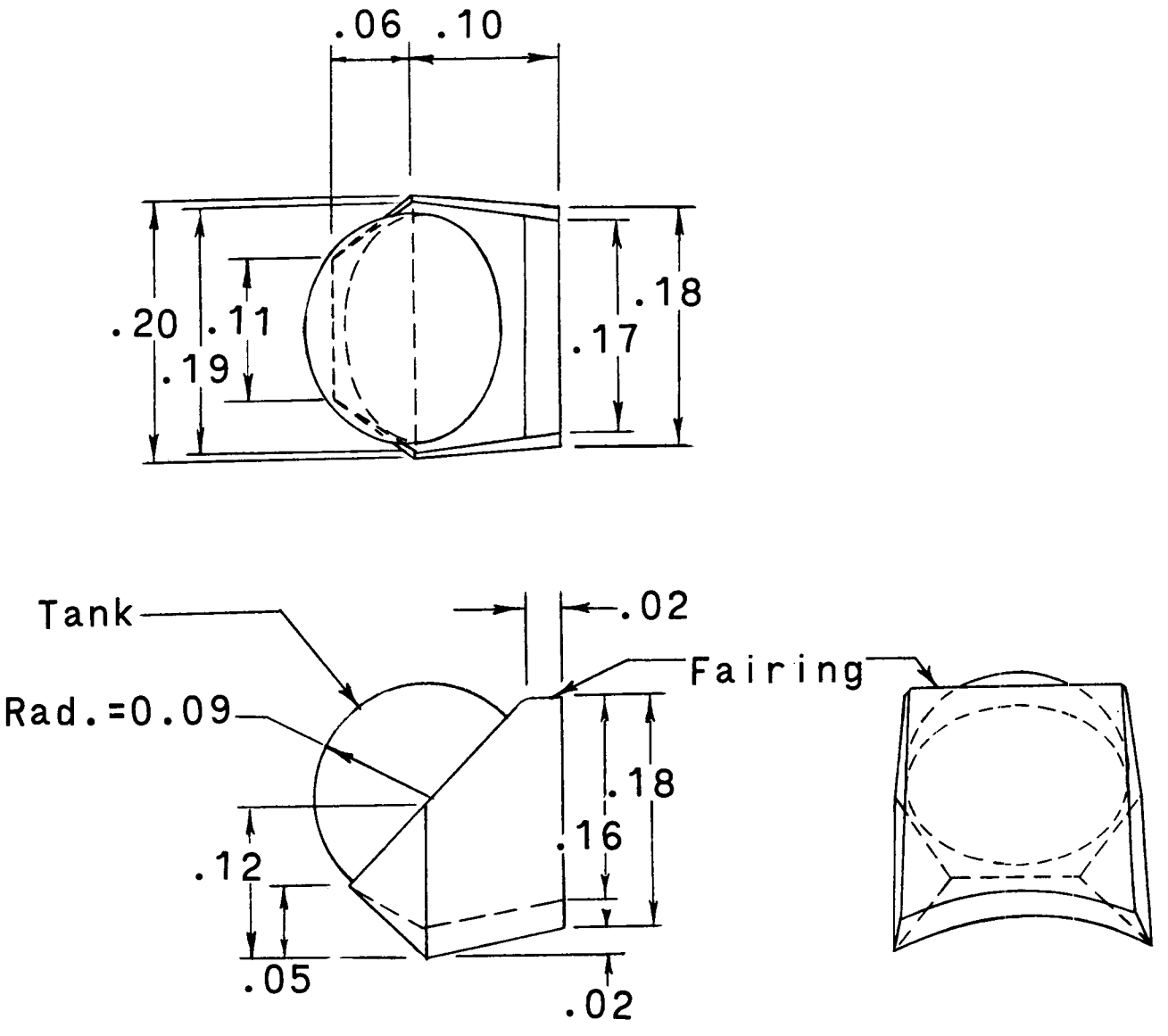

(c) Details of helium-tank installation.

Figure 1.- Concluded.

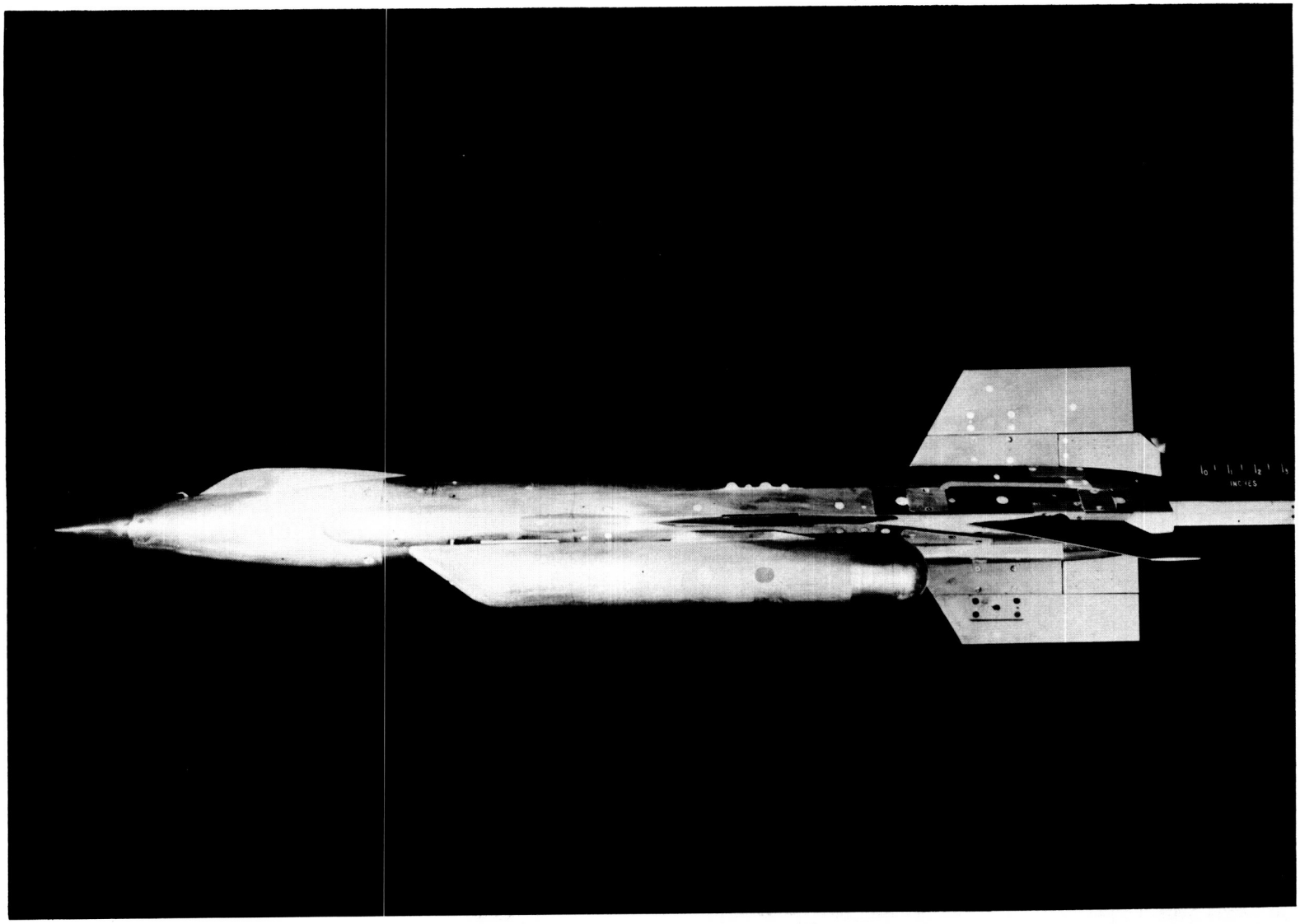

Figure 2.- Photograph of 0.0667-scale model of the X-15A-2.

L-64-5548

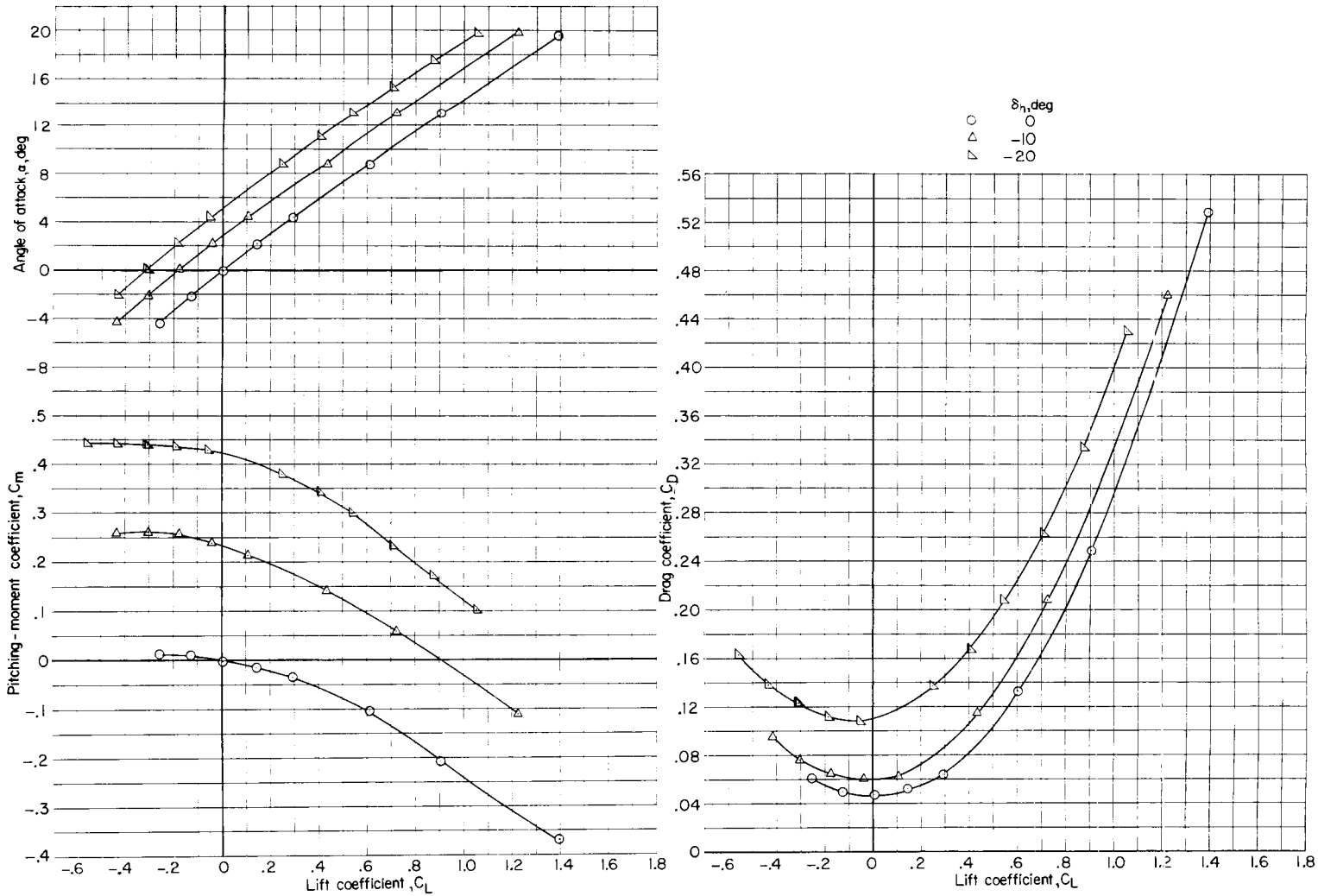

(a) M = 0.60.

Figure 3.- Effect of horizontal-tail deflection on longitudinal aerodynamic characteristics of the basic configuration. $\beta = 0^0$.

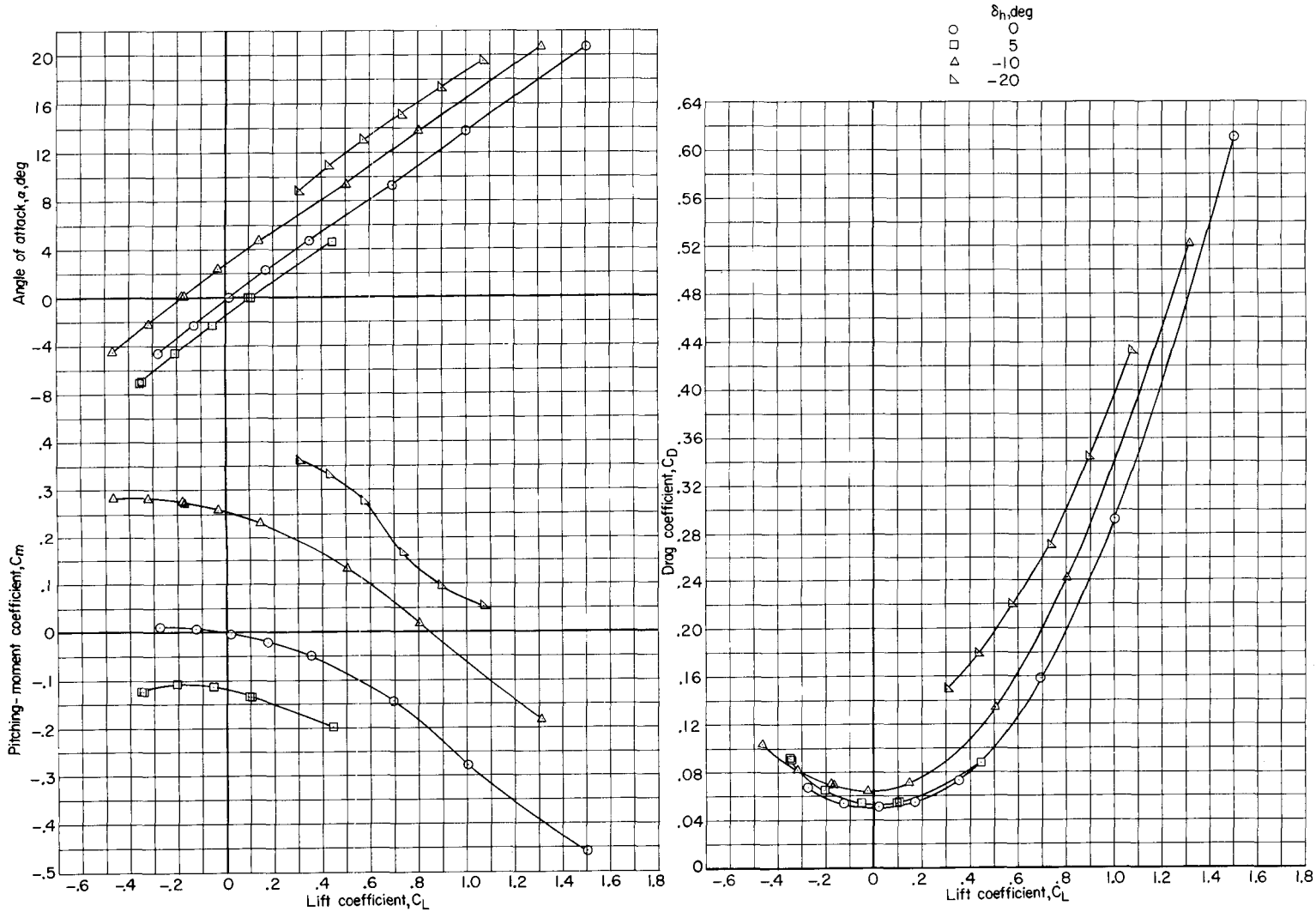

(b) M = 0.80.

Figure 3.- Continued.

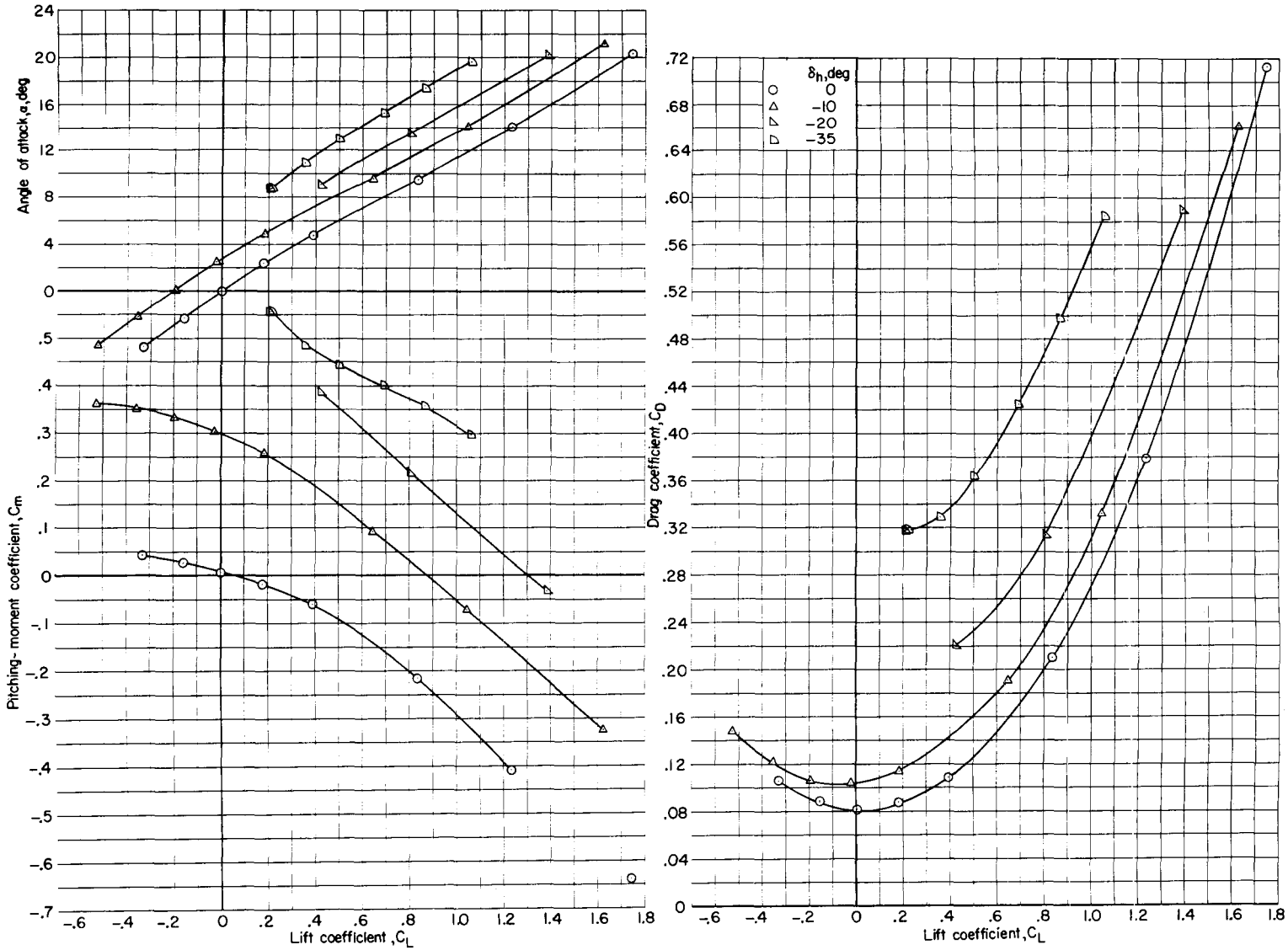

(c) M = 1.00.

Figure 3.- Continued.

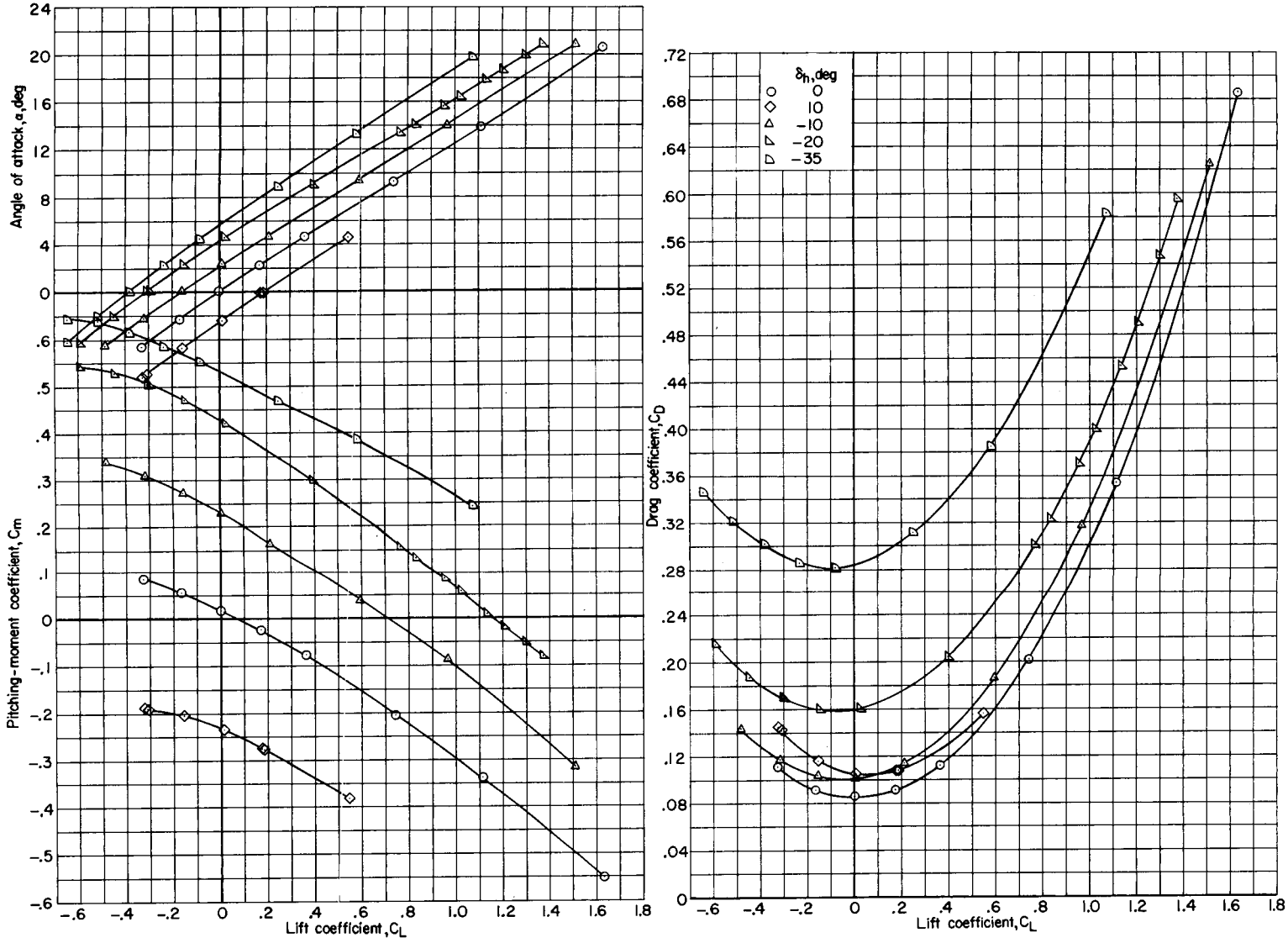

(d) M = 1.20.

Figure 3.- Concluded.

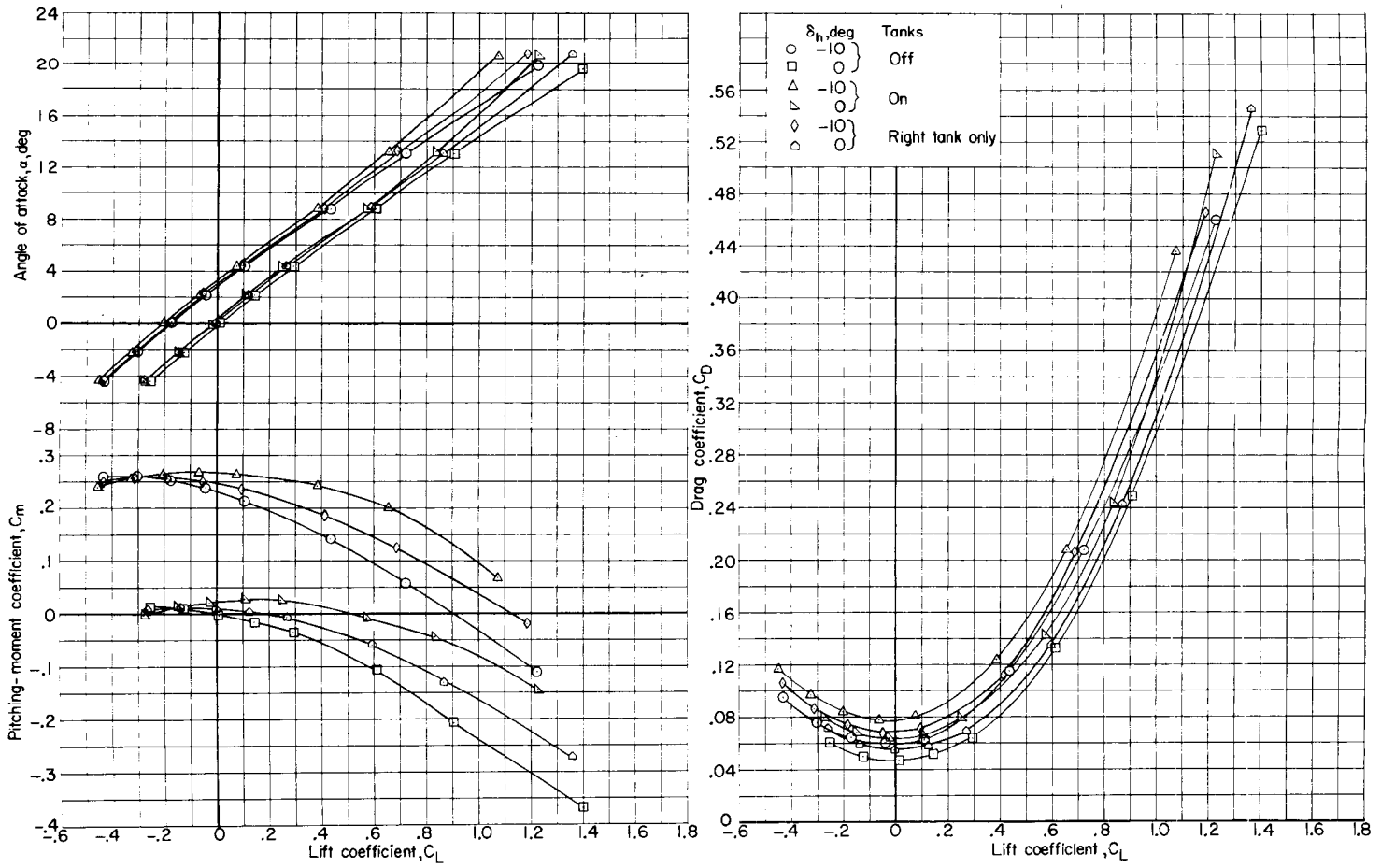

(a) M = 0.60.

Figure 4.- Effect of externally mounted fuel tanks on longitudinal aerodynamic characteristics of the basic configuration. $\beta = 0^0$.

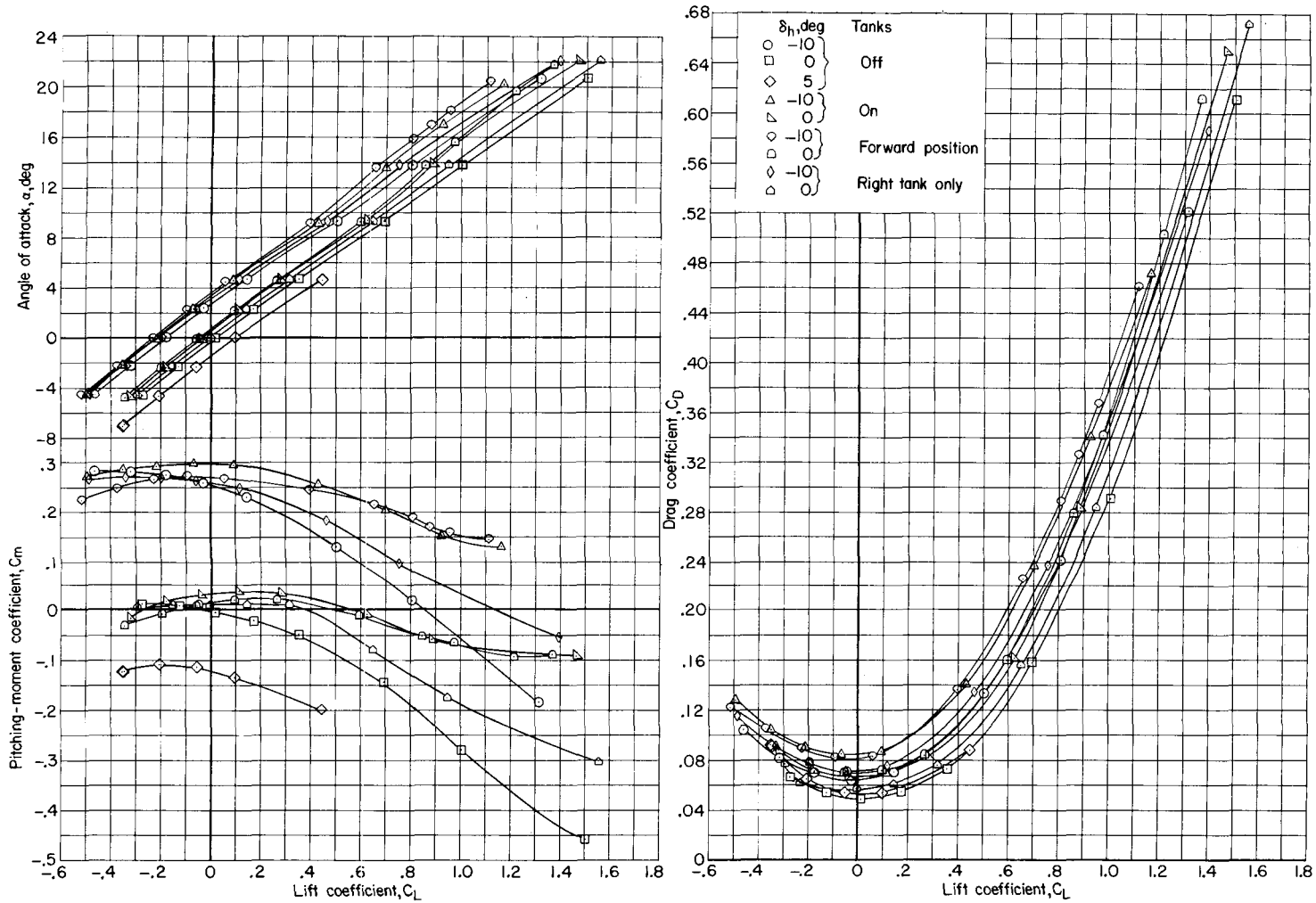

(b) M = 0.80.

Figure 4.- Continued.

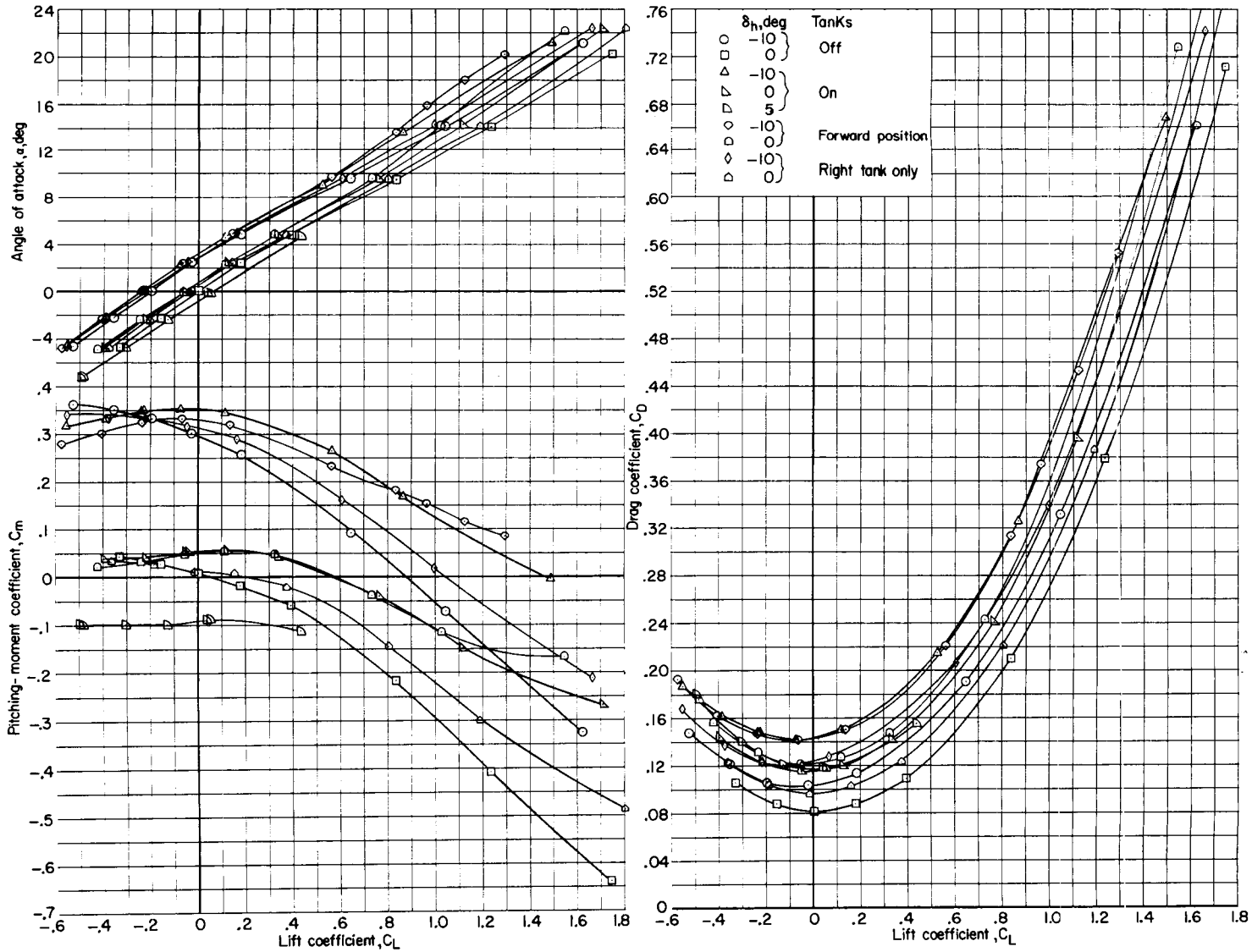

(c) M = 1.00.

Figure 4.- Continued.

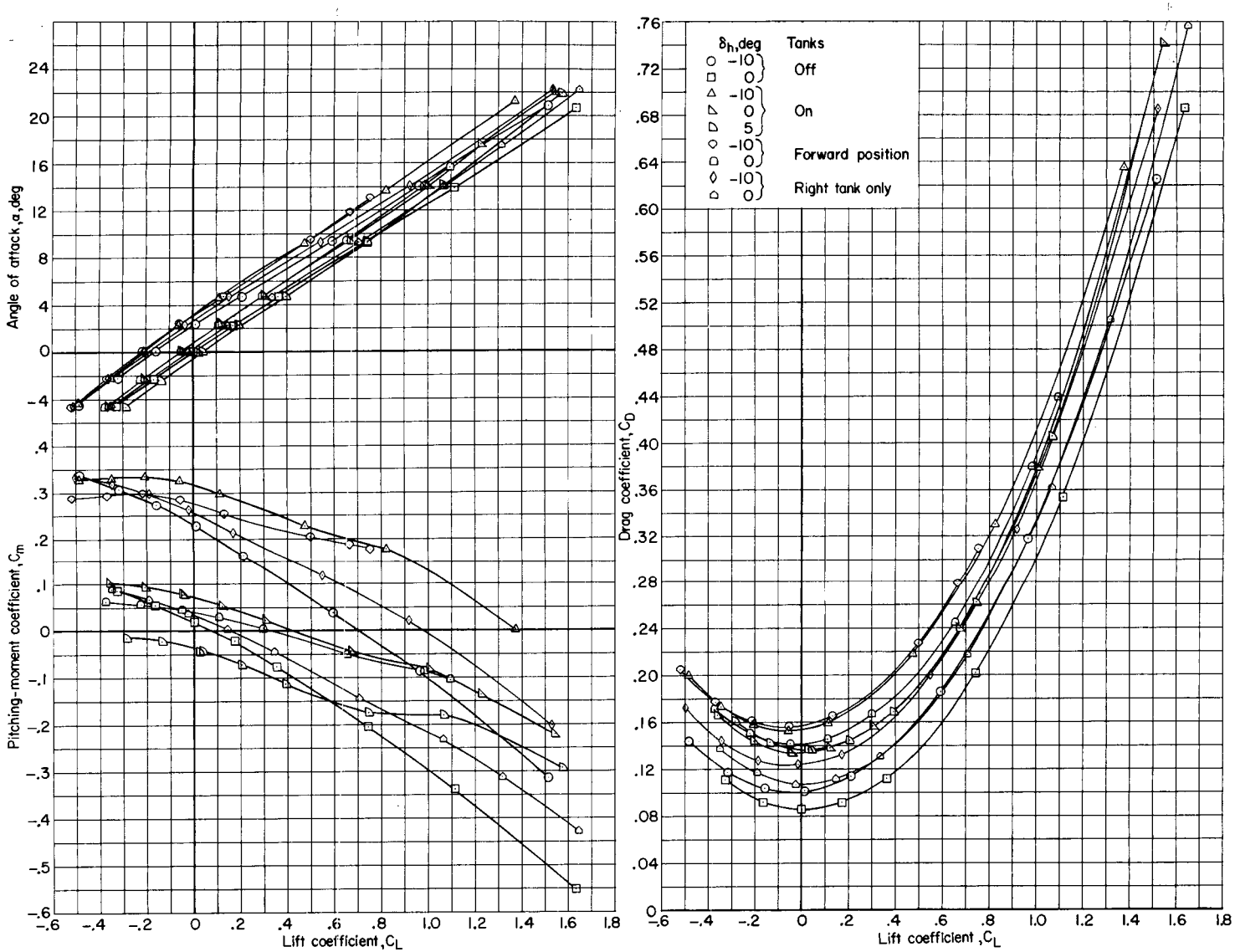

(d) M = 1.20.

Figure 4.- Concluded.

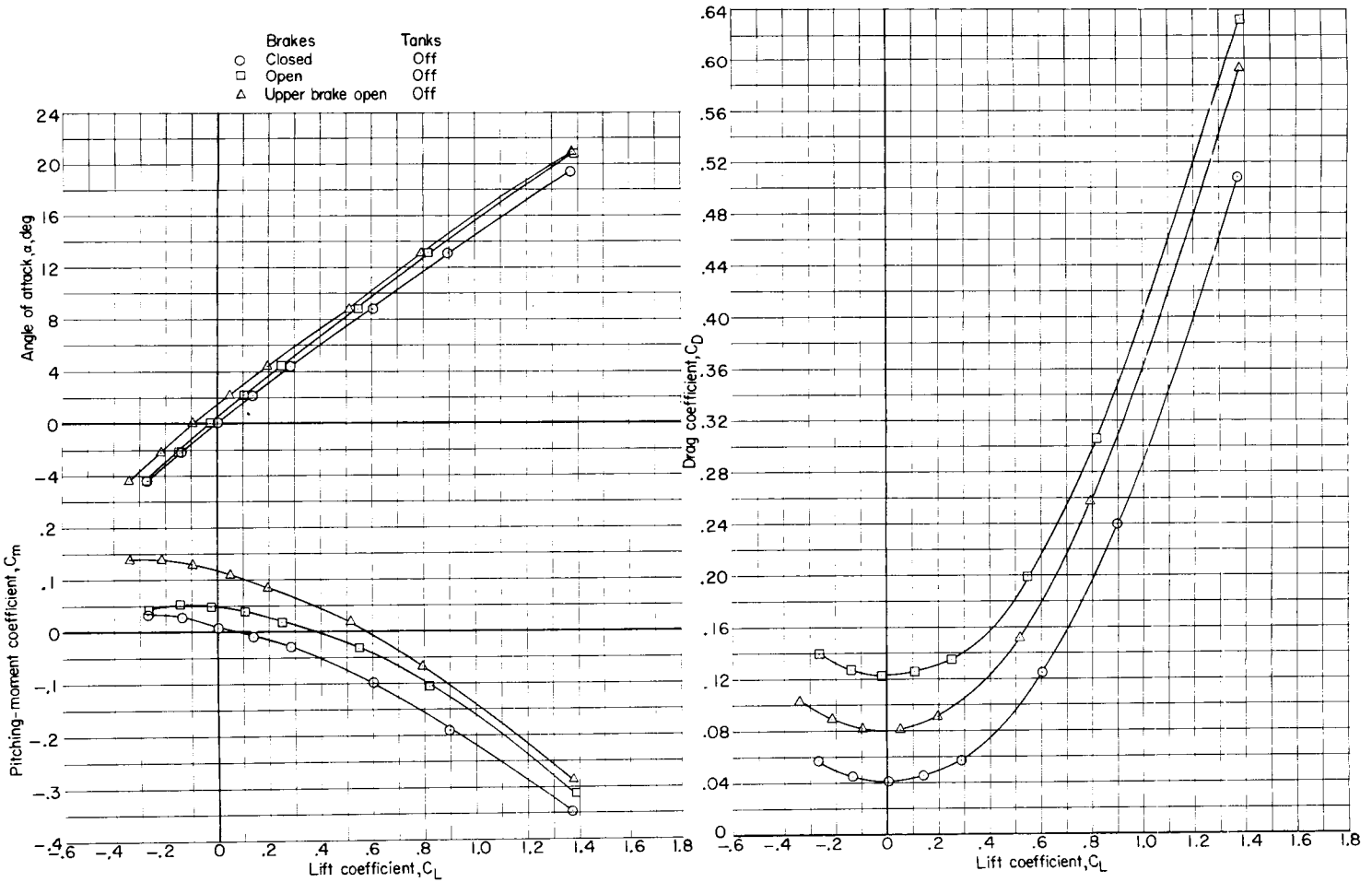

(a) M = 0.60.

Figure 5.- Effect of speed brakes on longitudinal aerodynamic characteristics. Vertical-tail configuration $V_{U5}V_{L8}$; $\beta = 0^{o}$.

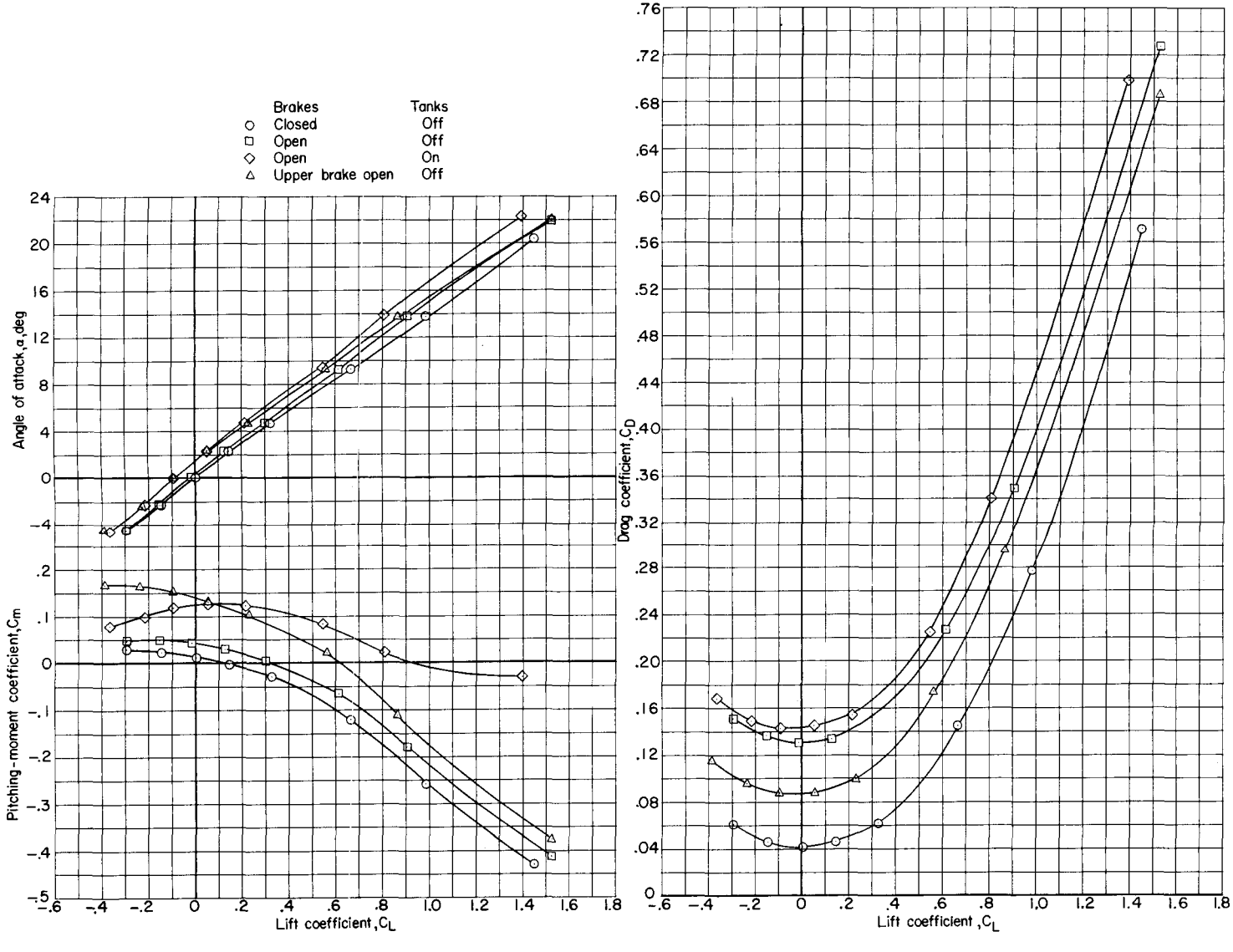

(b) M = 0.80.

Figure 5.- Continued.

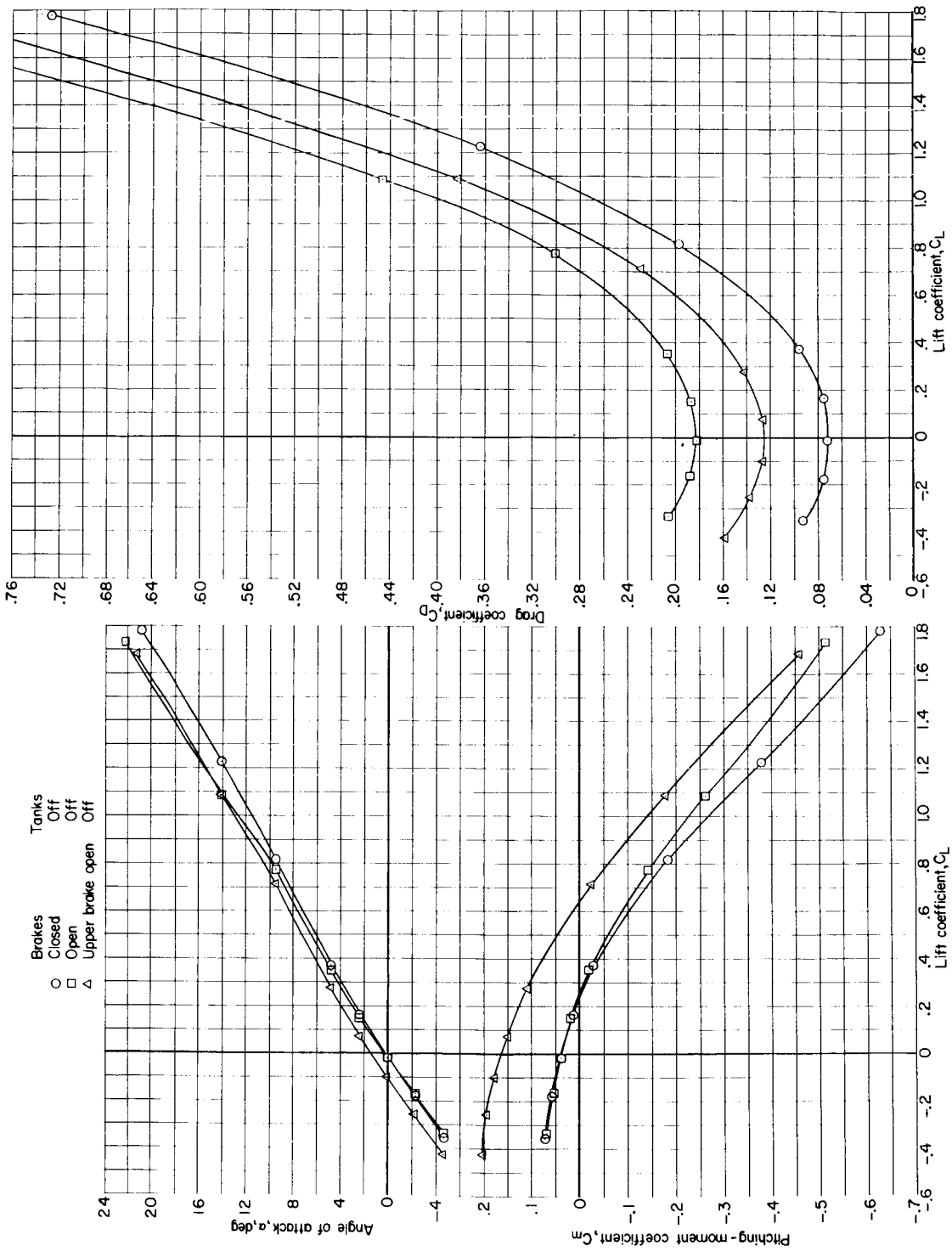

(c) M = 1.00.

Figure 5.- Continued.

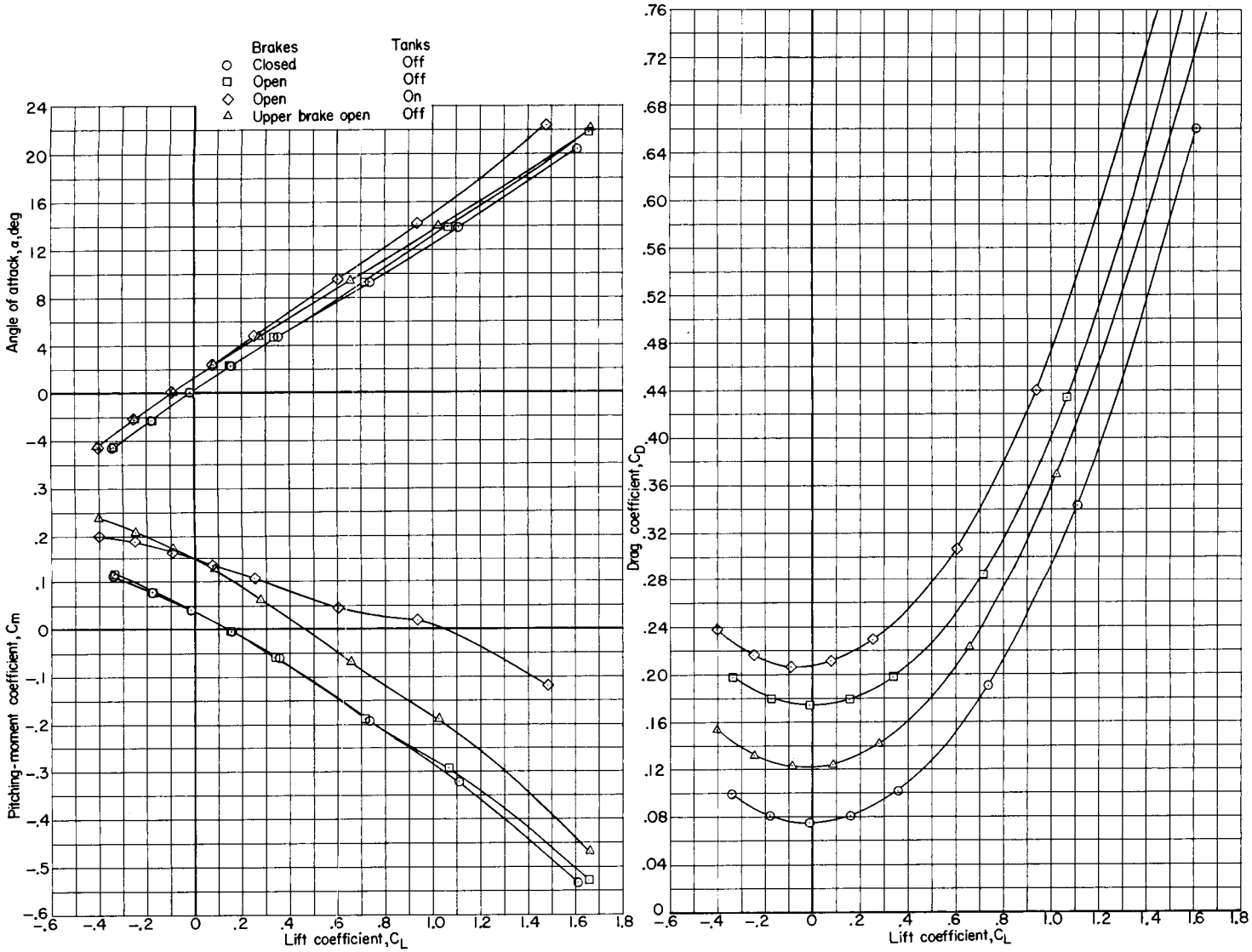

(d) M = 1.20.

Figure 5.- Concluded.

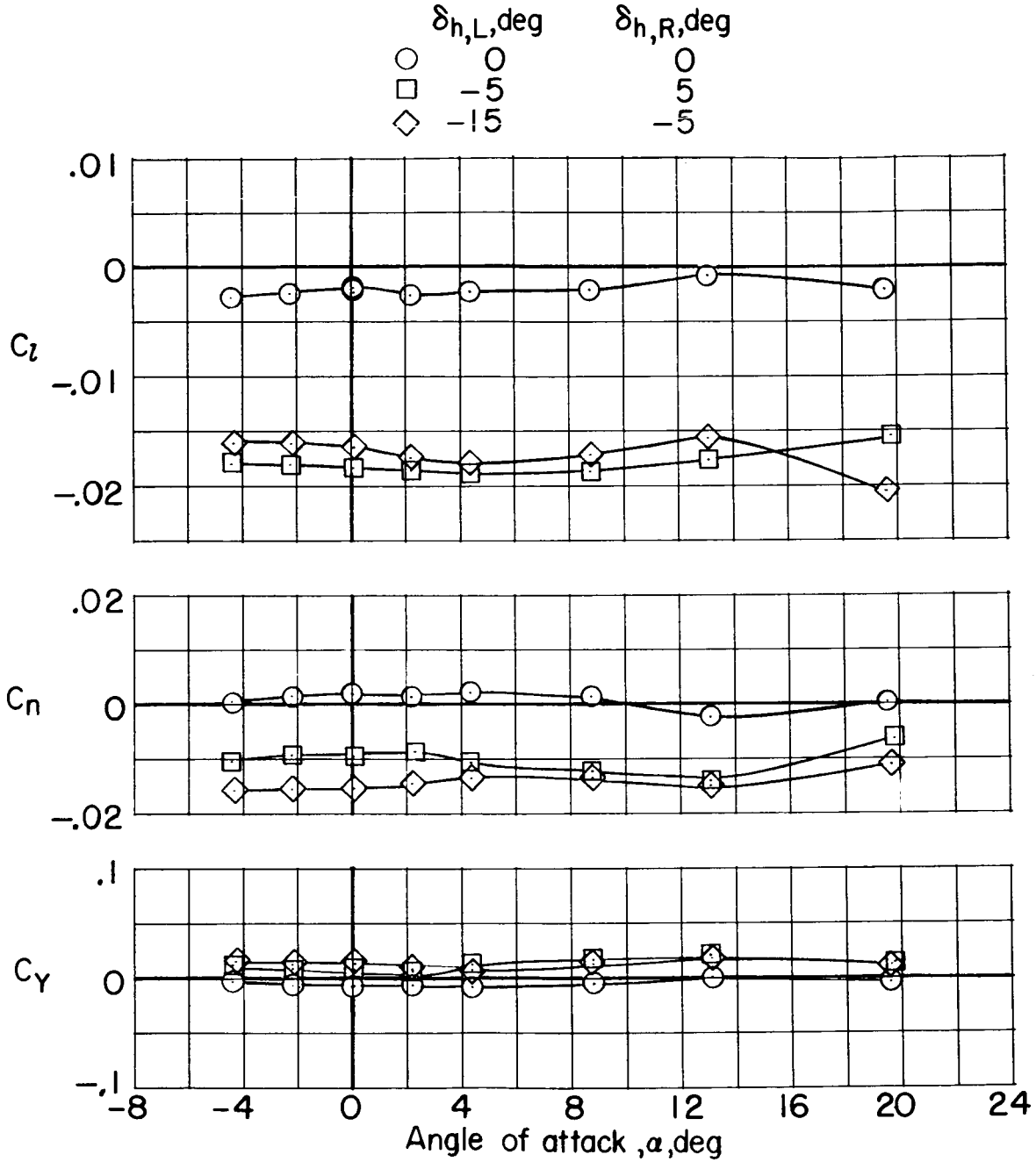

(a) M = 0.60.

Figure 6.- Effect of horizontal-tail differential deflection on lateral aerodynamic characteristics of the basic configuration. $\beta = 0^{o}$.

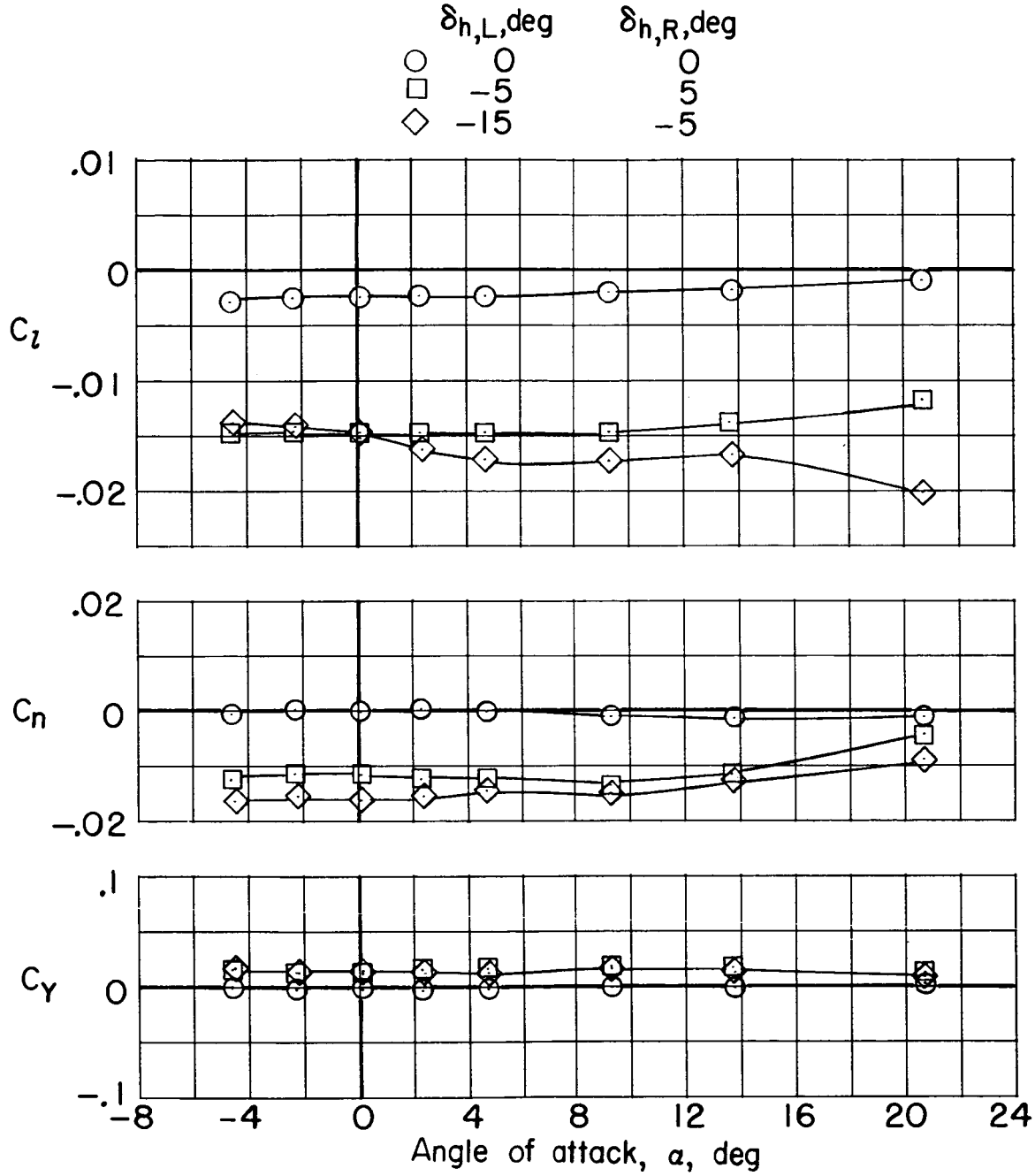

(b) M = 0.80.

Figure 6.- Continued.

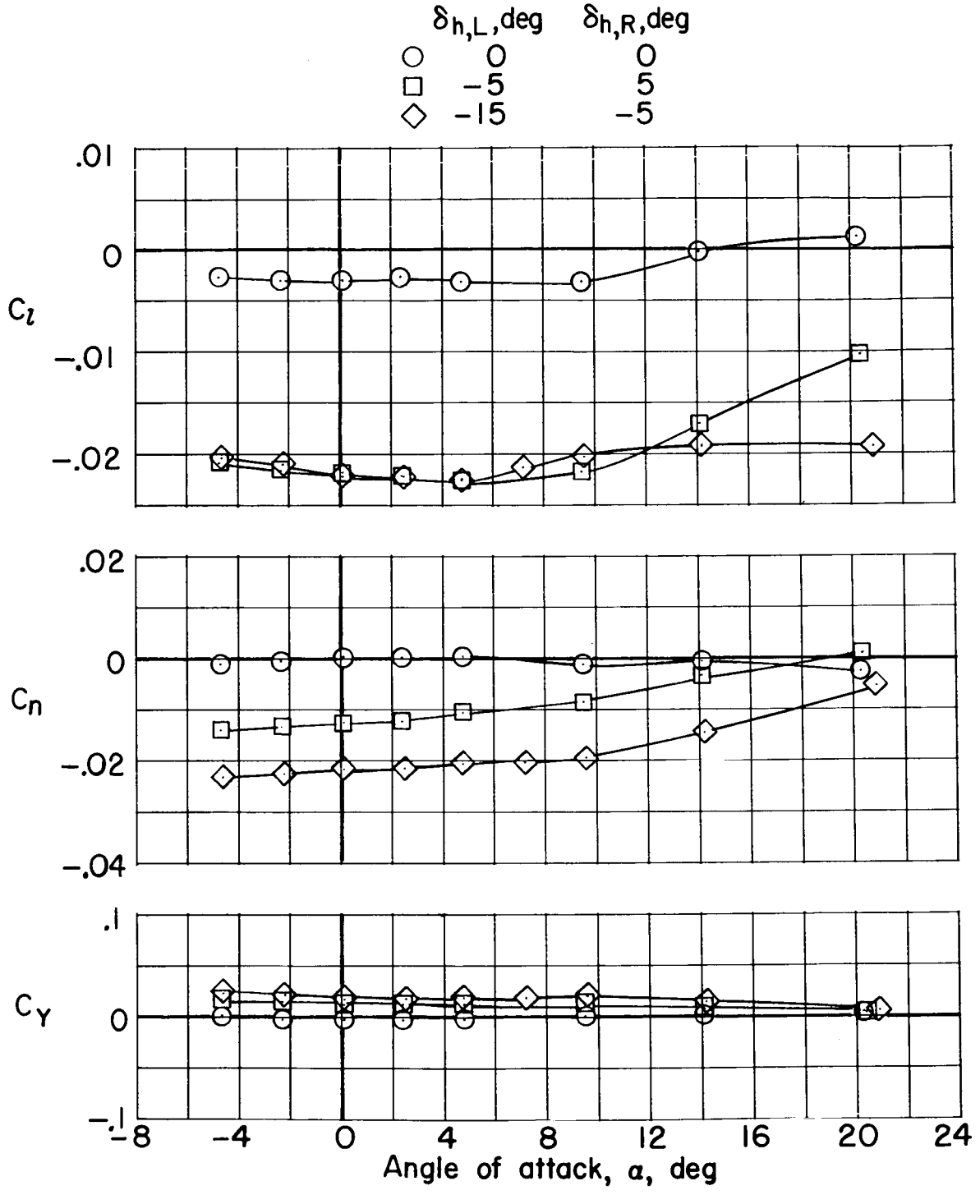

(c) M = 1.00.

Figure 6.- Continued.

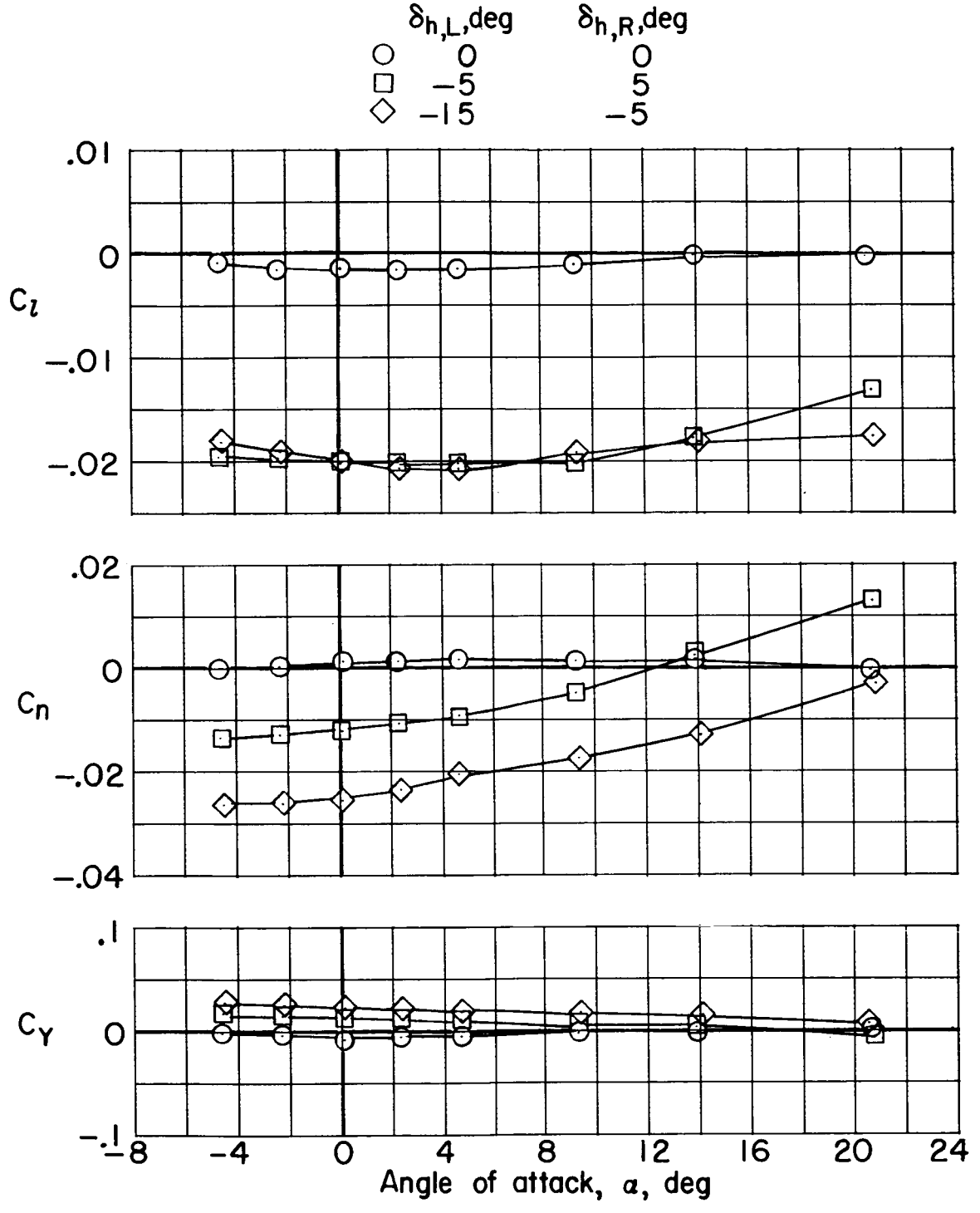

(d) M = 1.20.

Figure 6.- Concluded.

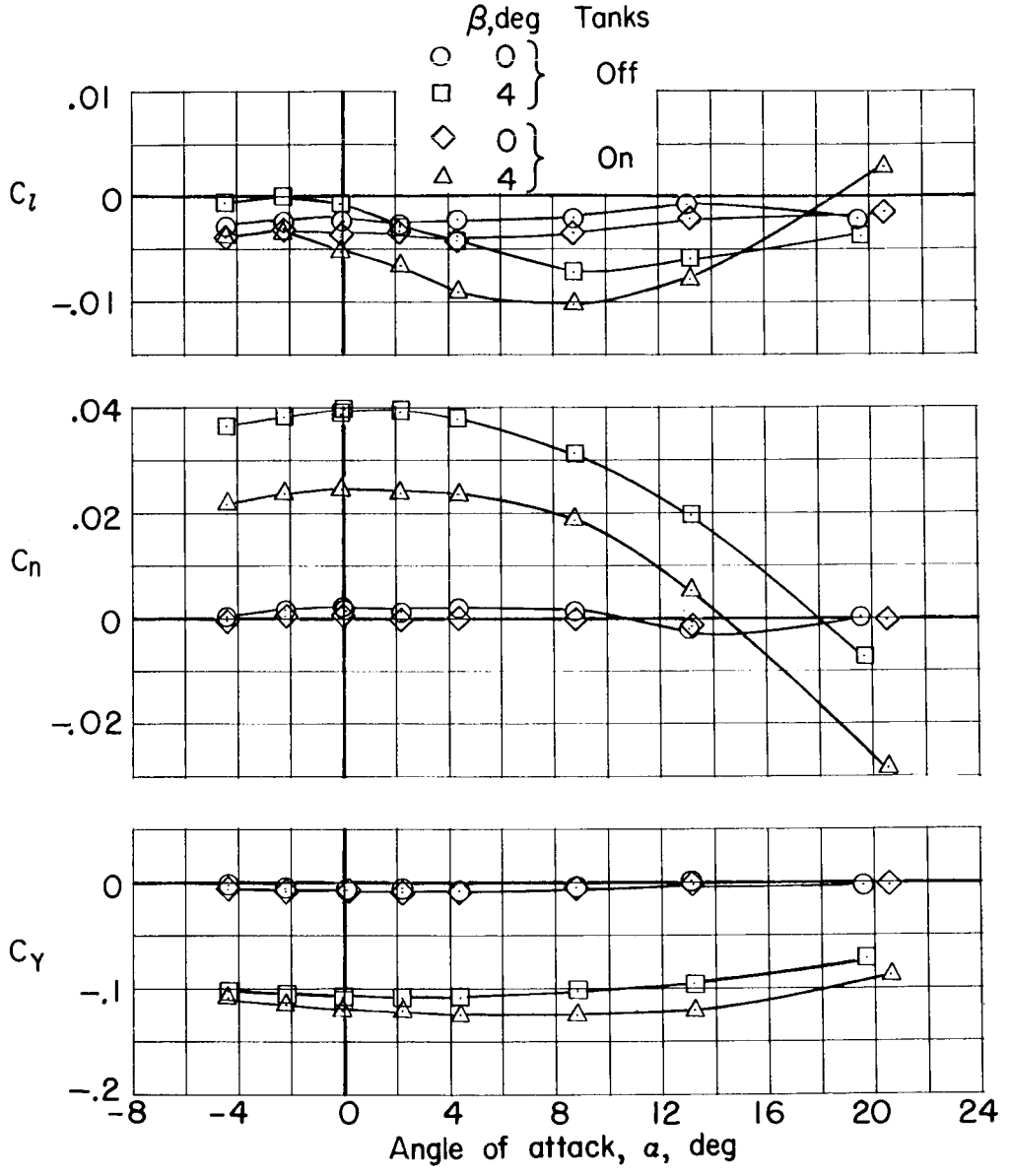

(a) M = 0.60.

Figure 7.- Effect of externally mounted fuel tanks on lateral aerodynamic characteristics of the basic configuration. $\beta = 0^0$ and 4^0.

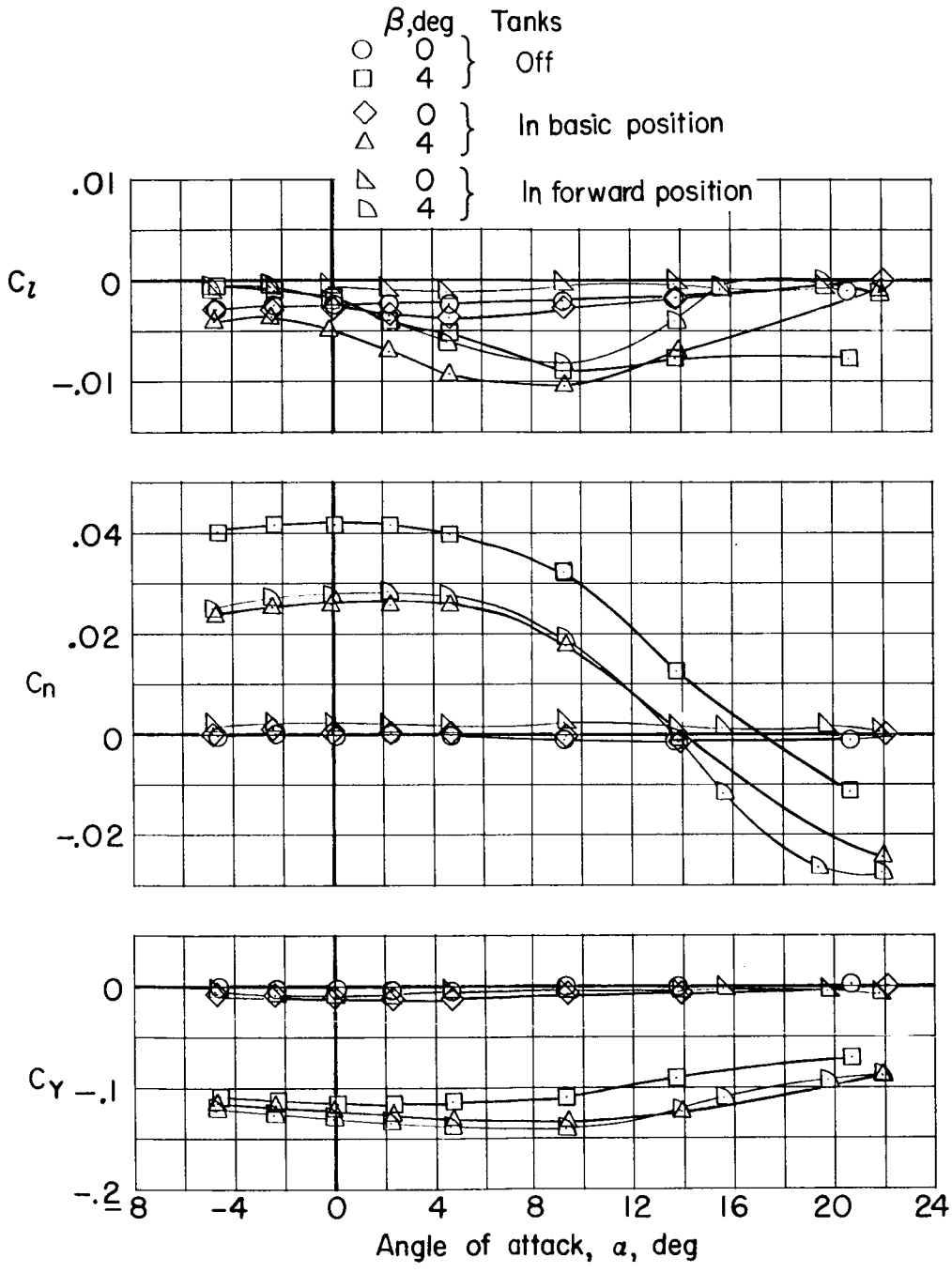

(b) M = 0.80.

Figure 7.- Continued.

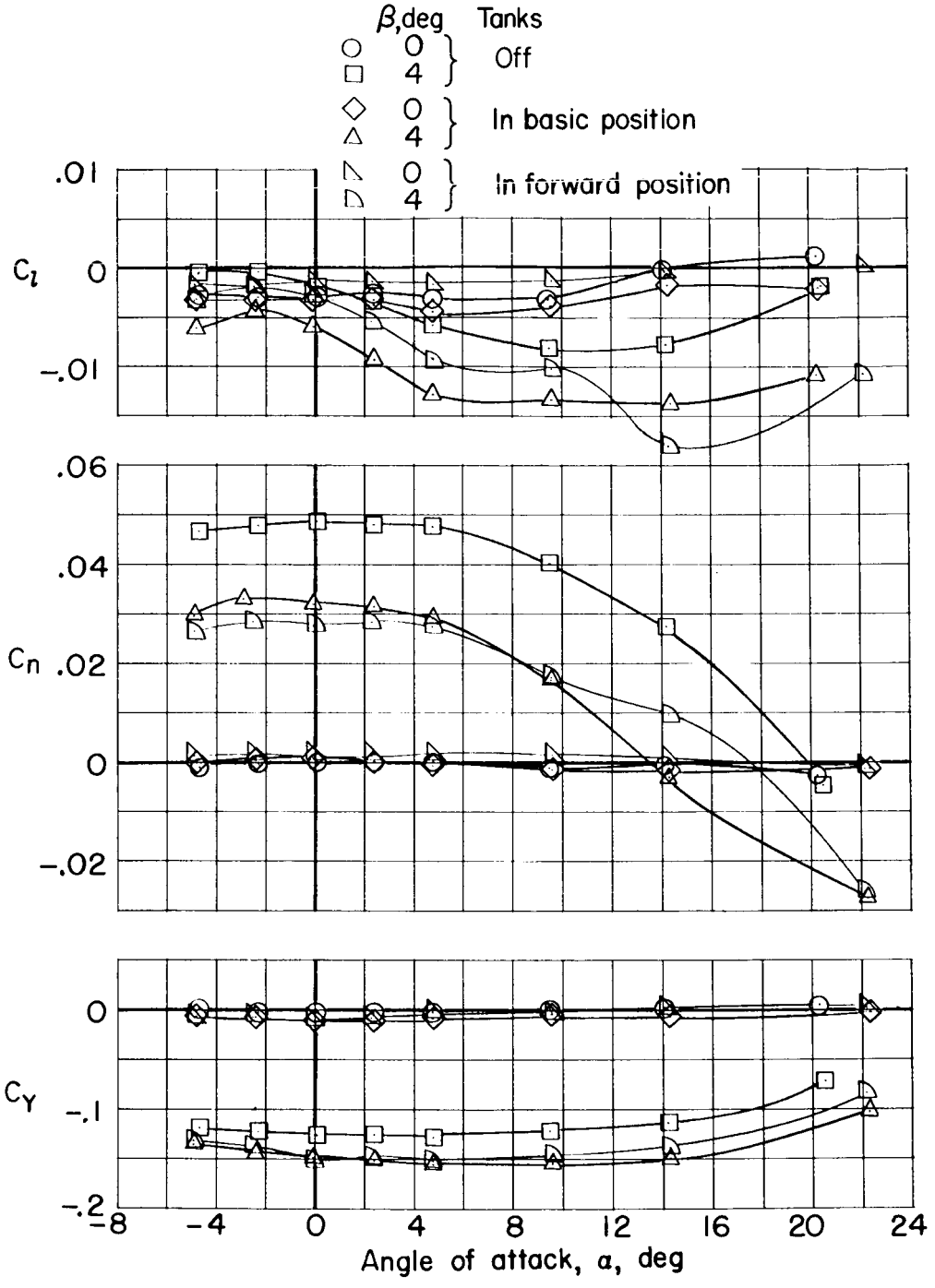

(c) M = 1.00.

Figure 7.- Continued.

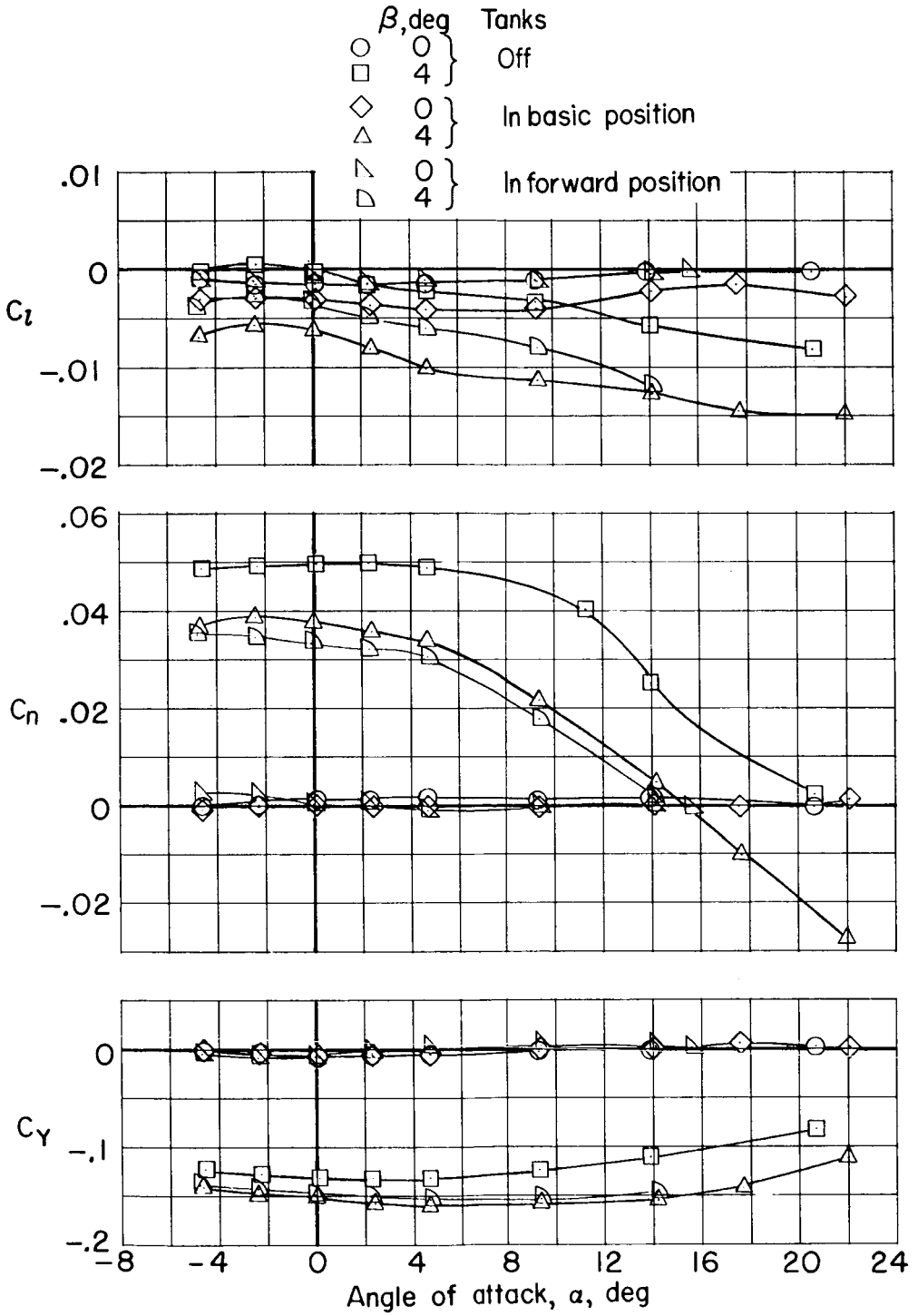

(d) M = 1.20.

Figure 7.- Concluded.

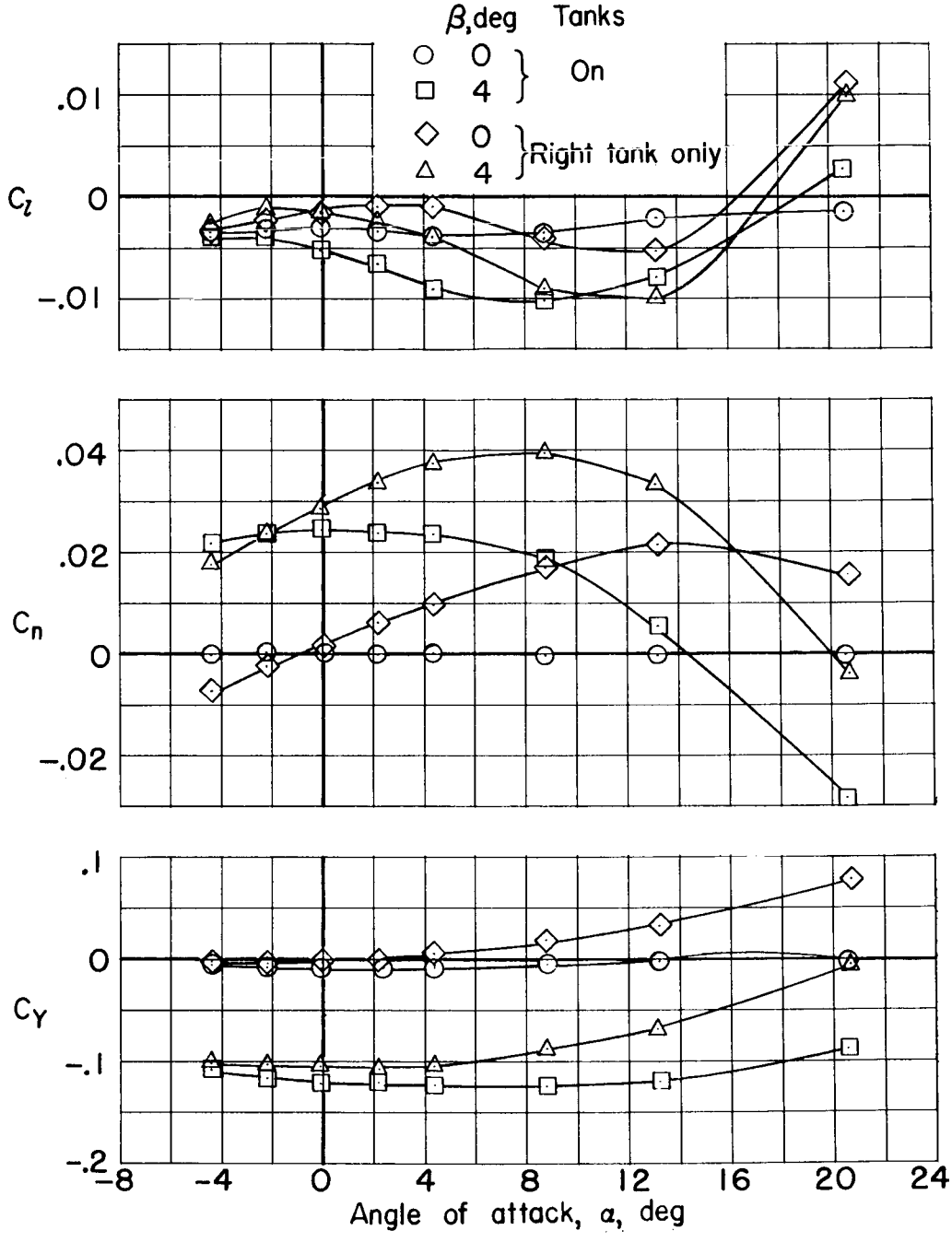

(a) M = 0.60.

Figure 8.- Effect of right externally mounted fuel tanks on the lateral aerodynamic characteristics of the basic configuration. $\beta = 0^0$ and 4^0.

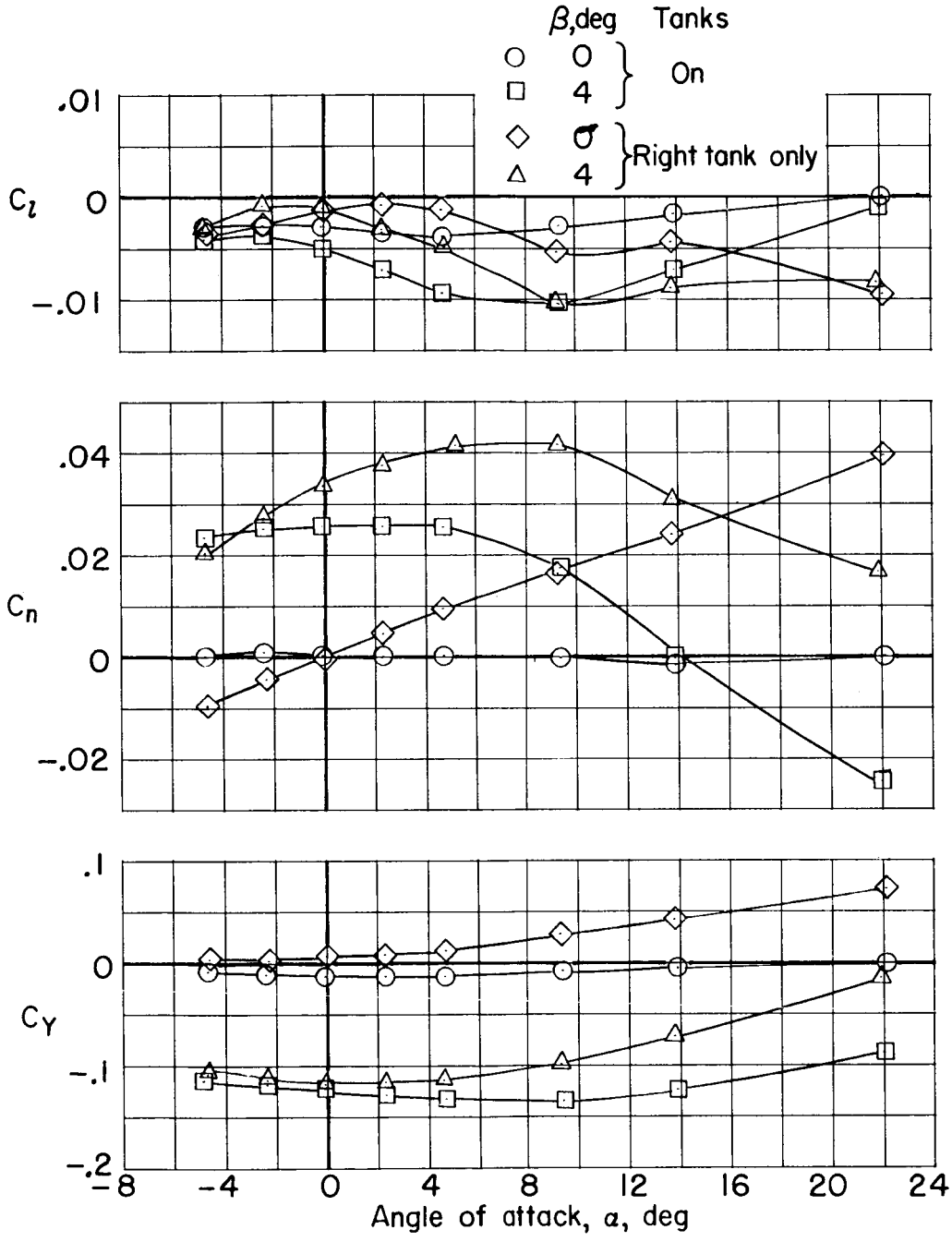

(b) M = 0.80.

Figure 8.- Continued.

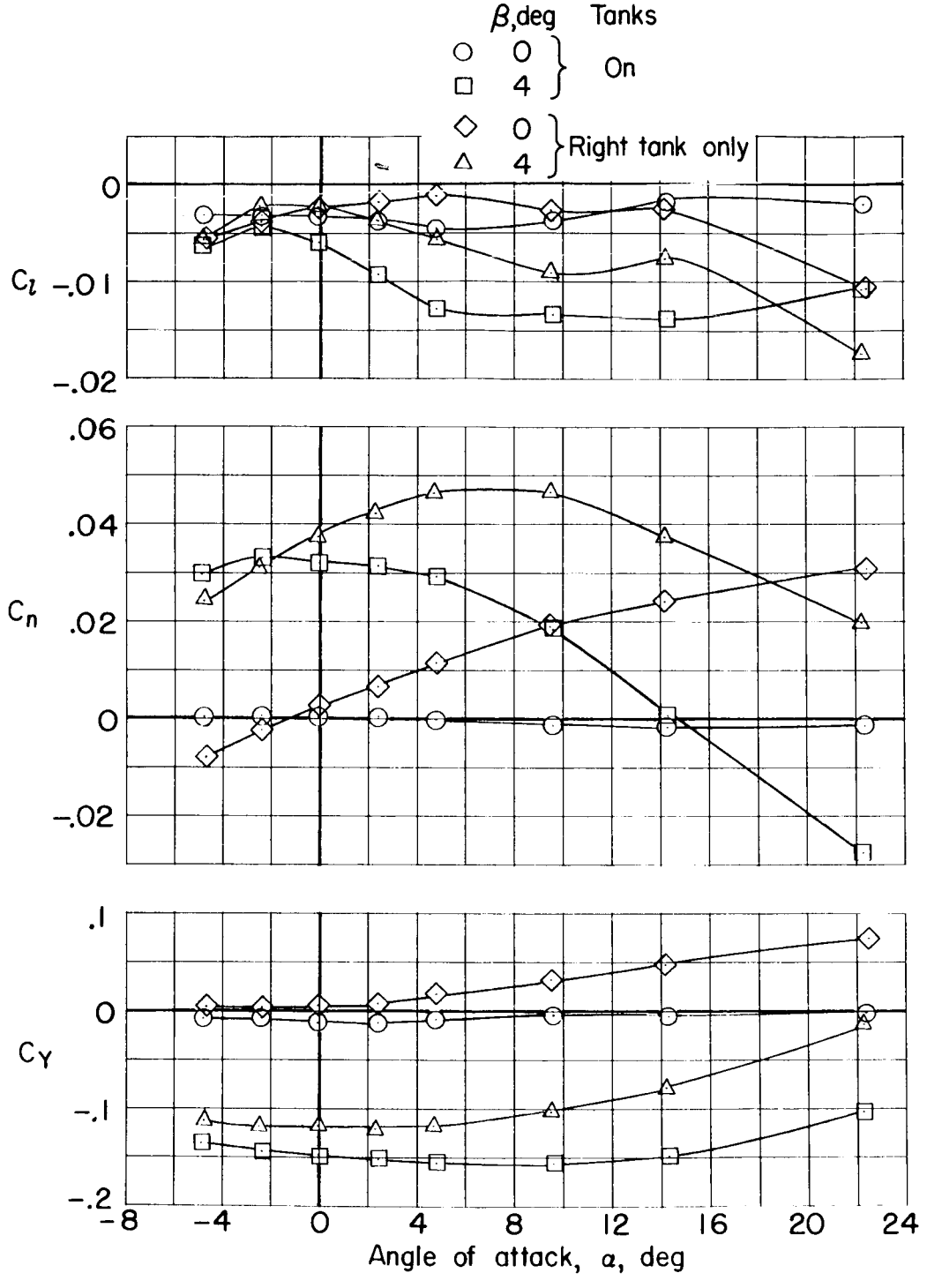

(c) M = 1.00.

Figure 8.- Continued.

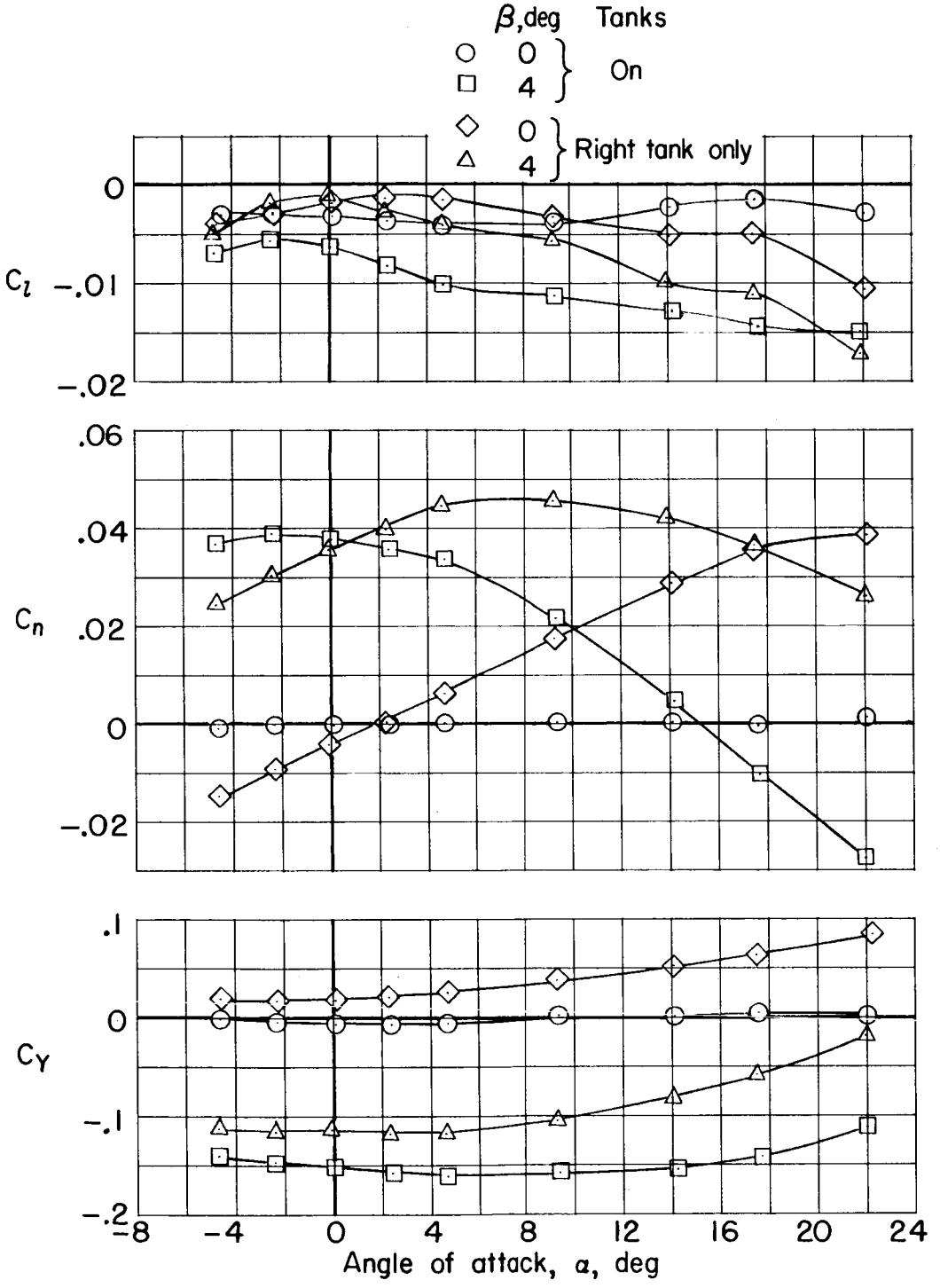

(d) M = 1.20.

Figure 8.- Concluded.

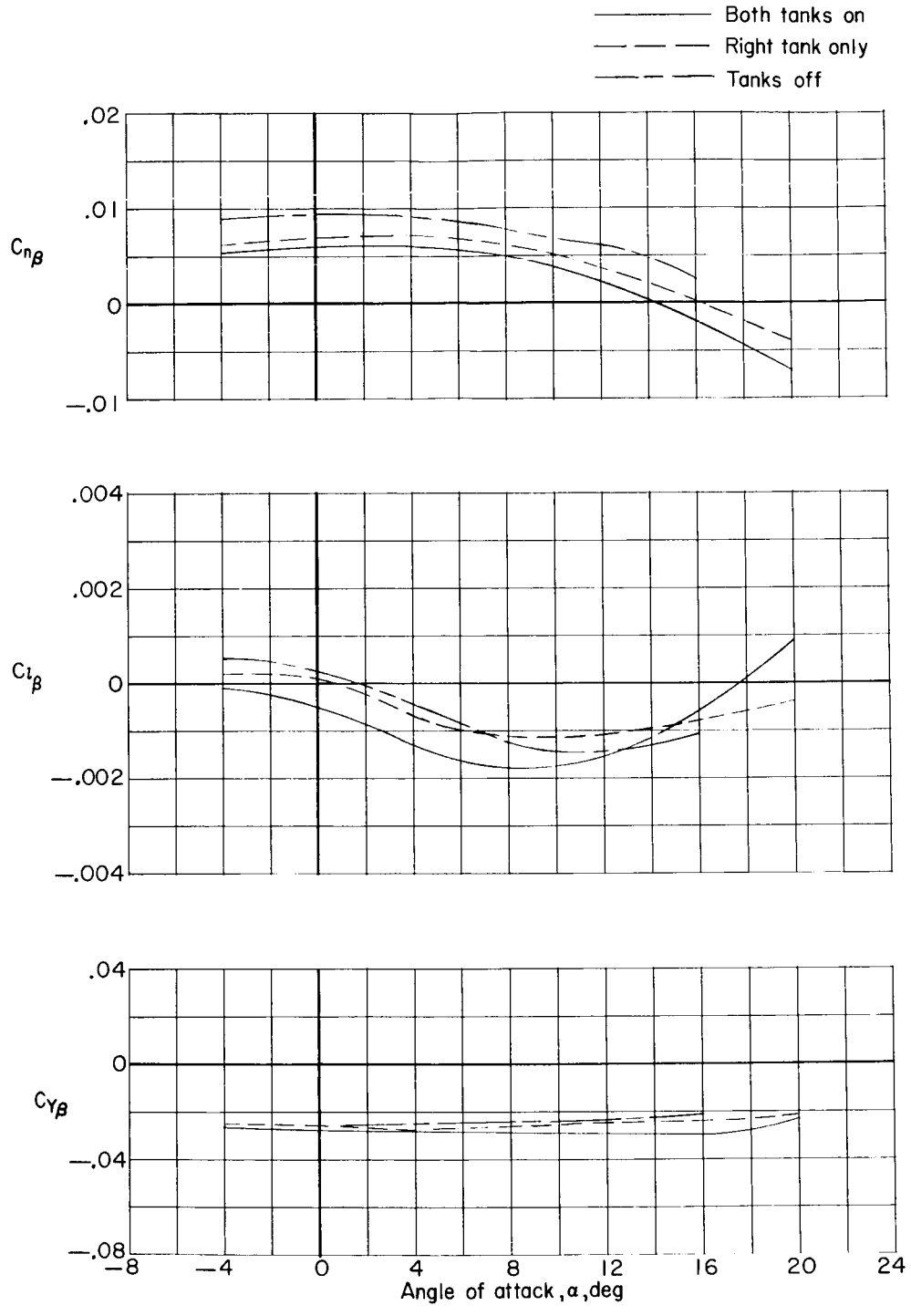

(a) M = 0.60.

Figure 9.- Variation with angle of attack of the lateral stability derivatives for externally mounted fuel tanks.

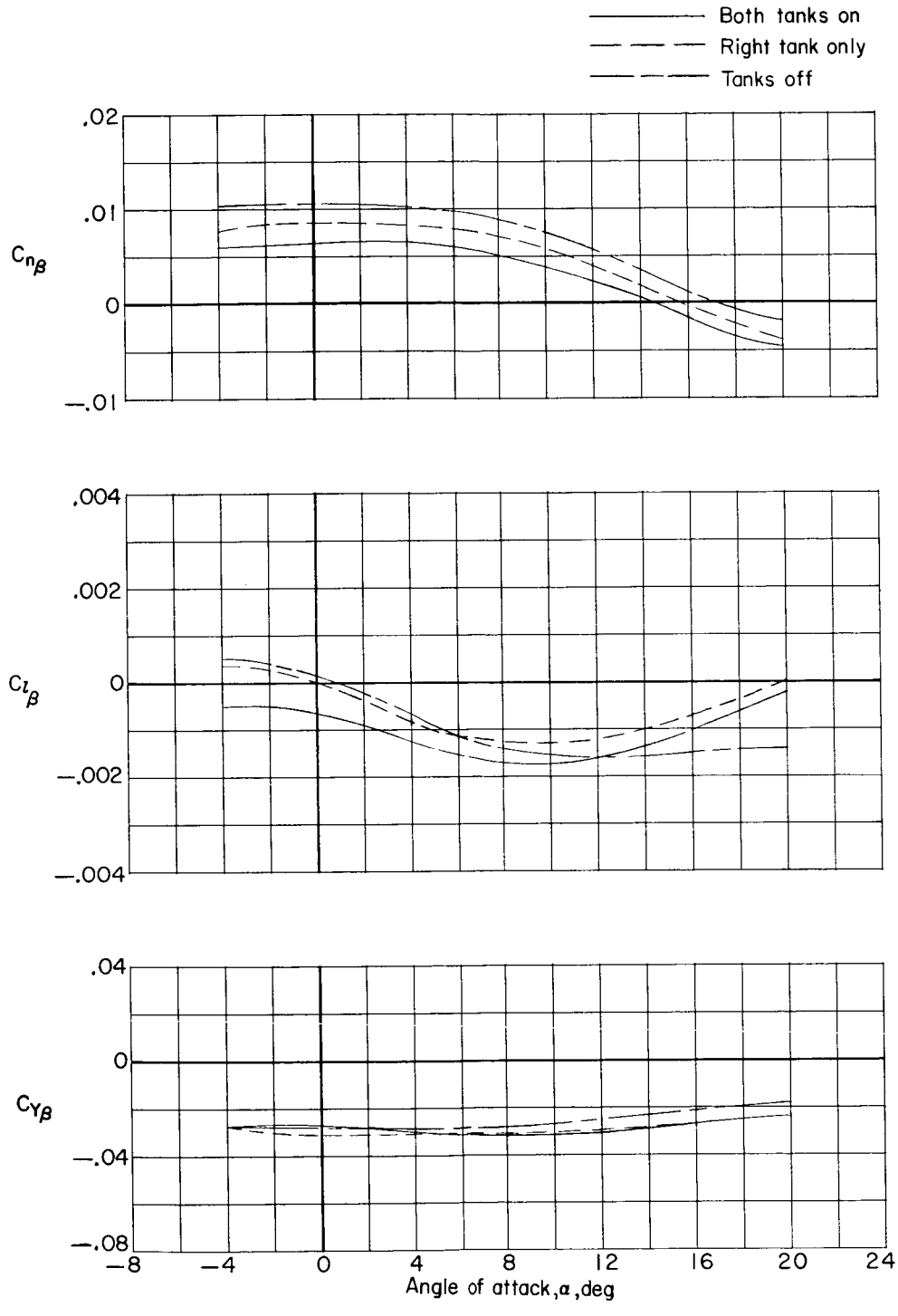

(b) M = 0.80.

Figure 9.- Continued.

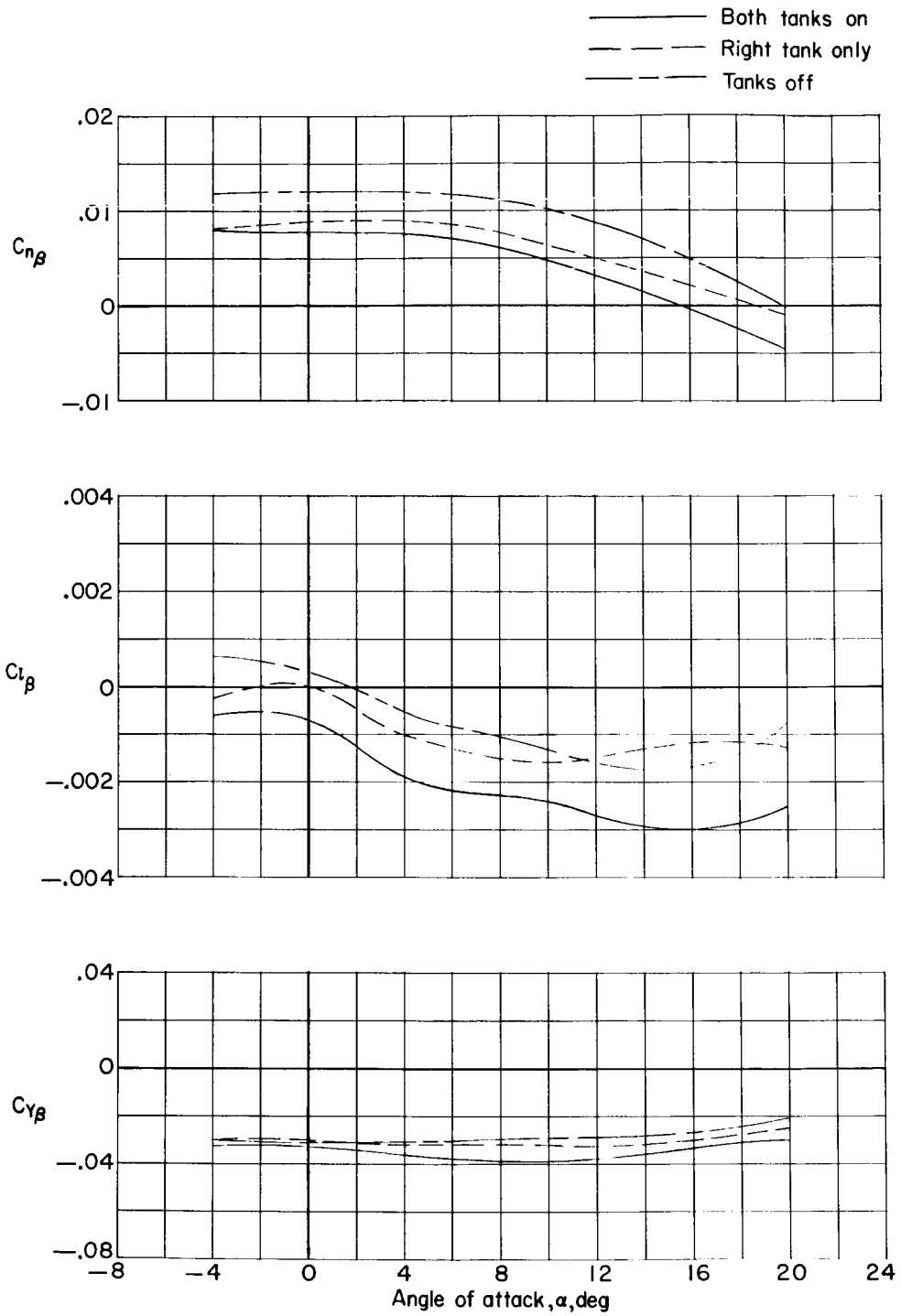

(c) M = 1.0.

Figure 9.- Continued.

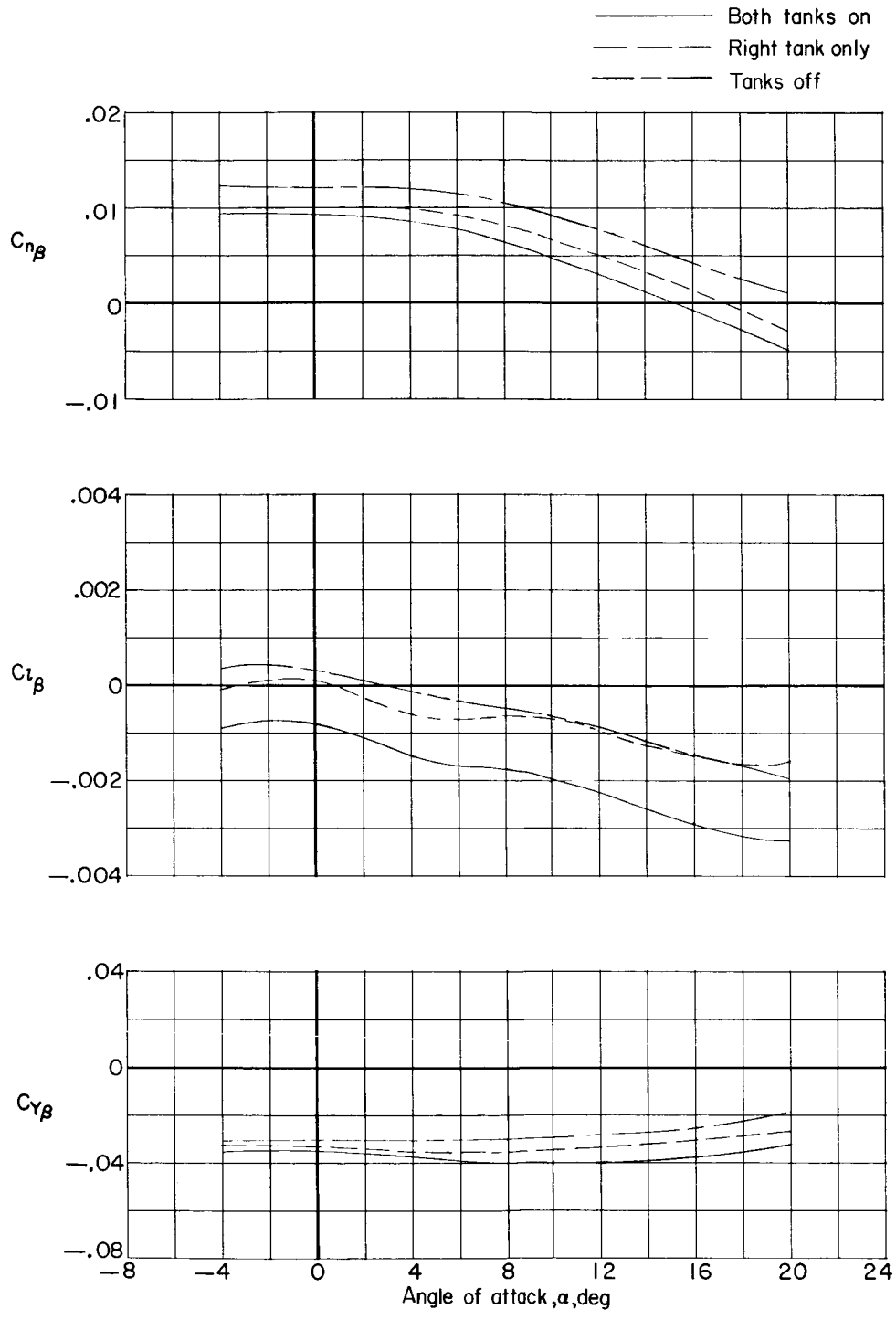

(d) M = 1.2.

Figure 9.- Concluded.

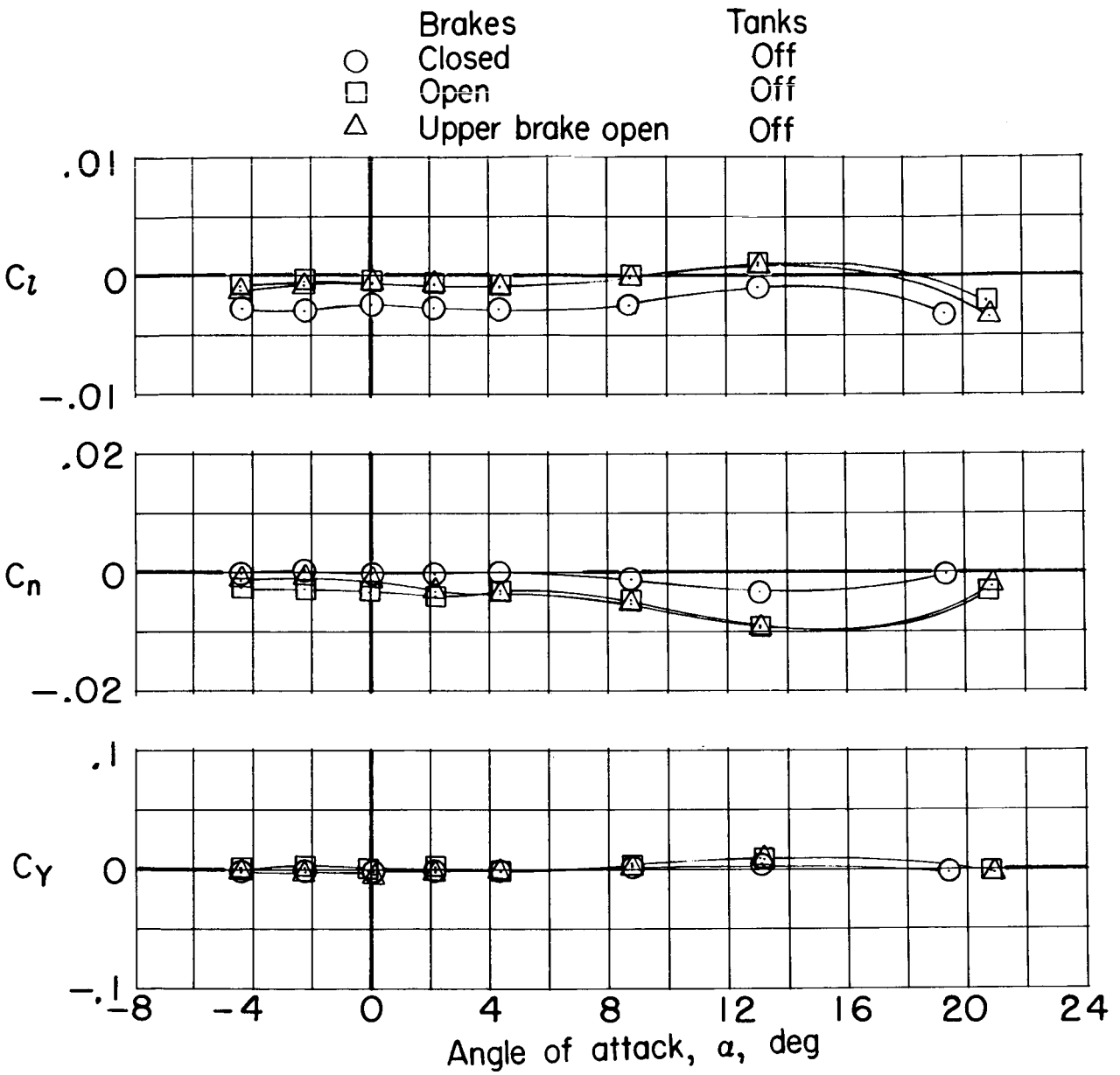

(a) M = 0.60.

Figure 10.- Effect of speed brakes on lateral aerodynamic characteristics. $\beta = 0^{o}$.

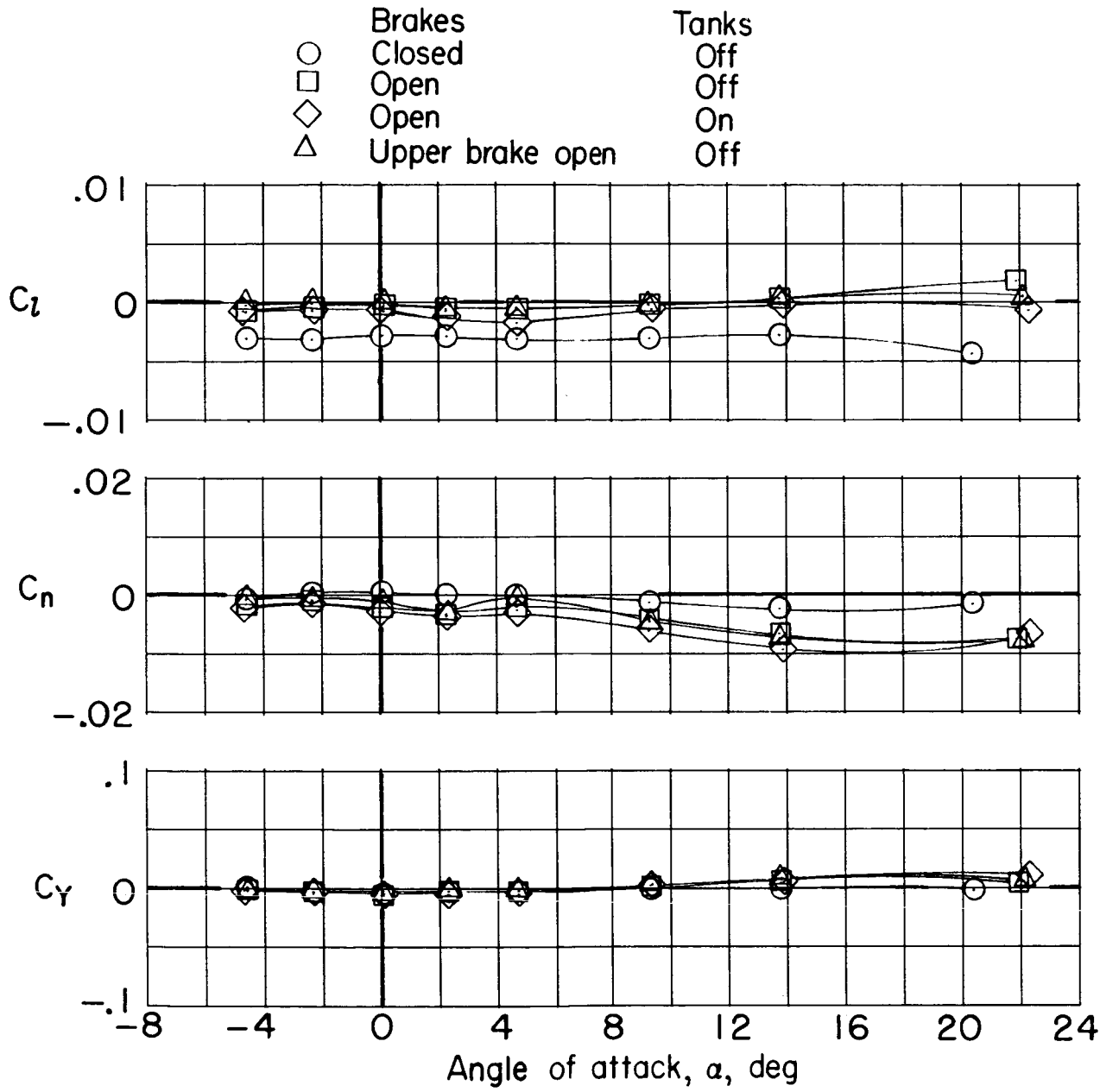

(b) M = 0.80.

Figure 10.- Continued.

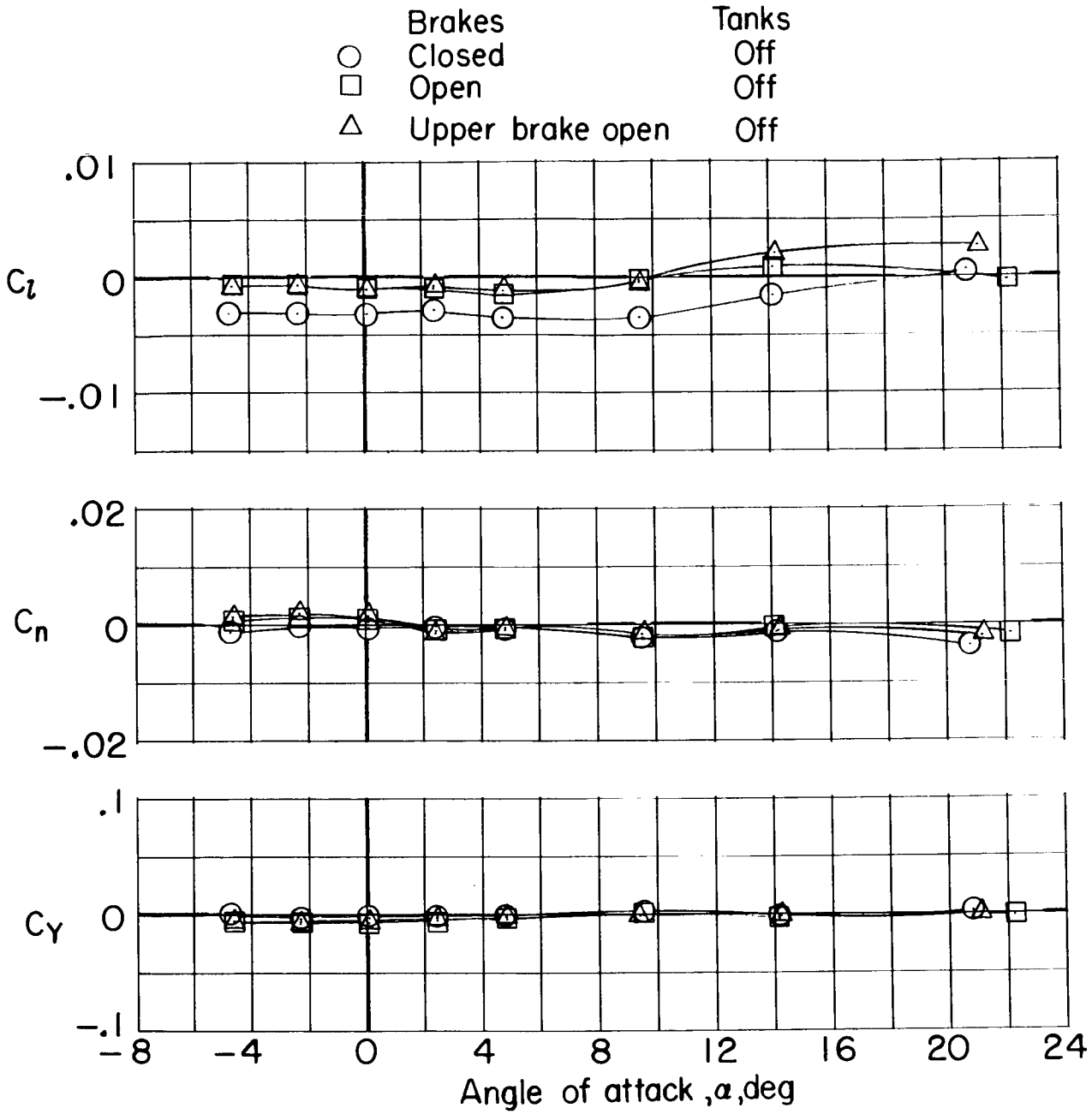

(c) M = 1.00.

Figure 10.- Continued.

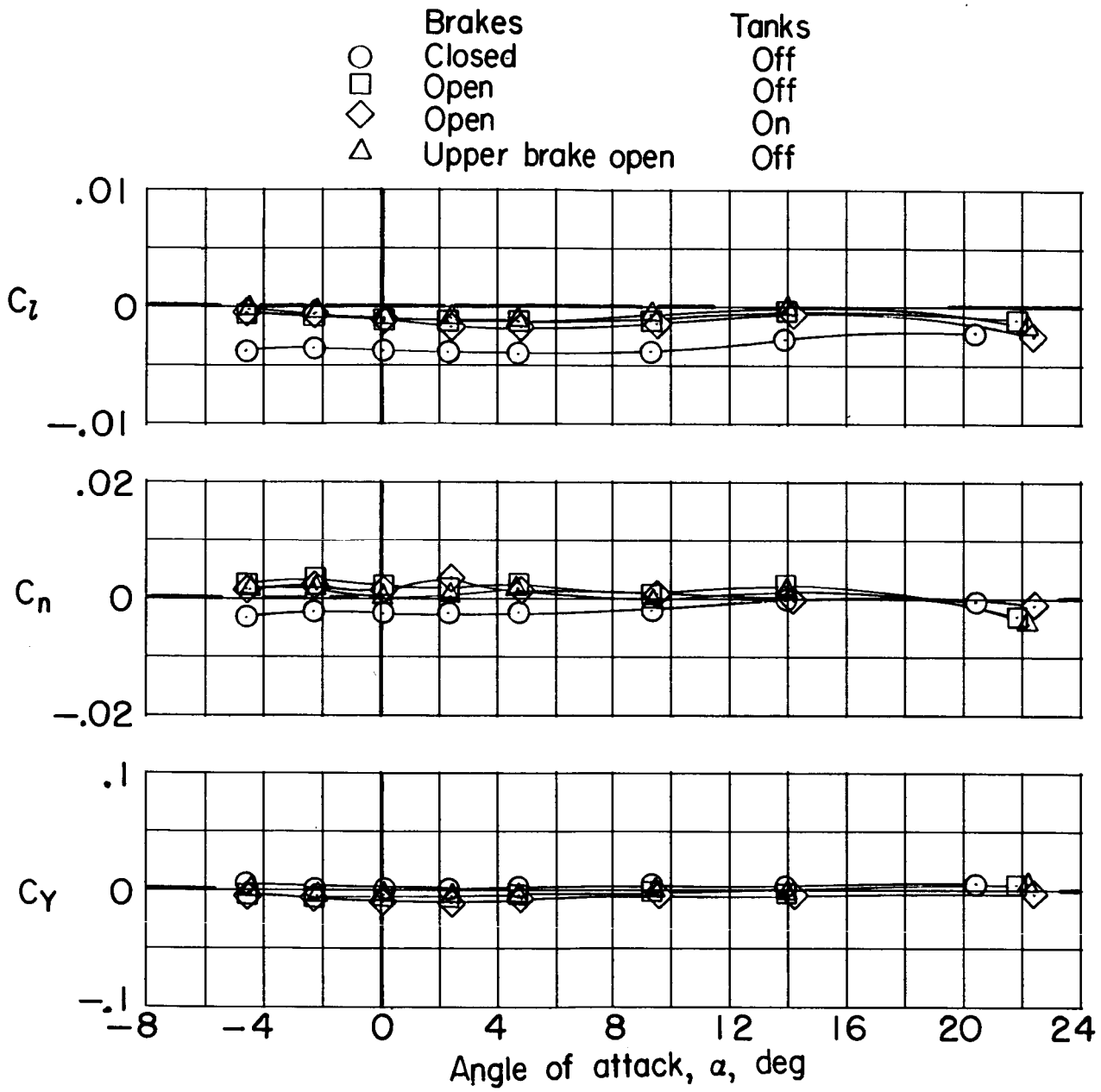

(d) M = 1.20.

Figure 10.- Concluded.

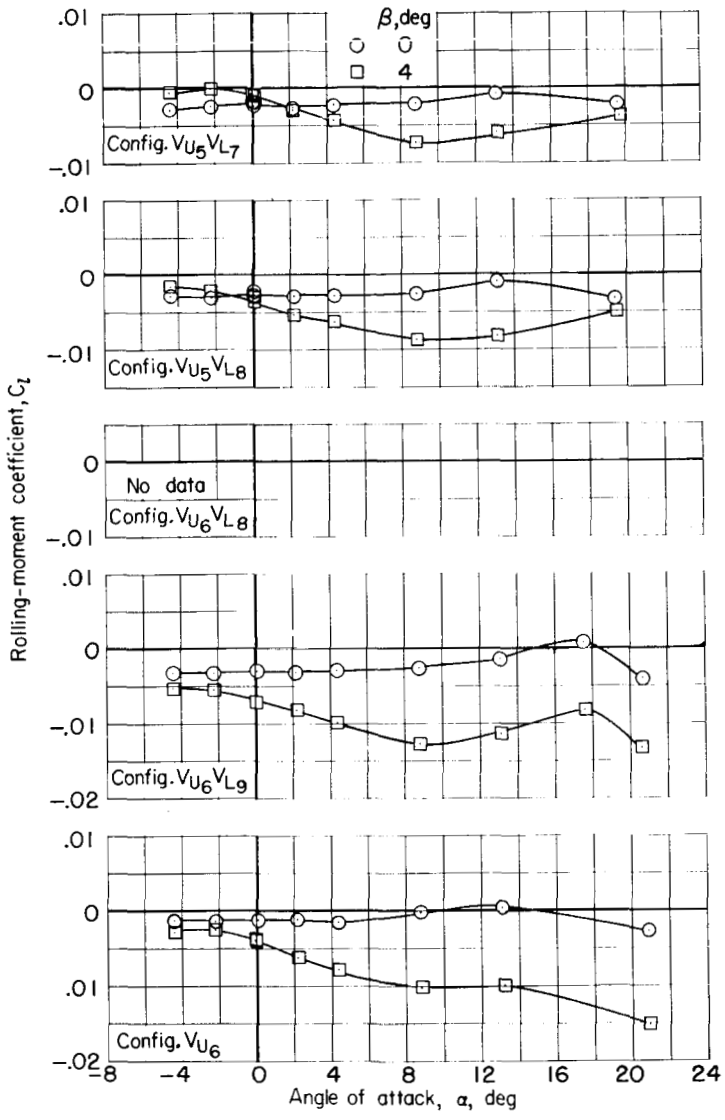

(a) M = 0.60.

Figure 11.- Effect of vertical-tail size on the lateral aerodynamic characteristics. $\beta = 0^0$ and 4^0.

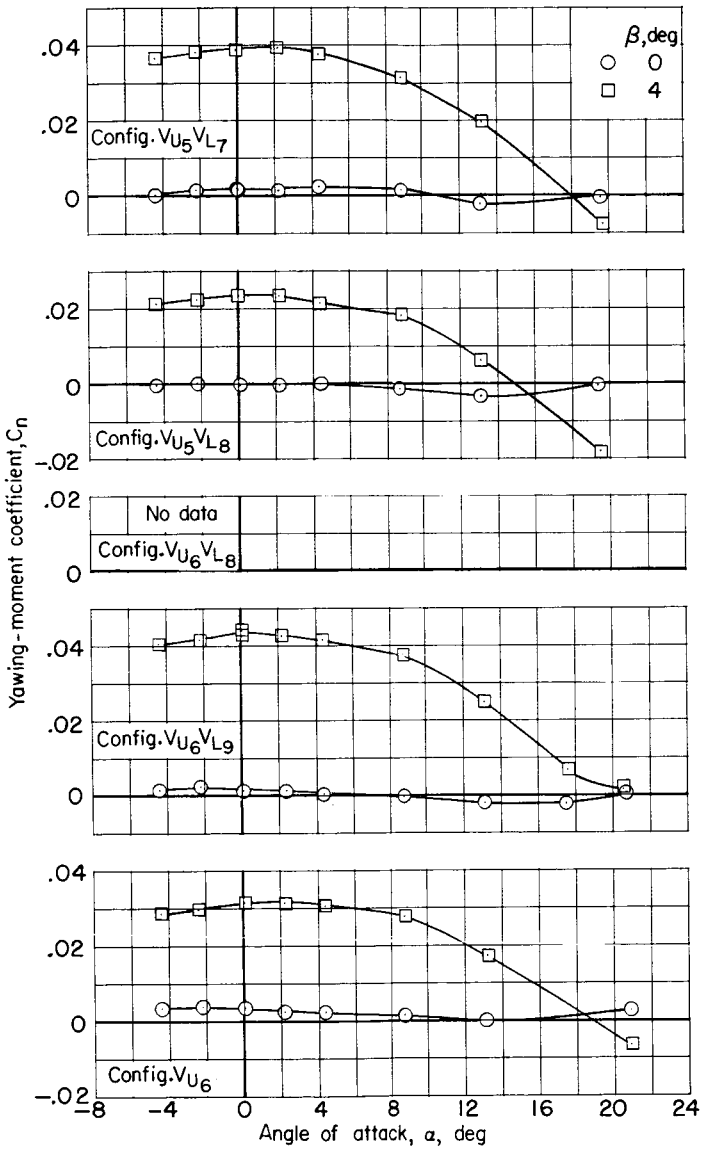

(a) M = 0.60. Continued.

Figure 11.- Continued.

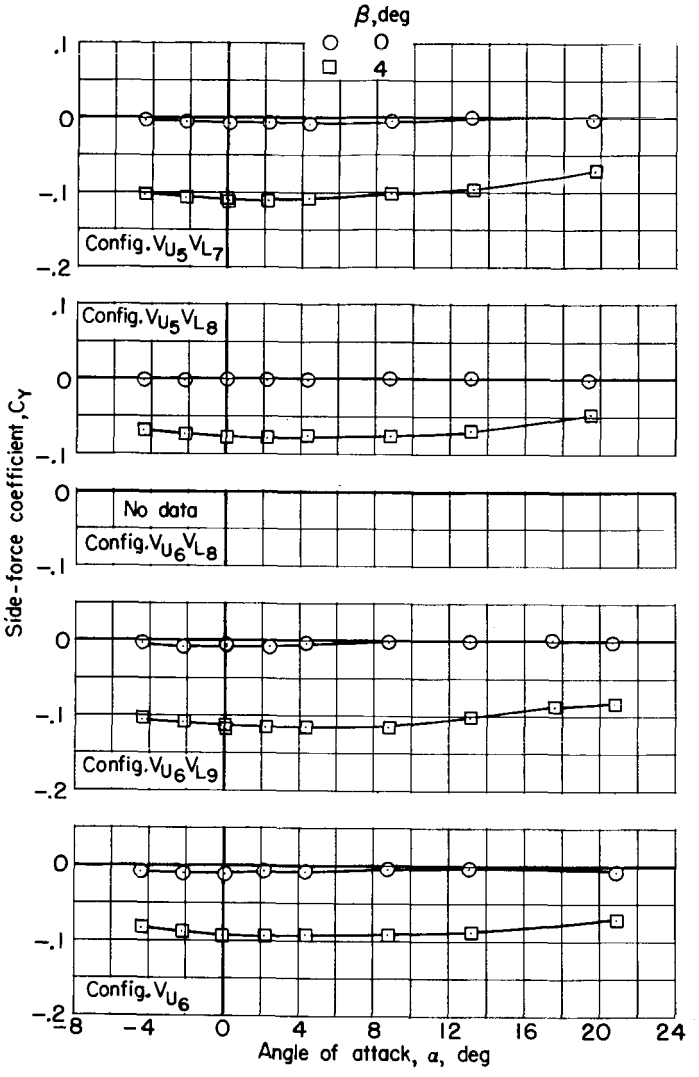

(a) M = 0.60. Concluded.

Figure 11.- Continued.

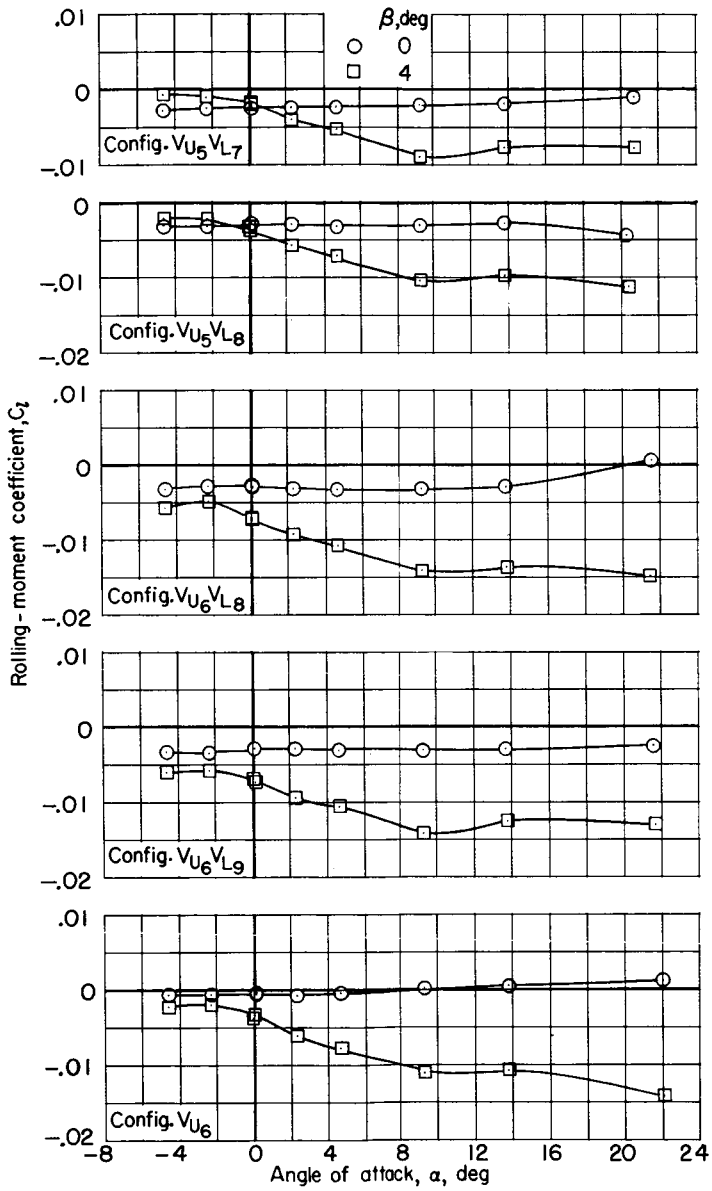

(b) M = 0.80.

Figure 11.- Continued.

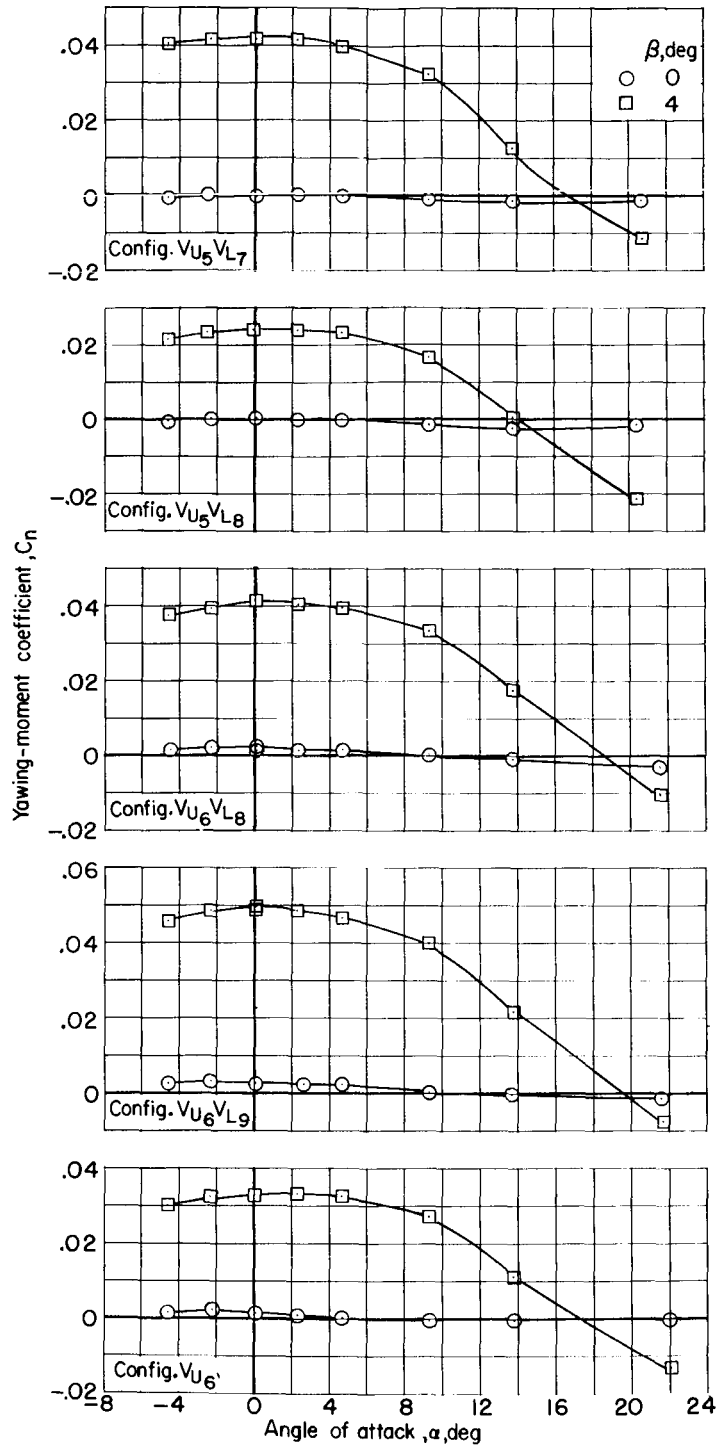

(b) M = 0.80. Continued.

Figure 11.- Continued.

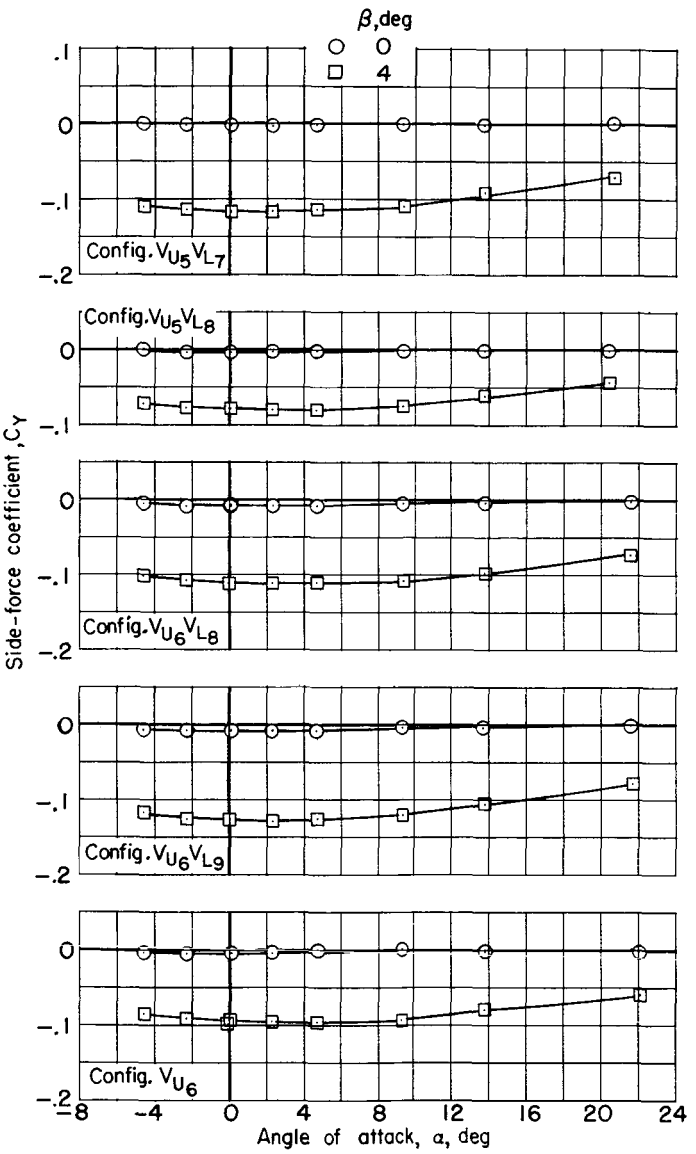

(b) M = 0.80. Concluded.

Figure 11.- Continued.

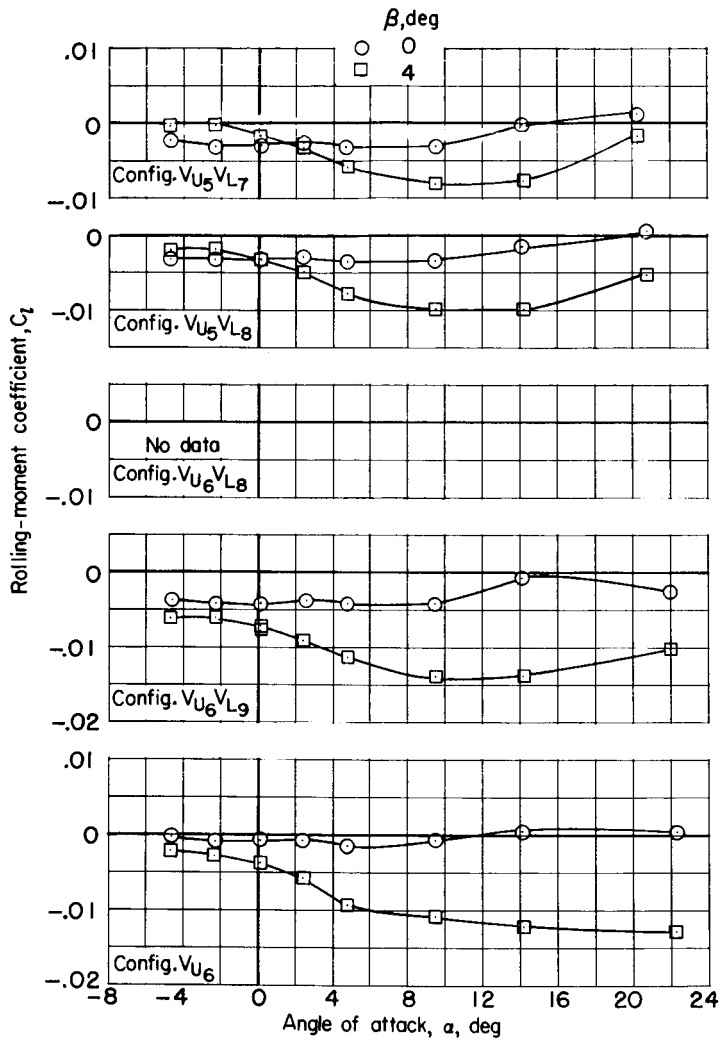

(c) M = 1.00.

Figure 11.- Continued.

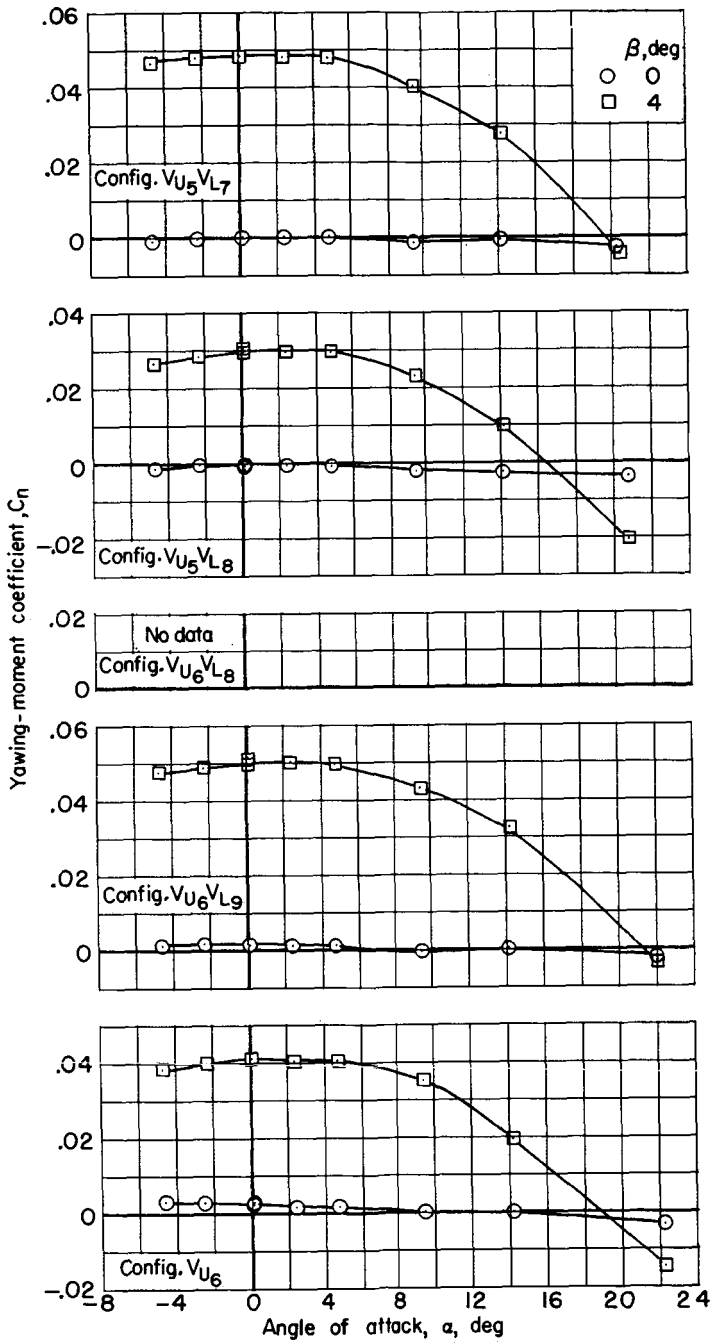

(c) M = 1.00. Continued.

Figure 11.- Continued.

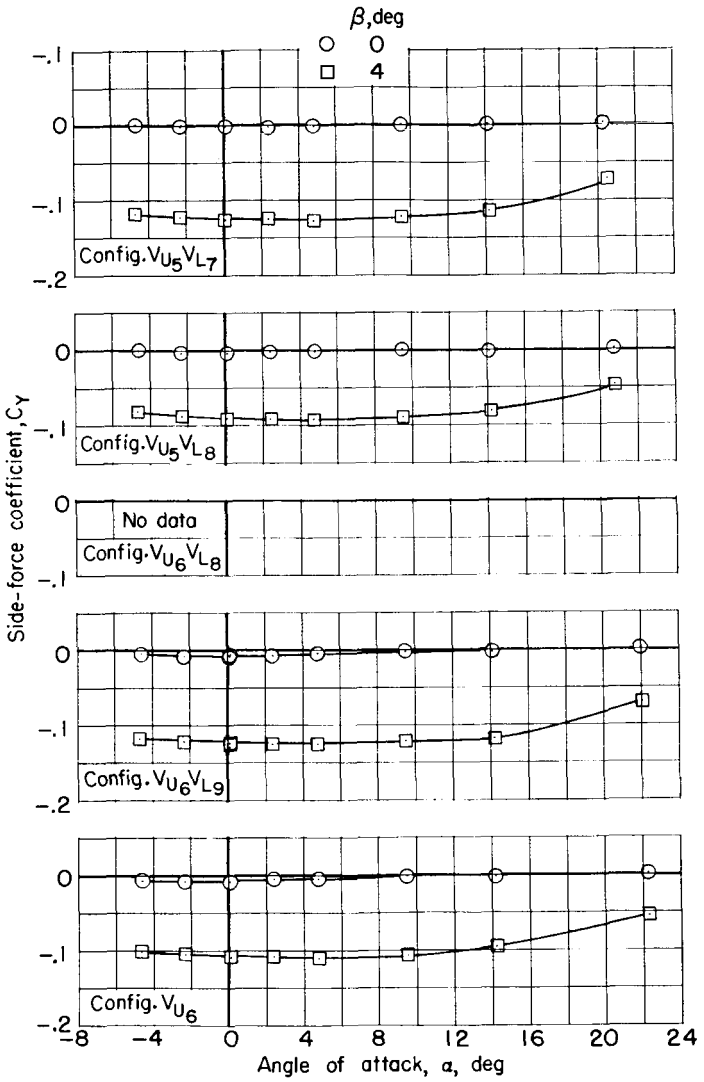

(c) M = 1.00. Concluded.

Figure 11.- Continued.

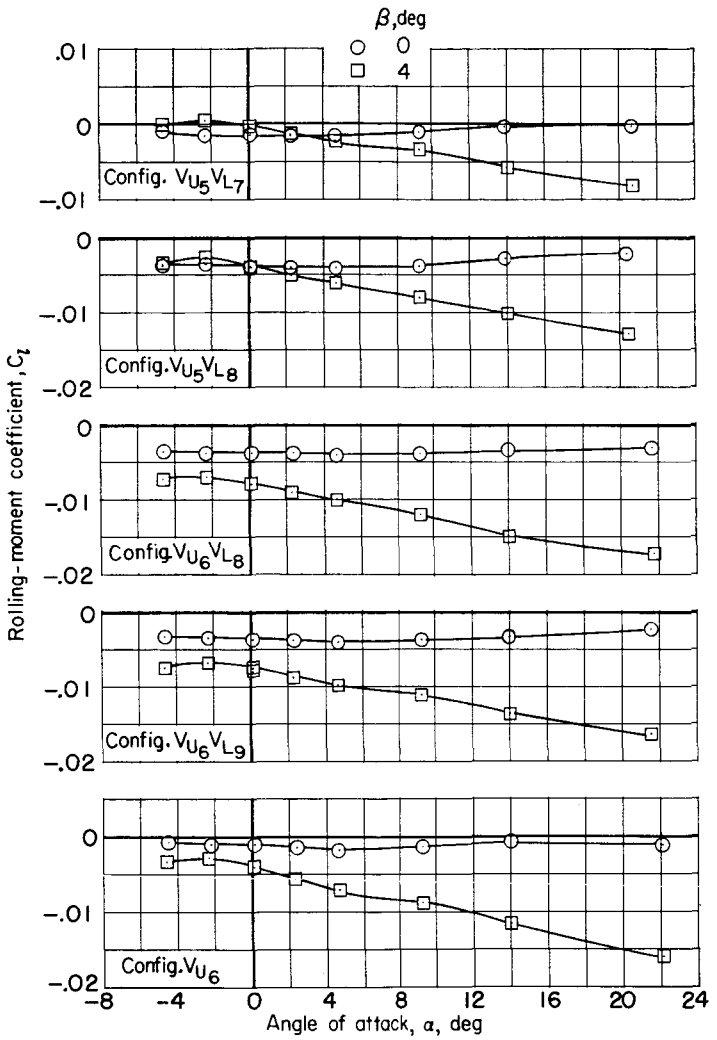

(d) M = 1.20.

Figure 11.- Continued.

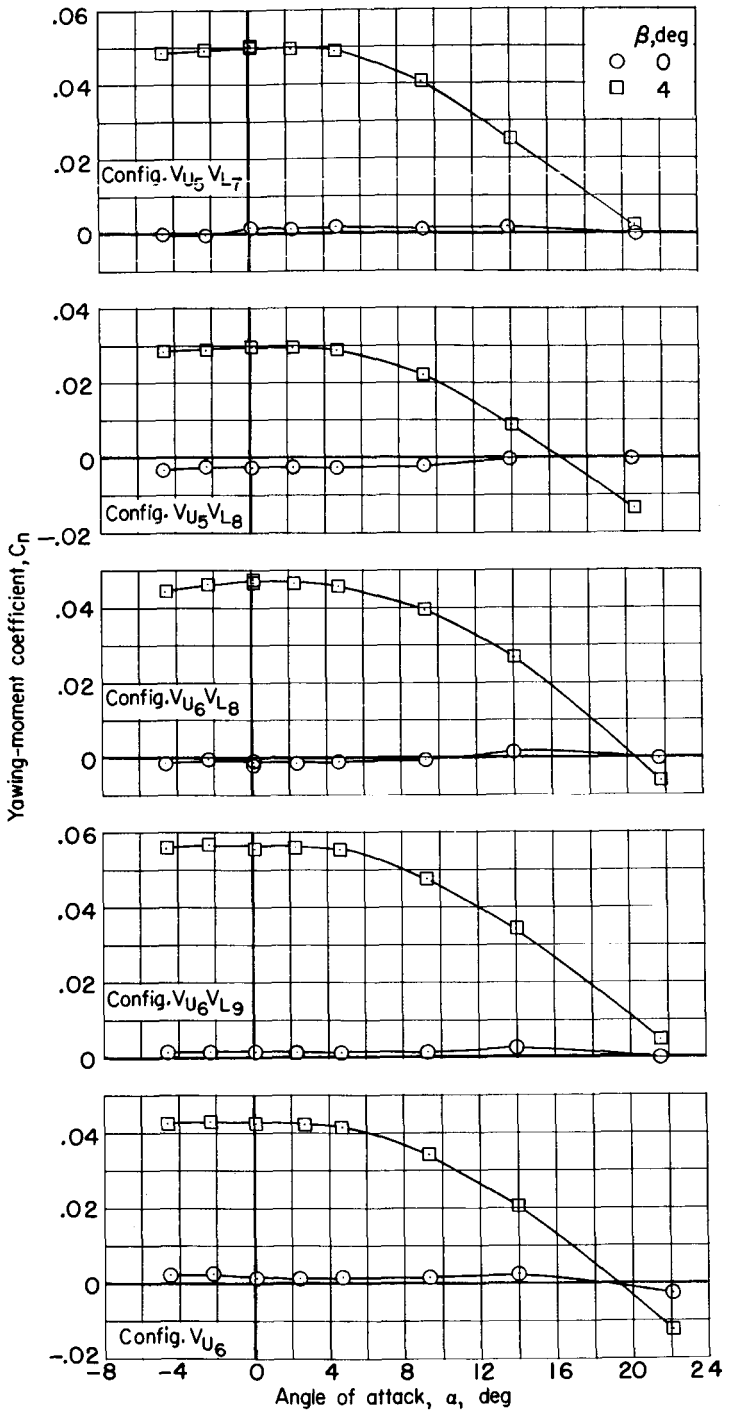

(d) M = 1.20. Continued.

Figure 11.- Continued.

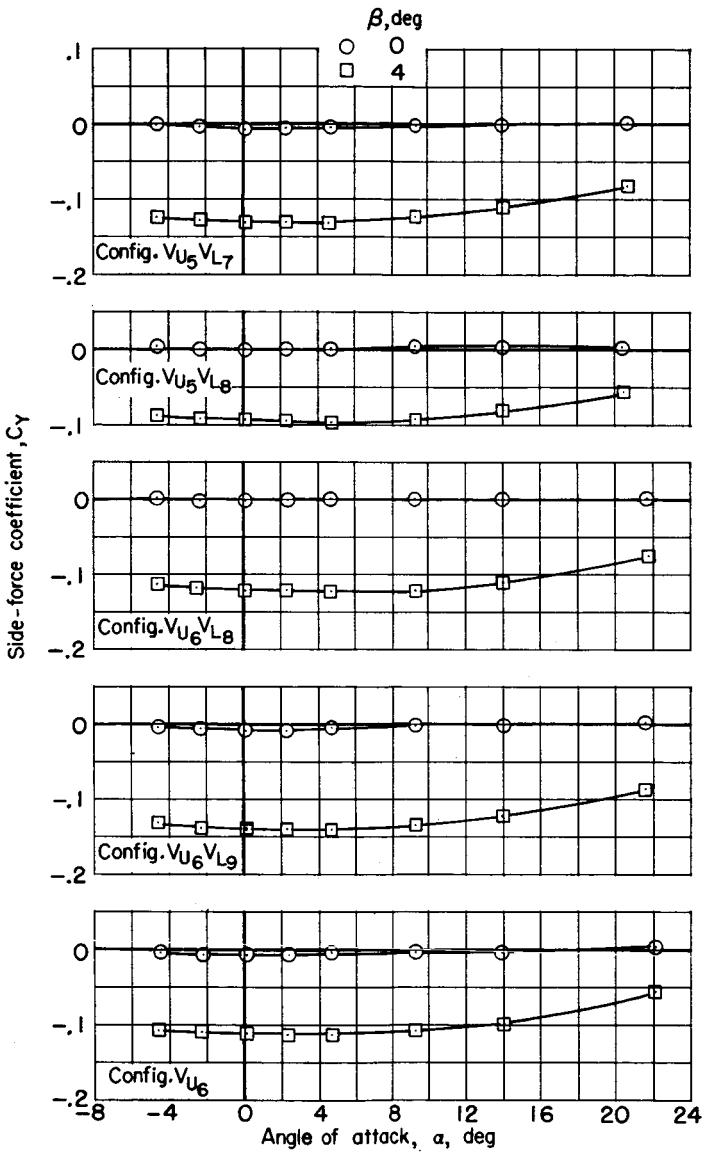

(d) M = 1.20. Concluded.

Figure 11.- Concluded.

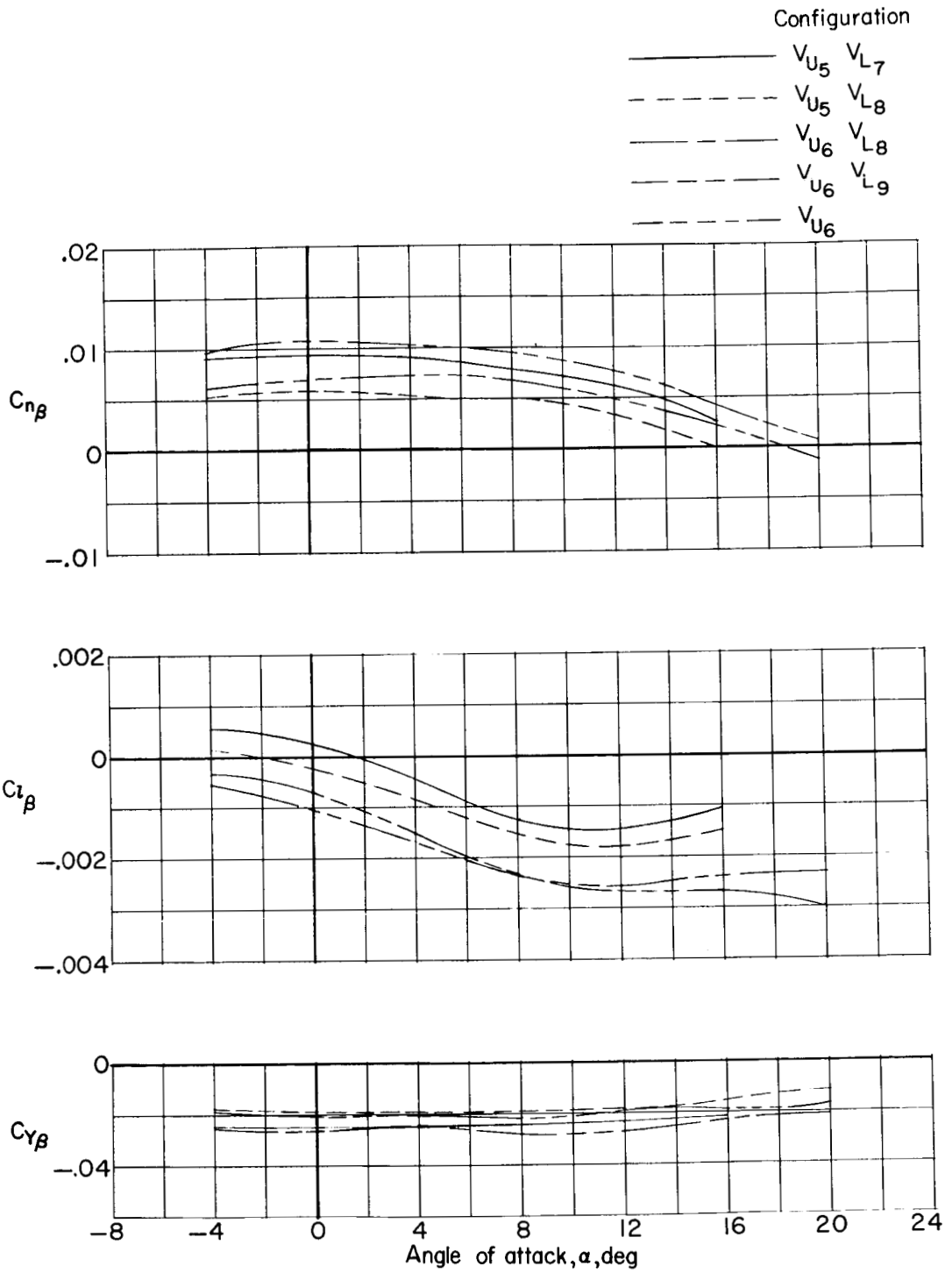

(a) M = 0.60.

Figure 12.- Variation with angle of attack of lateral stability derivatives for various vertical-tail configurations.

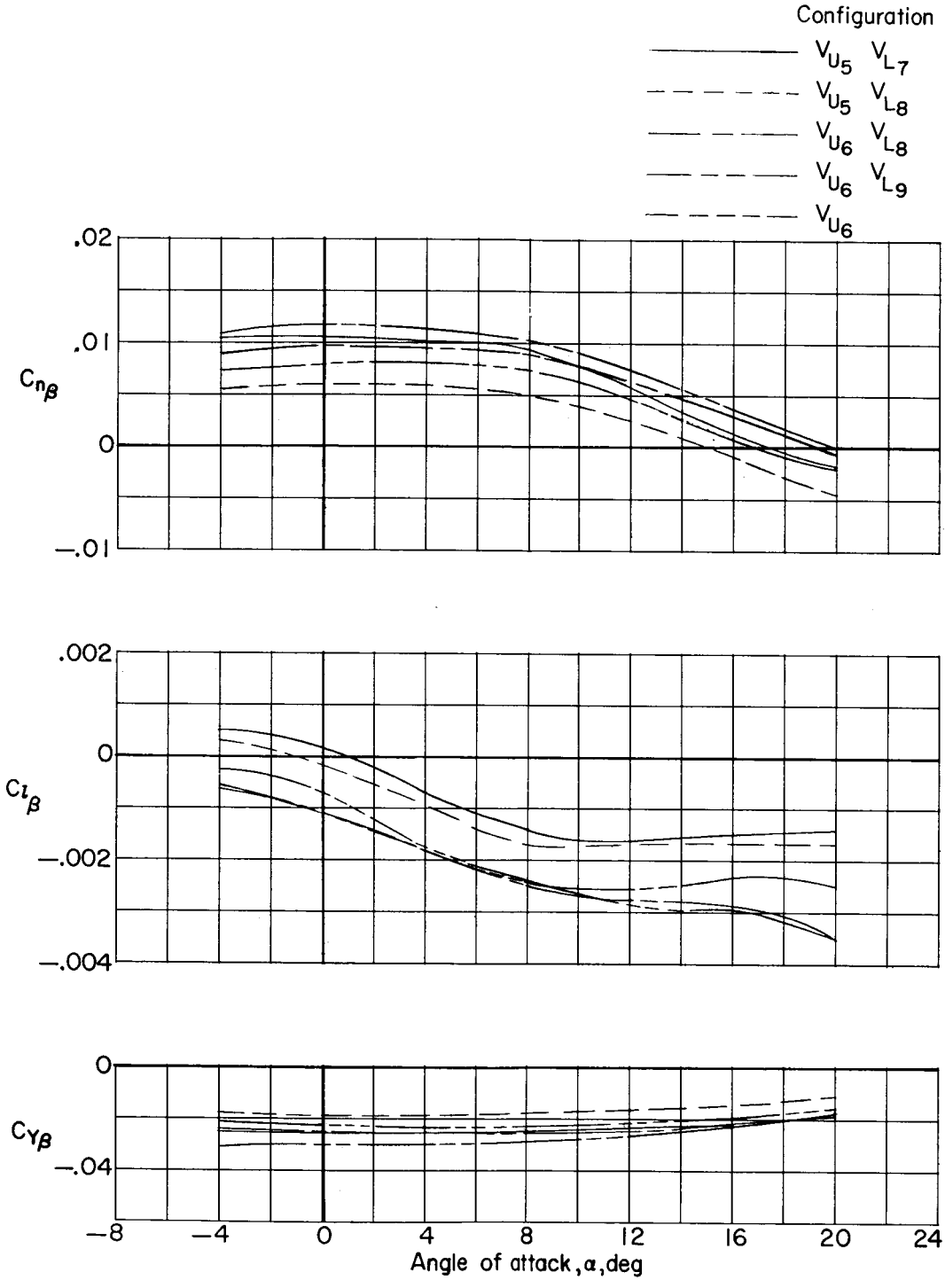

(b) M = 0.80.

Figure 12.- Continued.

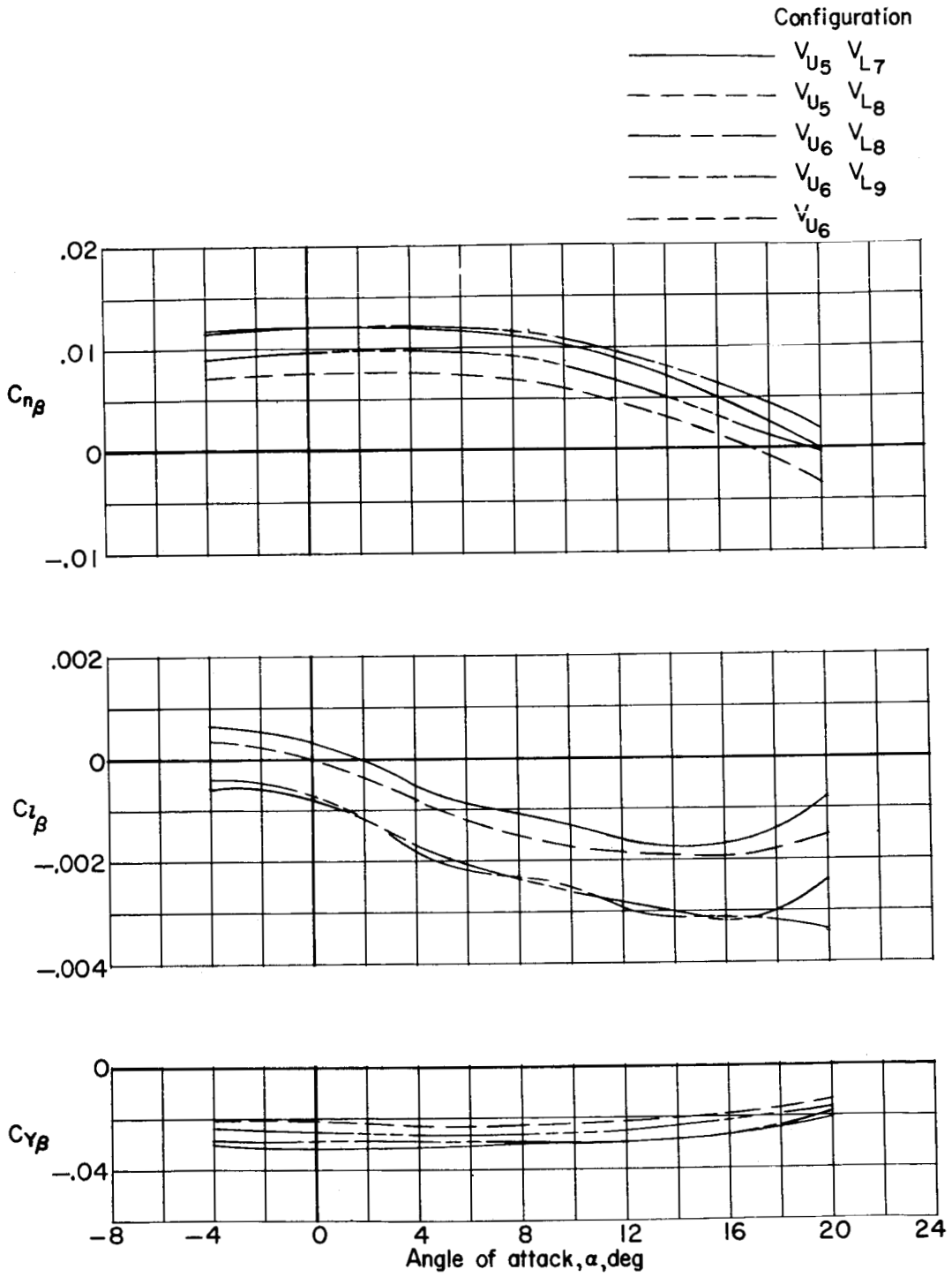

(c) M = 1.0.

Figure 12.- Continued.

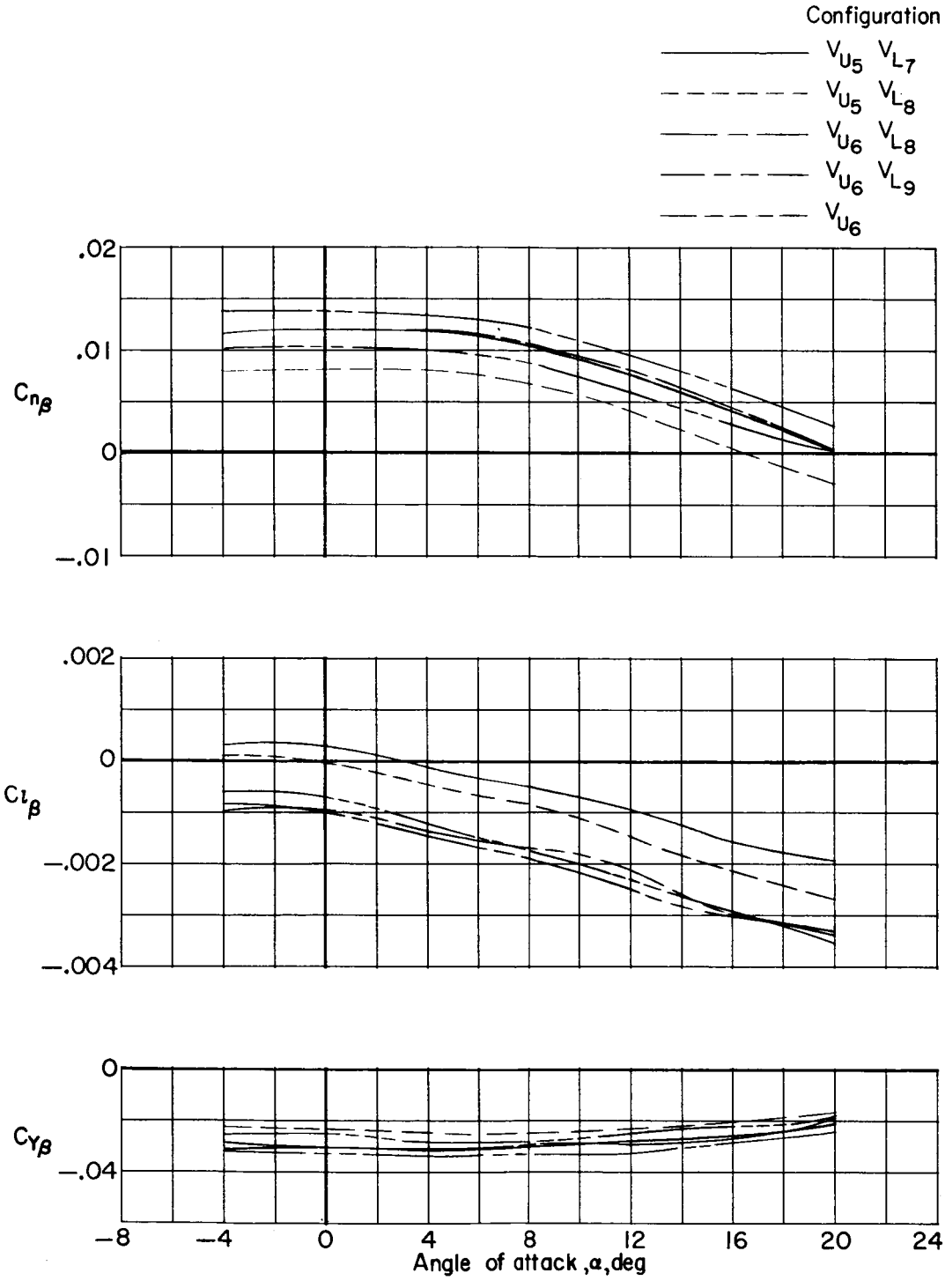

(d) M = 1.2.

Figure 12.- Concluded.

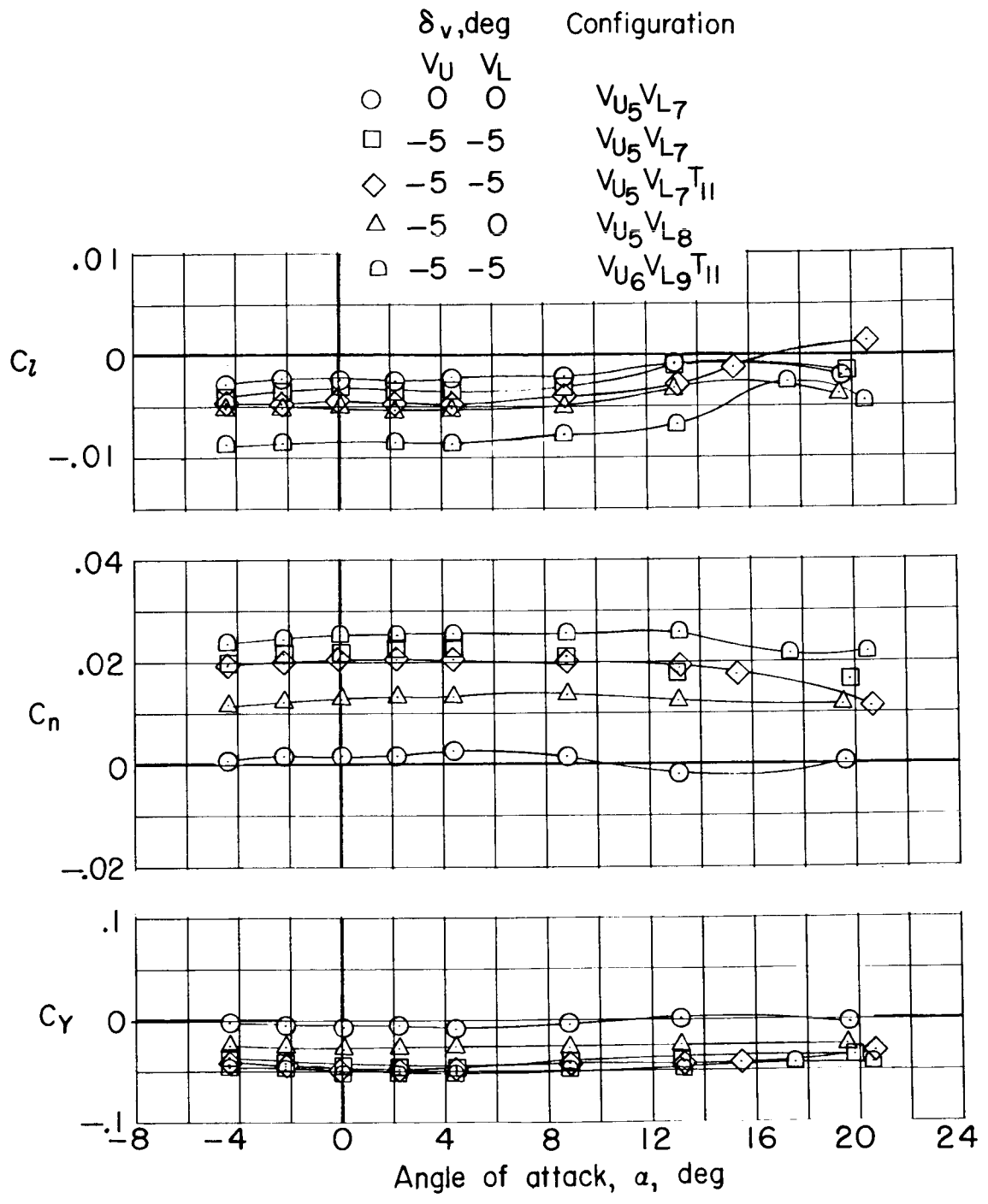

(a) M = 0.60.

Figure 13.- Effect of vertical-tail deflection on lateral aerodynamic characteristics. $\beta = 0^{o}$; $\delta_h = 0^{o}$.

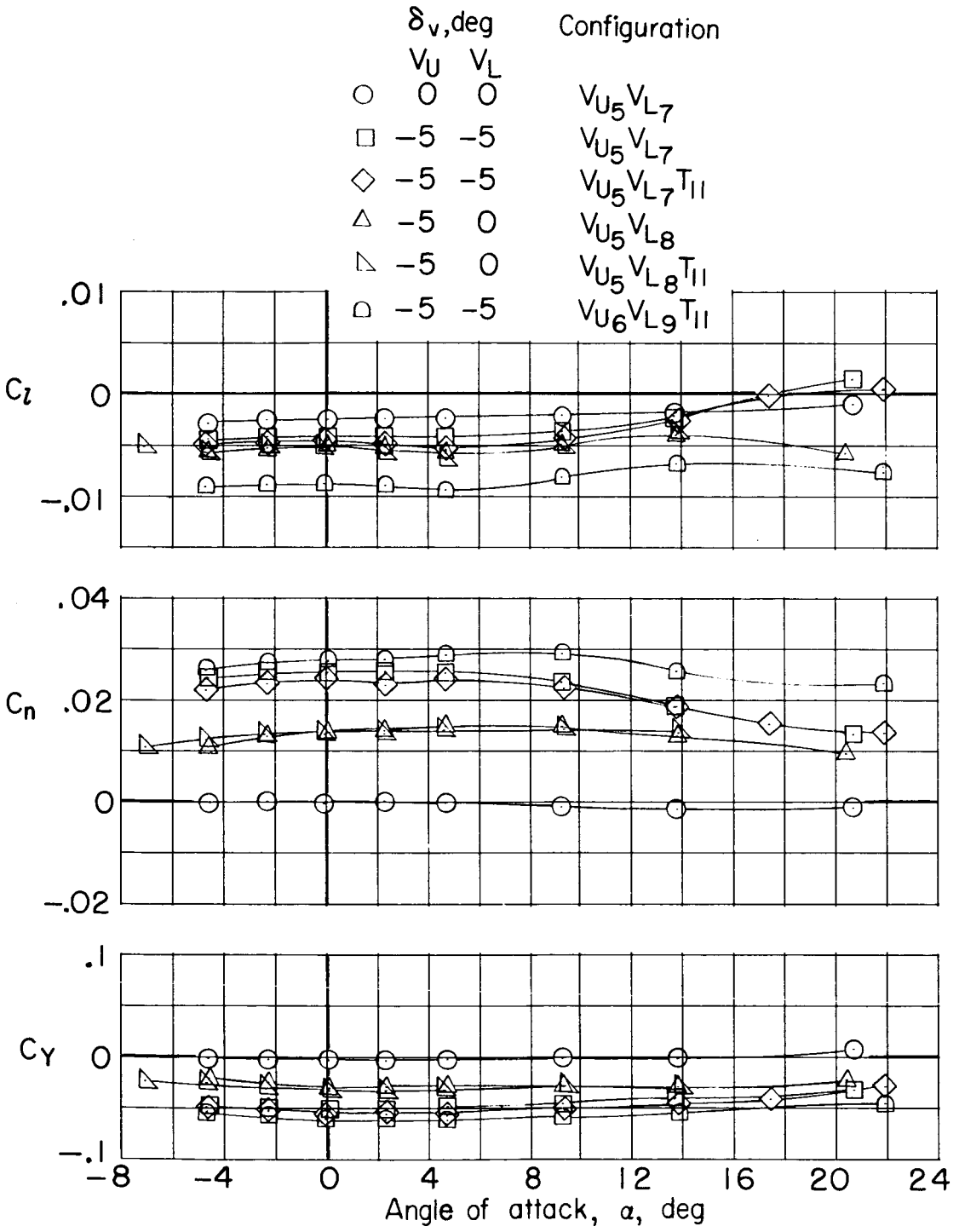

(b) M = 0.80.

Figure 13.- Continued.

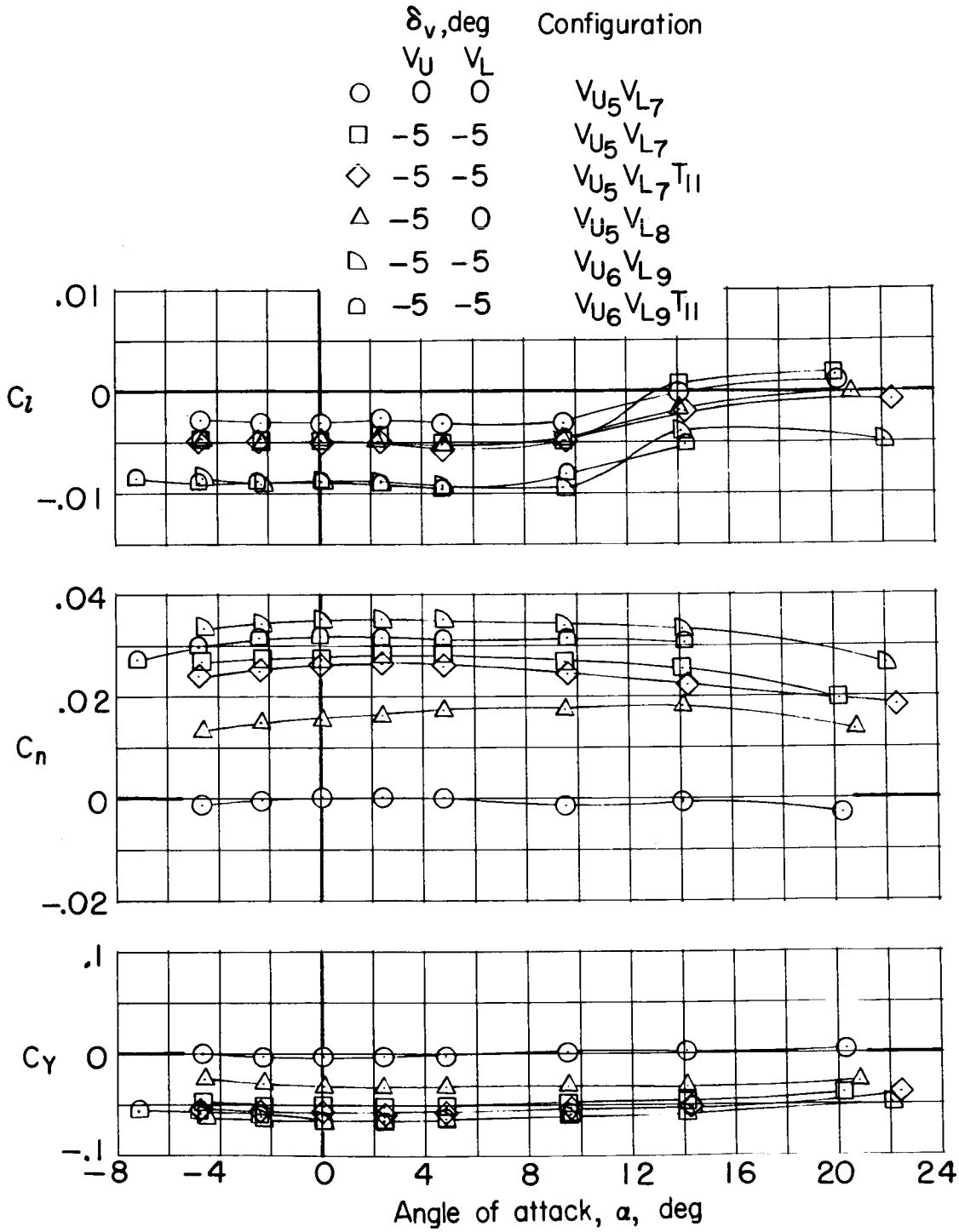

(c) M = 1.00.

Figure 13.- Continued.

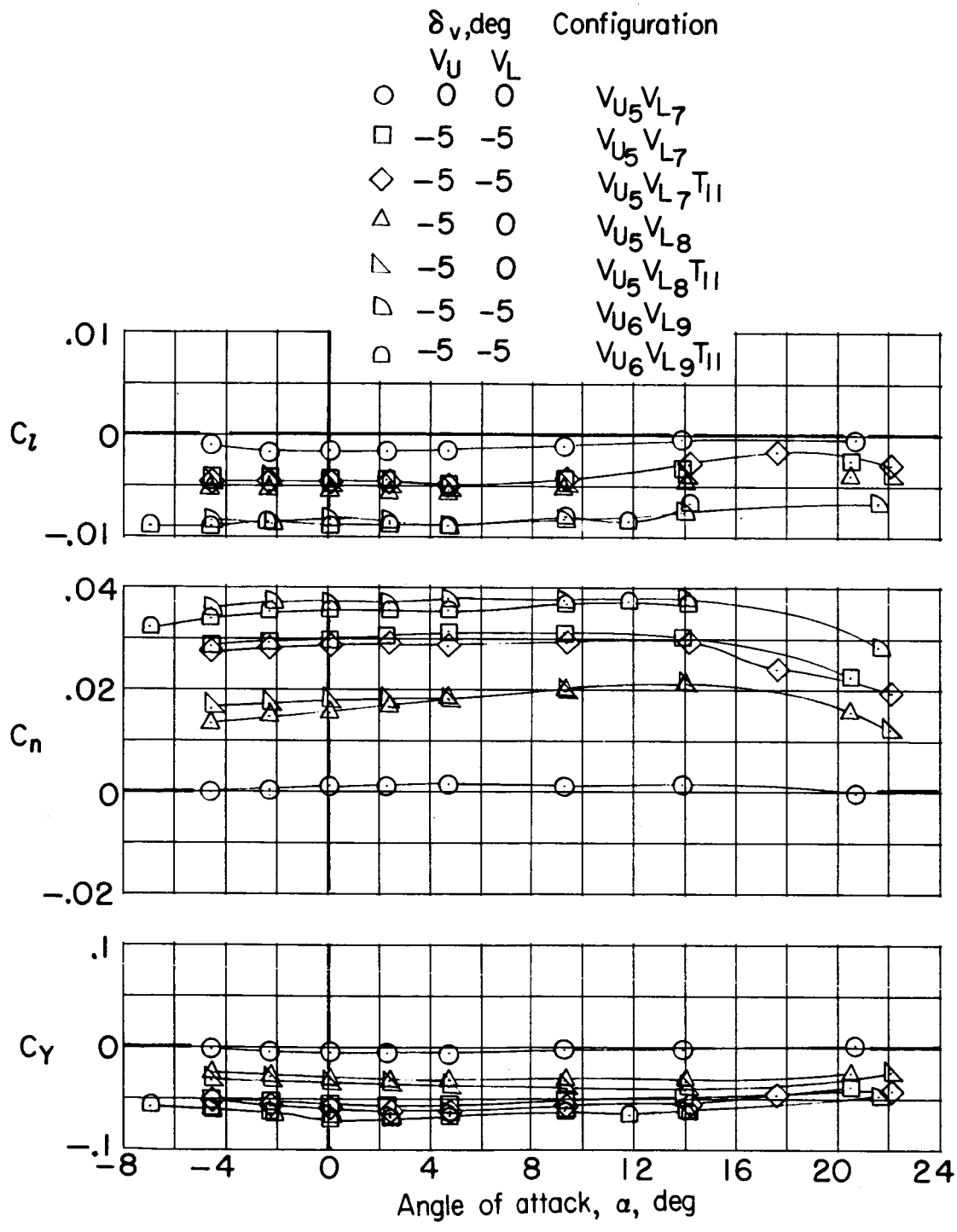

(d) M = 1.20.

Figure 13.- Concluded.

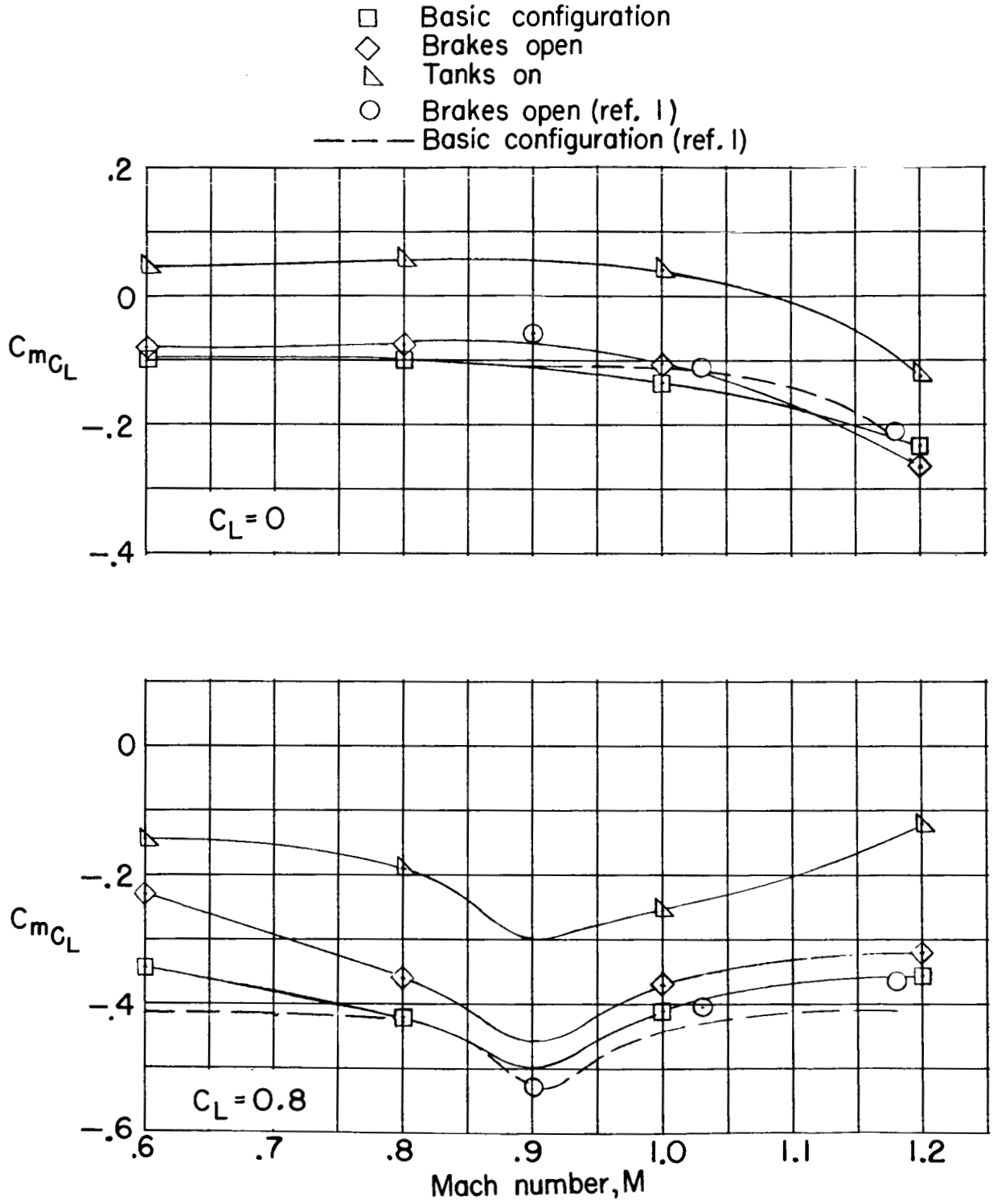

Figure 14.- Variation with Mach number of longitudinal stability parameter. Control surfaces undeflected.

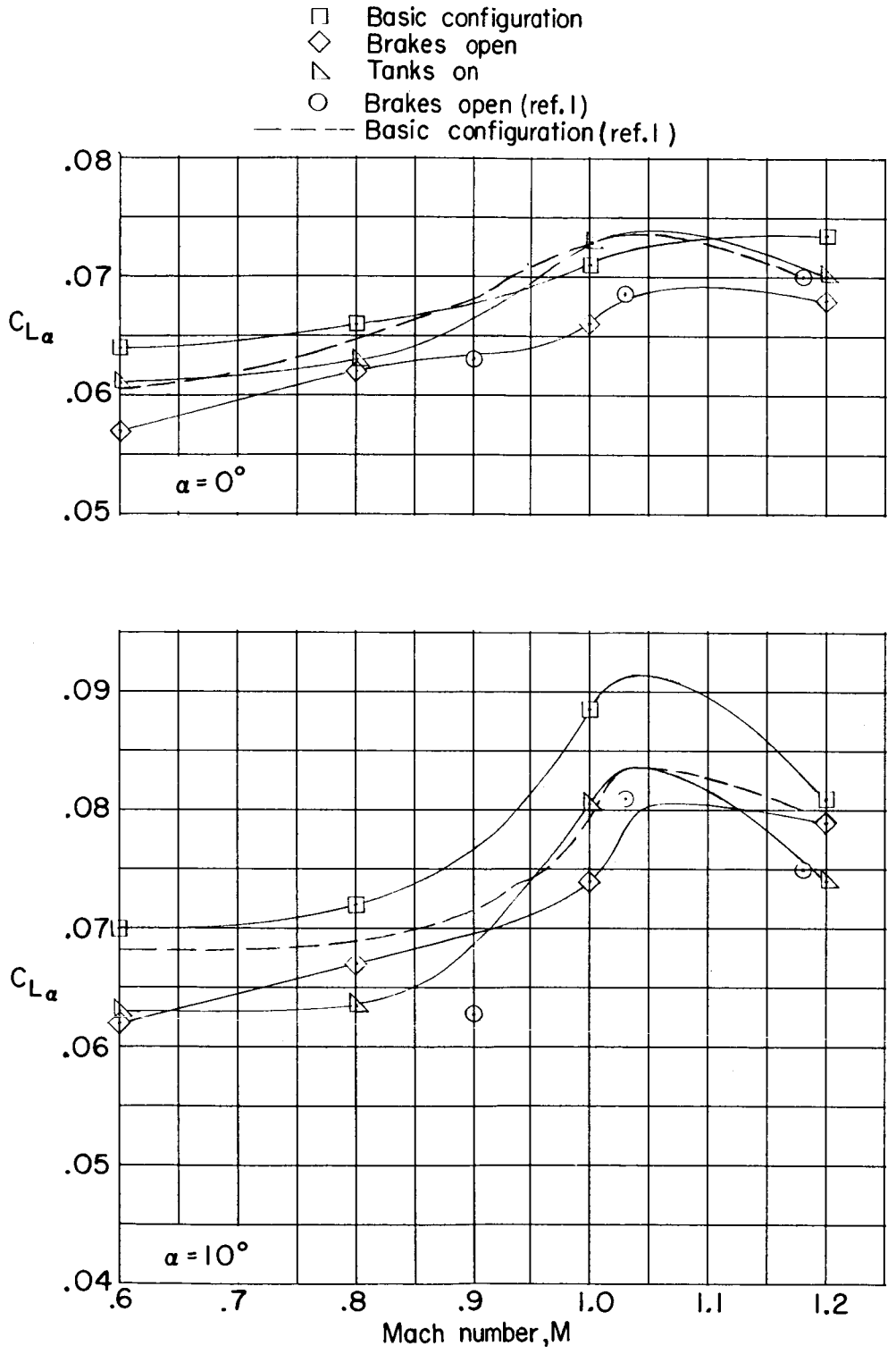

Figure 15.- Variation with Mach number of lift-curve slope. Control surfaces undeflected.

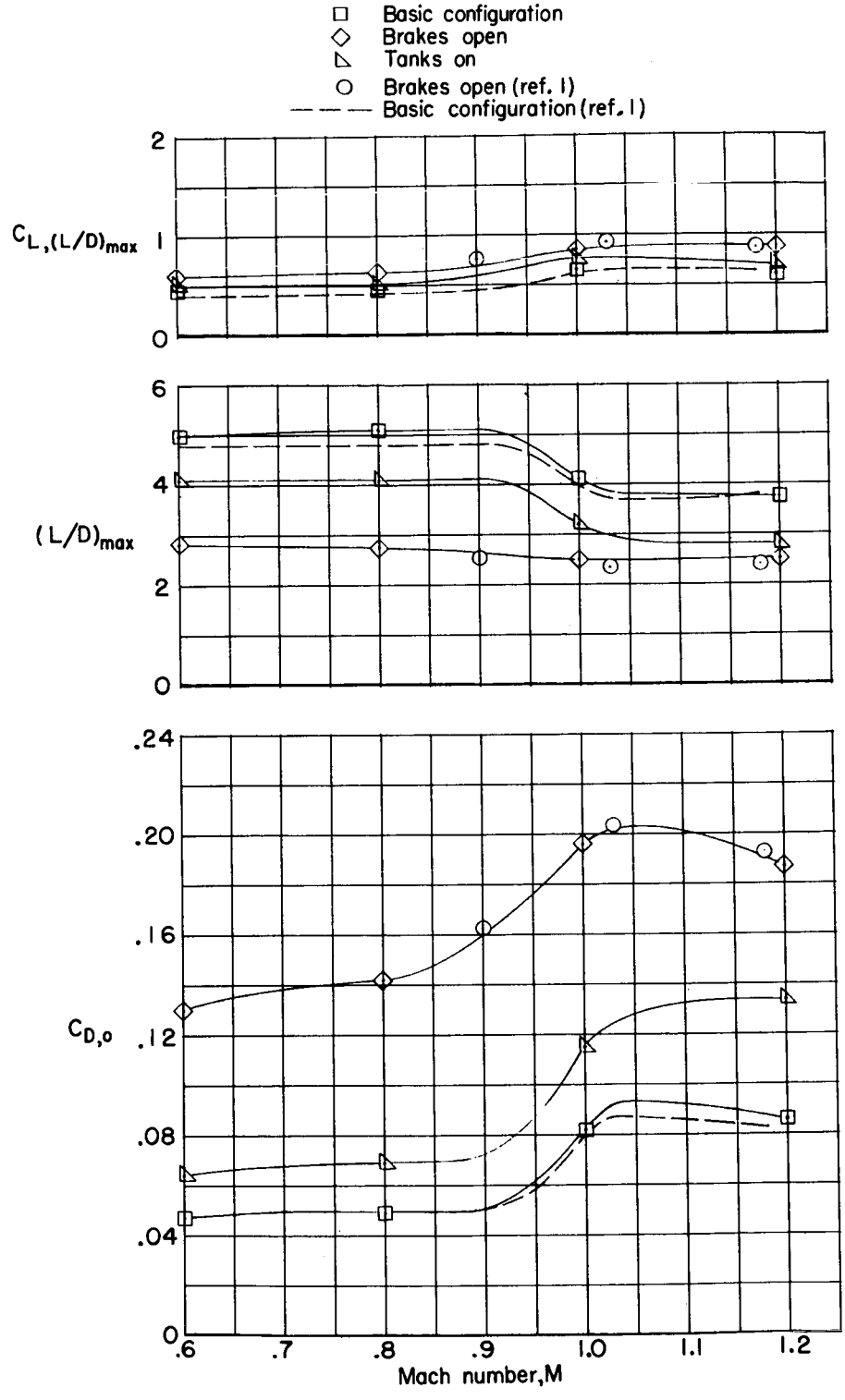

Figure 16.- Variation with Mach number of $C_{L,(L/D)_{max}}$, $(L/D)_{max}$, and $C_{D,o}$. Control surfaces undeflected.

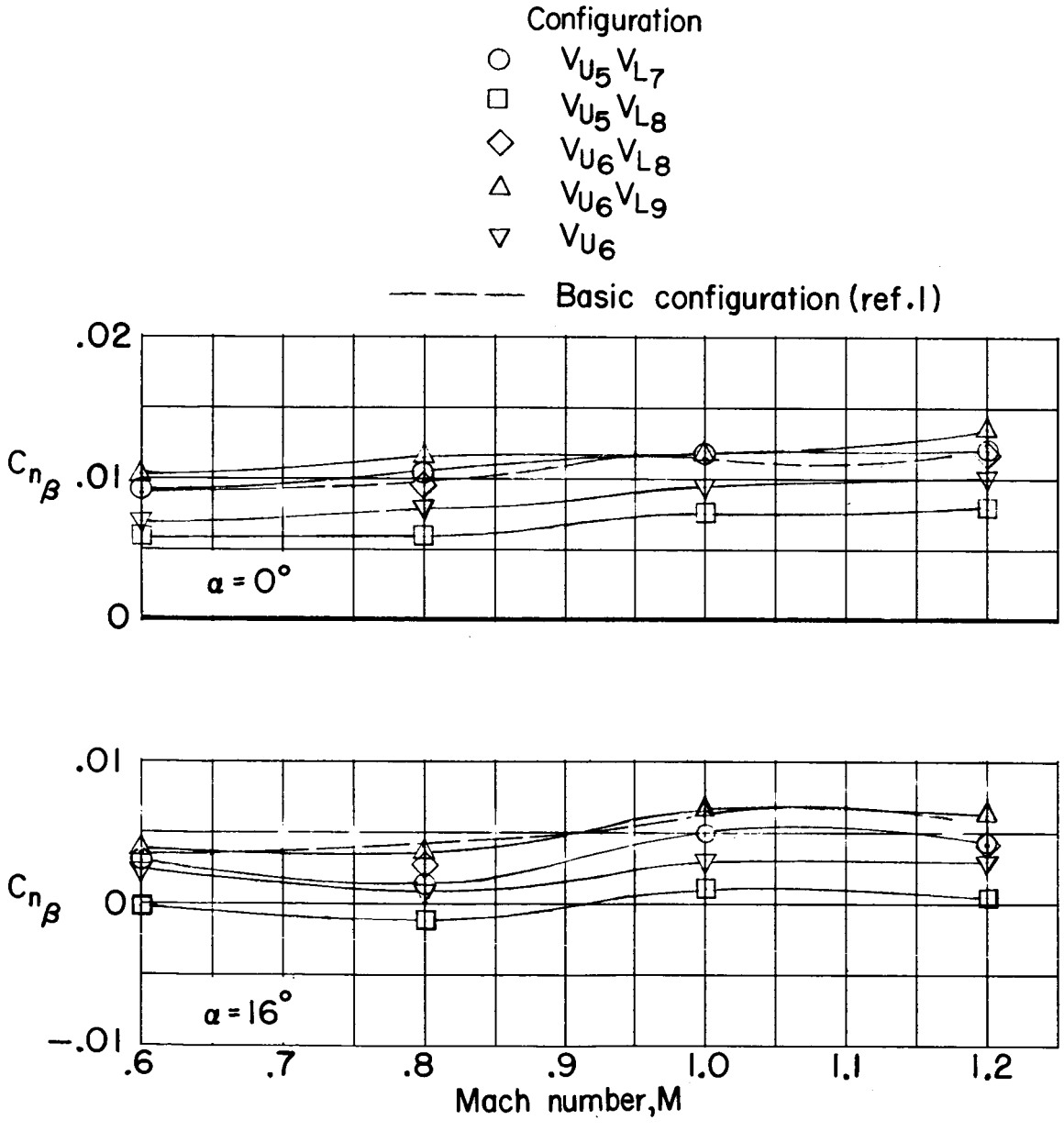

(a) C_{n_β} against M.

Figure 17.- Variation with Mach number of lateral stability derivatives for various vertical-tail configurations. $\delta_h = 0^o$.

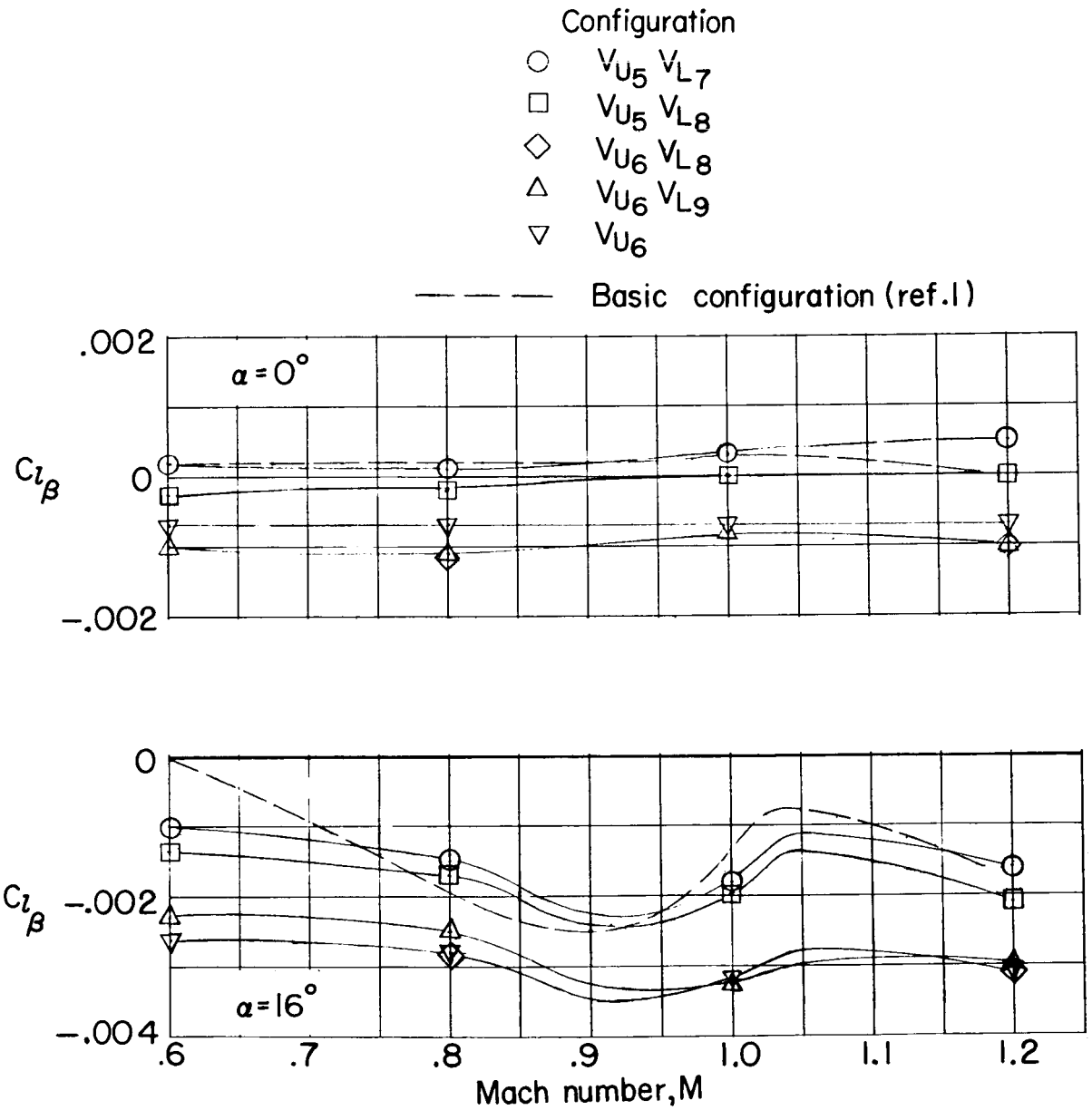

(b) C_{l_β} against M.

Figure 17.- Continued.

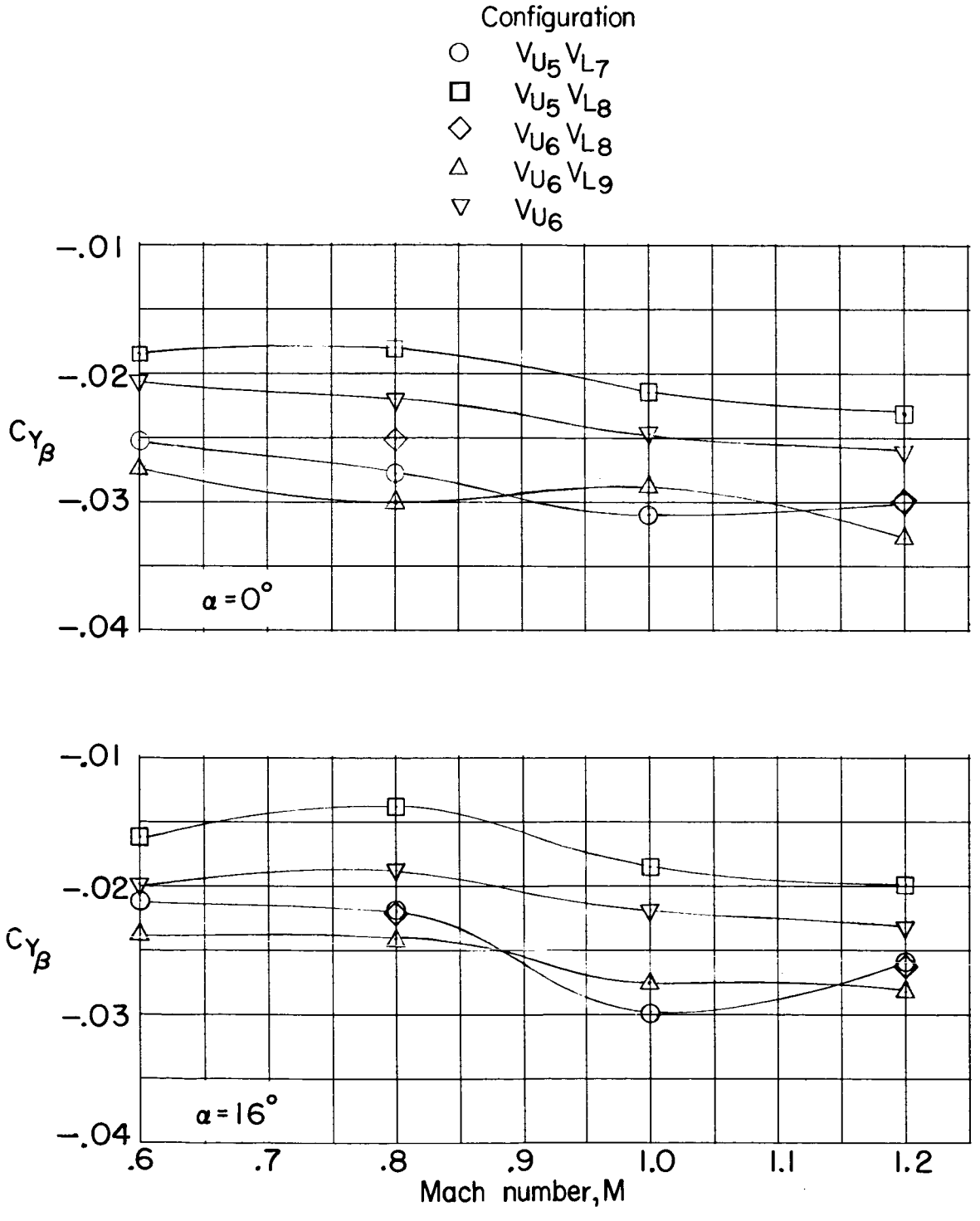

(c) C_{Y_β} against M.

Figure 17.- Concluded.

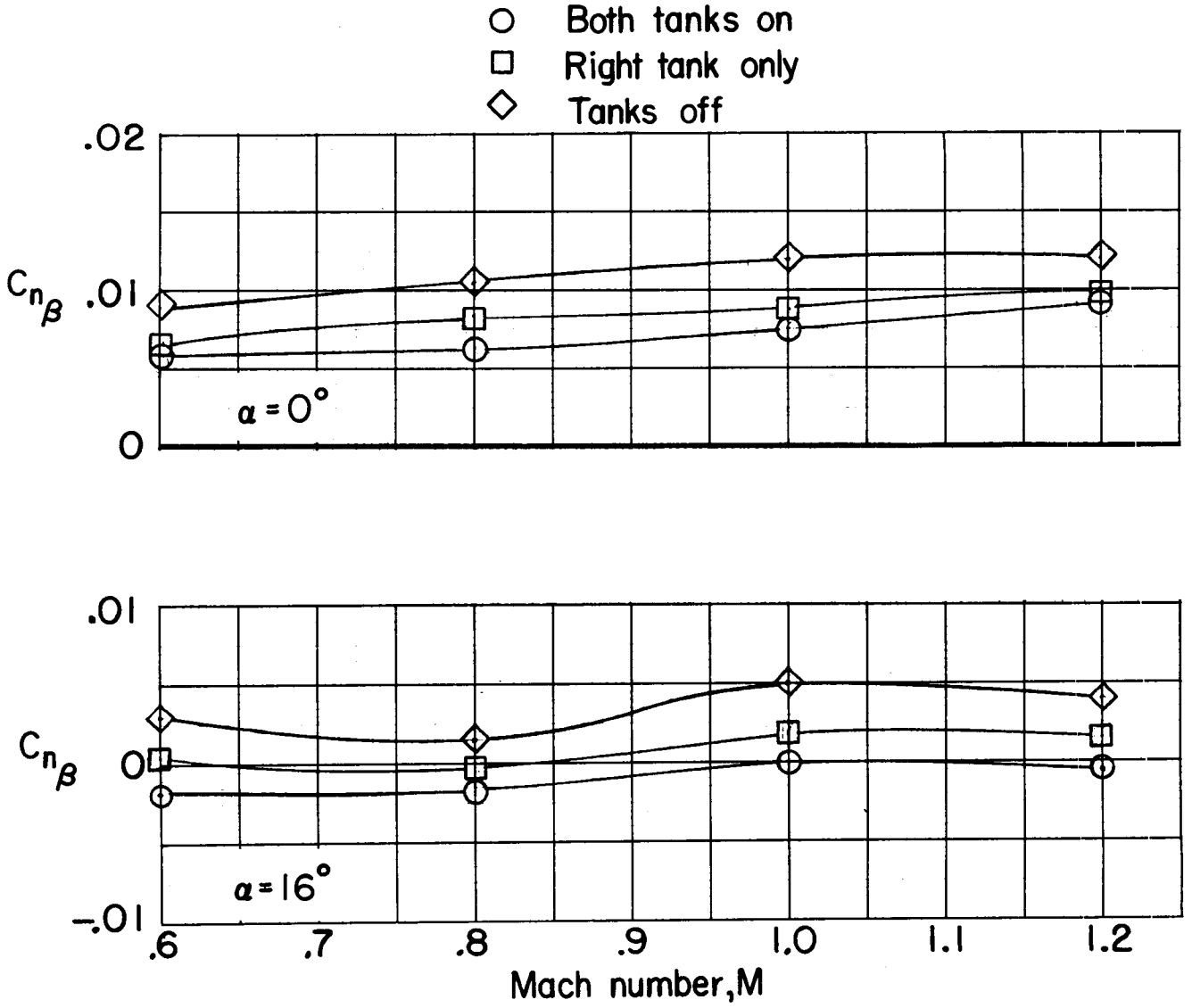

(a) C_{n_β} against M.

Figure 18.- Variation with Mach number of lateral stability derivatives for externally mounted fuel tanks.

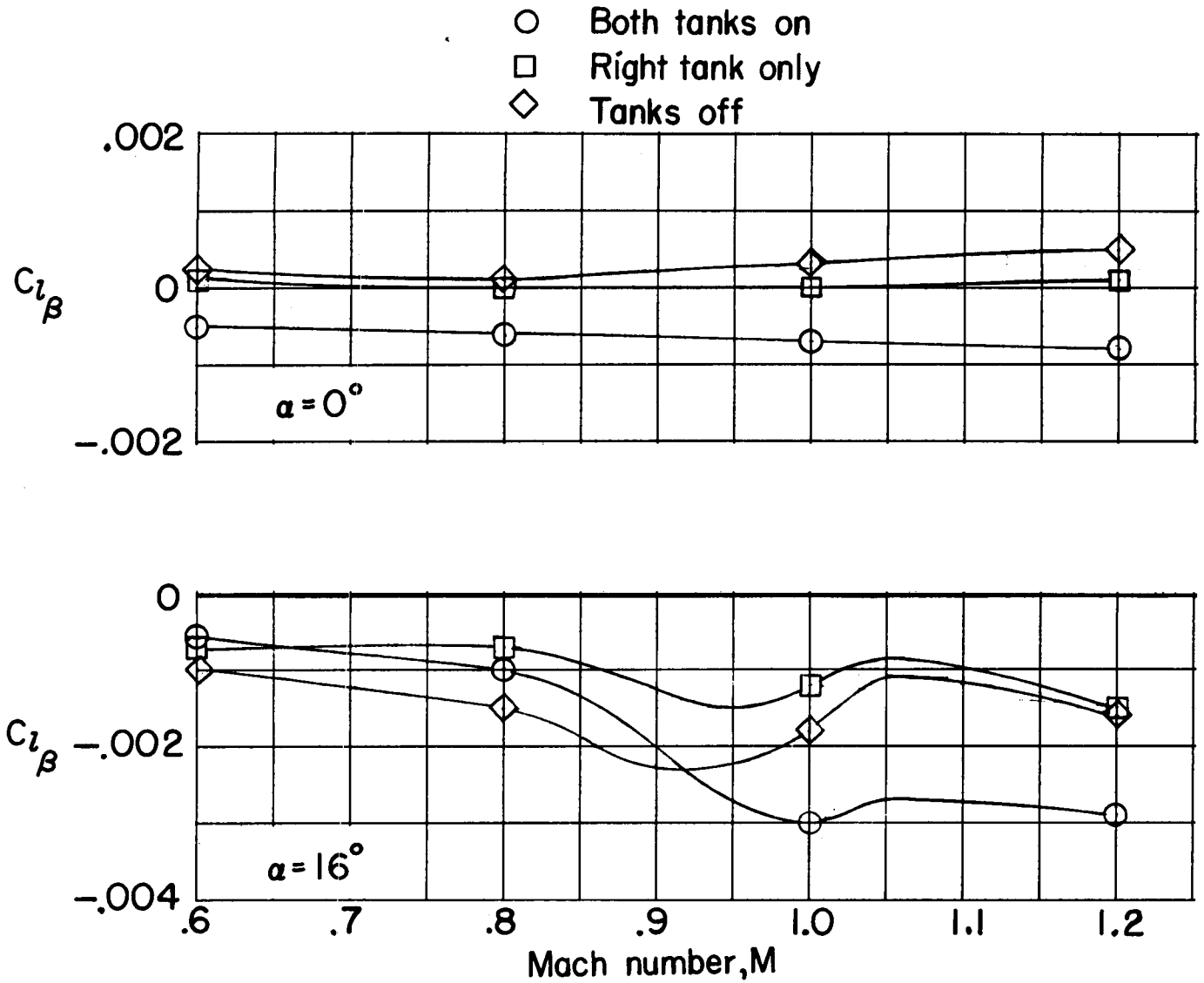

(b) C_{l_β} against M.

Figure 18.- Continued.

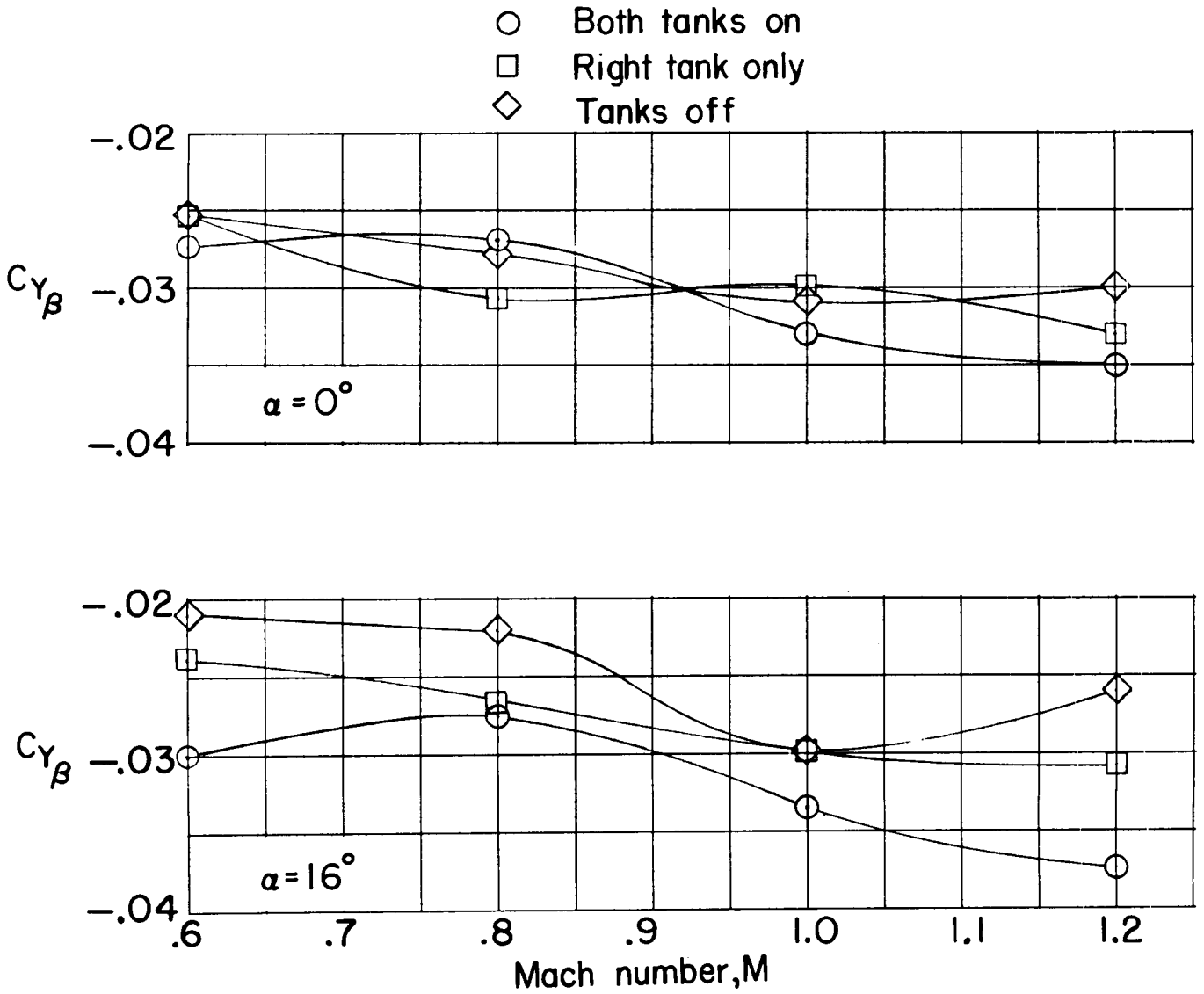

(c) C_{Y_β} against M.

Figure 18.- Concluded.